Modern X-ray spectroscopy

Zimmermann, Patric; Peredkov, Sergey; Abdala, Paula Macarena; DeBeer, Serena; Tromp, Moniek; Mueller, Christoph; van Bokhoven, Jeroen A.

Published in:
Coordination Chemistry Reviews

DOI:
10.1016/j.ccr.2020.213466

Publication date:
2020

Coordination Chemistry Reviews 423 (2020) 213466

Contents lists available at ScienceDirect

Coordination Chemistry Reviews

journal homepage: www.elsevier.com/locate/ccr

Review

Modern X-ray spectroscopy: XAS and XES in the laboratory

Patric Zimmermann [a], Sergey Peredkov [d], Paula Macarena Abdala [c], Serena DeBeer [d], Moniek Tromp [b], Christoph Müller [c], Jeroen A. van Bokhoven [a,e,*]

[a] Laboratory for Catalysis and Sustainable Chemistry, Paul Scherrer Institut, 5232 Villigen-PSI, Switzerland
[b] Zernike Institute for Advanced Materials – Materials Chemistry, Rijksuniversiteit Groningen, 9747 AG Groningen, The Netherlands
[c] Laboratory of Energy Science and Engineering, ETH Zürich, 8092 Zürich, Switzerland
[d] Max Planck Institute for Chemical Energy Conversion, 45470 Mülheim an der Ruhr, Germany
[e] Heterogeneous Catalysis, ETH Zürich, 8092 Zürich, Switzerland

ARTICLE INFO

Article history:
Received 2 April 2020
Accepted 22 June 2020
Available online 14 August 2020

Keywords:
Laboratory X-ray spectroscopy
WDX
XAS
non-resonant XES
VtC
Catalysis

ABSTRACT

X-ray spectroscopy is an important tool for scientific analysis. While the earliest demonstration experiments were realised in the laboratory, with the advent of synchrotron light sources most of the experiments shifted to large scale synchrotron facilities. In the recent past there is an increased interest to perform X-ray experiments also with in-house laboratory sources, to simplify access to X-ray absorption and X-ray emission spectroscopy, in particular for routine measurements. Here we summarise the recent developments and comment on the most representative example experiments in the field of in-house laboratory X-ray spectroscopy. We first give an introduction and some historic background on X-ray spectroscopy. This is followed by an overview of the detection techniques used for X-ray absorption and X-ray emission measurements. A short paragraph also puts related high energy resolution and resonant techniques into context, though they are not yet feasible in the laboratory. At the end of this section the opportunities using wavelength dispersive X-ray spectroscopy in the laboratory are discussed. Then we summarise the relevant details of the recent experimental laboratory setups split into two separate sections, one for the recent von Hamos setups, and one for the recent Johann/Johansson type setups. Following that, focussing on chemistry and catalysis, we then summarise some of the notable X-ray absorption and X-ray emission experiments and the results accomplished with in-house setups. In a third part we then discuss some applications of laboratory X-ray spectroscopy with a particular focus on chemistry and catalysis.

Contents

* Corresponding author.
E-mail address: jeroen.vanbokhoven@chem.ethz.ch (J.A. van Bokhoven).

https://doi.org/10.1016/j.ccr.2020.213466
0010-8545/

1. Introduction

The field of X-ray spectroscopy underwent a dramatic evolution during the past decades and there have been enormous developments and technological improvements, experimentally as well as in theory and modelling [1,2]. Nowadays X-ray spectroscopy is employed in almost every thinkable field of technology and research. To give just a few examples, applications range from fundamental research in chemistry [3–8], physics [9–15] and material science[16,17], to environmental research [18,19], architecture [20], art [19,21,22], archeology [19,23–25] and industrial applications [19], to even forensics [19], security systems [26,27] and astronomy [28–31]. In a scientific context X-ray spectroscopy is also known as *core-level- or core-spectroscopy* [32,33] and it has become an essential tool for the study of a vast number of systems. Two of the key attributes of X-rays are the intrinsic elemental selectivity due to the characteristic energy of the core-level transitions and, especially for hard X-rays, the methods are bulk sensitive, referring to the ability to penetrate a material allowing one to 'look inside'. Over the years many books on core-spectroscopy have been written making it essentially impossible to create a complete list, hence we only refer to a few example sources [1,2,19,32,34] for the interested reader.

Historically, in most cases W.C. Röntgen is with his article *Uber eine neue Art von Strahlen*, published in 1895 [35,36], credited for the discovery of X-rays. For his work he received in 1901 the Nobel Prize in Physics *in recognition of the extraordinary services he has rendered by the discovery of the remarkable rays subsequently named after him* [37]. However, as Lederman [38] and Grubbé [39] point out others have used X-rays prior to Röntgen and much of the ground work had been done several years before by Plücker (1859) [40,41], Crookes (1875) and Lenard (1893) (both cited by Grubbé [39]). Nonetheless, in German speaking countries X-rays are called *'Röntgenstrahlung'* crediting Röntgen as the discoverer of this new kind of light.

In the early days X-rays were a physical curiosity and mostly used only for therapeutical or medical applications [39]. The last years of the 19th and the first decades of the 20th century were a revolutionary time in physics with a lot of controversy [42]. During these years, among the well-known figures including Planck, Heisenberg and Einstein many others such as Born [43,44], Sommerfeld [45,46] and Bohr [42,47] made significant contributions laying the foundation of quantum-mechanics and the fundamental understanding of the atomic structure. This was the beginning of modern physics and core spectroscopy as we know it today.

One of the fundamental discoveries relevant to the field of X-rays came from Lawrence Bragg and his father William H. Bragg which they published in 1913 [48]. They systematically studied *The Reflection of X-rays by Crystals*, for which they both received the Nobel price in physics in 1915, and *Bragg's law* was subsequently named after them. Also in 1913 De Broglie published his remarkable article *Recherches sur la diffraction des rayons de Röntgen par les milieux cristallins* [49] in which he uses Bragg's law employing salt crystals (NaCl and $K_3[Fe(CN)_6]$) to disperse the emission of an X-ray tube and to measure one of the first *X-ray absorption spectra* (XAS). Other early notable spectroscopic experiments with X-rays were carried out in the laboratory by Coster [50,51], Sommerfeld [45,46], Siegbahn [52] and Kronig [53] in the 1920s and 30s.

One of the first reports of an *X-ray Emission Spectrum* (XES), published by Lundquist [54] in 1925, was based on measurements using an X-ray tube with a copper anode, operating at approximately 200 Watts. In this early experiment the dispersive component was a natural calcite ($CaCO_3$) crystal employed for the investigation of the Kβ emission lines of phosphorus (P) and potassium (K). This experiment done almost one century ago is in its essence still one of the important methods in regard to chemical speciation [3].

As in recent years some notable developments took place with respect to laboratory X-ray spectroscopy setups, we take the opportunity here to summarise and comment on the most notable developments and publications in this field.

1.1. X-ray sources and X-ray detection

Before we discuss the existing in-house setups, we review in this section the essential techniques required for the production and detection of X-rays. Due to the fact that hard X-rays can be used at ambient conditions, while measurements in the soft X-ray energy range typically require a vacuum setup, we focus on the hard X-ray energy range. However, some of the sources mentioned are employed for the generation of soft X-rays and where appropriate we also give some references with respect to the soft energy range.

Nowadays, there are various kinds of X-ray sources. Though we will focus here on laboratory sources, we cannot omit the most important source of X-rays today, being the third and fourth generation of modern and highly brilliant synchrotron light sources, which have boosted the advance of high-resolution spectroscopies in the X-ray energy range [17].

In 1974 the first machine designed as dedicated X-ray light source using a 300 MeV storage ring was built in Japan [55–57]. Though some earlier machines did exist, they were not designed as light sources and the light was rather used in a parasitic mode. Since these early days of synchrotron radiation huge improvements have been made. Most importantly the development of the so-called *insertion devices* (wigglers, undulators) around 1980 can be considered as one of the big milestones for modern X-ray spectroscopy leading to a broad application in many research fields [57–59].

Since then great efforts have been made to improve and use the various unique properties of synchrotron radiation. For example the increased intensity across a broad energy range, the high coherence and low angular divergence (brilliance), but also the tunability using undulators and sophisticated single and double bounce monochromators, and taking advantage of the intrinsic pulsed time structure and high degree of polarisation are important properties of synchrotron light [57]. All these properties are

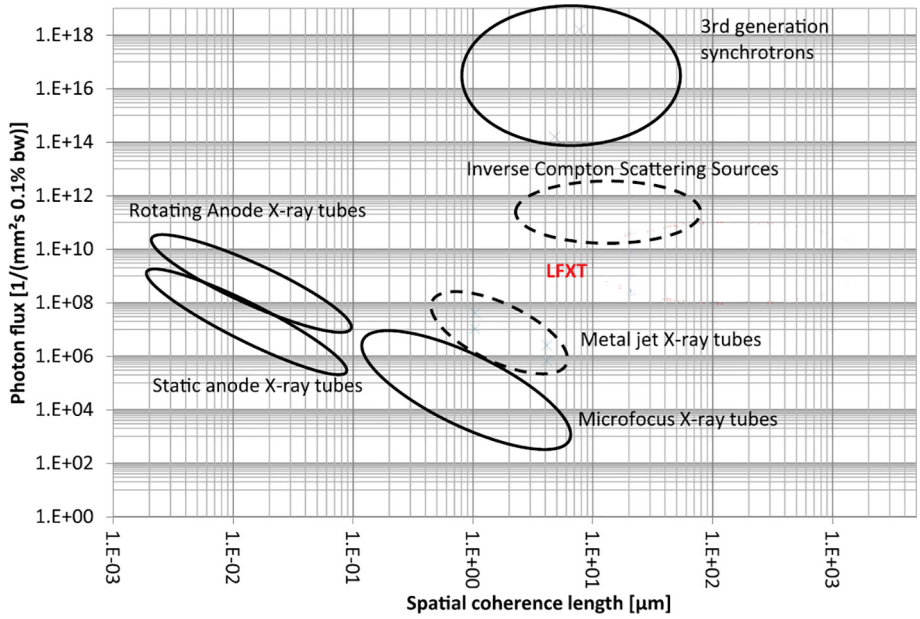

Fig. 1. A comparison of the Flux and coherence for difference X-ray sources. (Image reused from Bartzsch [73] published Open Access/CC3.0).

often highly desirable making the currently existing third and fourth generation of synchrotron light sources still irreplaceable for many applications and without doubt an essential tool in modern research. Hence, we are now seeing some of theses machines being either in the planning-phase or in the process to be upgraded to deliver even higher brilliance and coherence (ERSF upgrade completed in 2020 [60], SOLEIL upgrade planned for 2022–25 [61], SLS upgrade planned for 2021–24 [62]).

Synchrotrons are and will be for the foreseeable future irreplaceable for many applications. However, as access to large scale infrastructure is limited and highly competitive, we are seeing in the recent years more efforts being made to bring the know-how from the synchrotron back into the lab in order to simplify access and to increase the available measurement time. Hence, modern lab sources are being utilised as a valuable alternative for some applications, or as a means to allow for preliminary tests for X-ray spectroscopic studies. Moreover, lab-based spectrometers also enable to perform different types of experiments, such as for example long-term measurements or the study of systems which are toxic or dangerous and hence not allowed at many synchrotrons. [63,64] Thus, there are attempts by Lyncean to employ 'mini synchrotrons' in the lab, which they call *Compact Light Source* (CLS). [65–67].

The most common laboratory sources in the hard X-ray energy range are, due to their relatively simple working principle the classic, though highly improved [68] X-ray tubes using various anode materials. It is well known that X-ray tubes convert only about 1% of the energy applied to the anode into radiation, while the majority of 99% is lost due to the conversion into thermal energy. [68,2] Thus a 100 W tube (f.e. with an acceleration potential of $U = 25$ kV and an electron beam current of $I = 4$ mA) delivers only 1 W of light across its entire spectrum. This translates to an order of magnitude of roughly $10^{12} - 10^{13}$ photons per second integrated over all energies. The result is, depending on the photon energy and aperture of the slits used, approximately $10^{2} - 10^{4}$ photons per second when monochromatised to a sub-eV bandwidth. The characteristic lines, however, of course yield notably higher count rates. Overall this illustrates that X-ray tubes are obviously a very inefficient source of radiation.

Since most of the energy transferred to the anode dissipates as heat, in fact, the melting point of the anode material sets the limit for the maximum power of the tube, making substantial cooling necessary for high-power X-ray tubes [2]. To address this problem, rotating and even liquid metal anodes are used as a target in high-power X-ray tubes [69–71]. An alternative approach is presented by Tuohimaa et al. [72] who introduced a methanol jet as a non-metal liquid target excited by an electron beam. A promising recent development are so-called *Line Focus X-ray Tubes* (LFXTs) which employ an extremely small focal spot in one direction. It is essentially a very thin line allowing for a much more efficient heat dissipation when compared to conventional point source X-ray tubes. The photon flux and coherence length of such a LFXT is predicted to be comparable to inverse Compton scattering sources (see Fig. 1) [73].

Yet another approach addressing the issue of heat-dissipation is offered by Sigray, who have developed a microstructured anode material comprised of arrays of metal, such as copper (Cu) or tungsten (W), embedded in a diamond substrate. This allows for highly localised and large thermal gradients for rapid passive cooling. Additionally the linear accumulation across the embedded microstructures notably increases the emitted photon flux produced by the source [74]. A different approach is to use laser driven X-ray sources, though they are typically limited to the soft X-ray energy range $E < 500$ eV. Their working principle is essentially that a very intense laser creates a plasma from various target materials, which then recombines under emission of X-rays, hence they are called *Laser Plasma Source* (LPS) or more specifically *Laser Plasma X-ray Source* (LPXS) [75–79]. One of the major advantages of a LPS is that a Laser can create well-defined pulses translating into pulses of X-rays which then enable time-resolved X-ray experiments.

An overview with various details on X-ray sources, the detection of X-rays and more can be found in the textbooks *Handbook of Practical X-ray Fluorescence Analysis* [19] and in *X-ray Absorption and X-ray Emission Spectroscopy* [2].

Also the detection of X-rays has dramatically improved during the last century [80]. On the one hand there are *Energy Dispersive X-ray* (EDX) detectors, such as solid state *Silicon Drift Detectors*

(SDDs) with an energy resolution up to $\Delta E \approx 120$eV (due to the Fano limit [2,81,82]), and even spatially resolving 1D line and 2D area EDX pixel detectors [83–86]. The latter ones are essentially a 'color camera' for the X-ray energy range. Typically EDX detectors can cover a large energy range, from approximately 1 keV to 40 keV [87].

Wavelength Dispersive X-ray (WDX) detection on the other hand is commonly used to achieve the highest possible energy resolution by trading flux for resolution. WDX configurations take advantage of Bragg's law [48], where a grating or crystal is used to spatially disperse the photons wavelength selectively. In the soft X-ray energy range below 2 keV, gratings are usually preferred, while at higher energies for hard X-rays crystal analysers are used [76,82]. Under ideal conditions they can reach a sub-eV energy resolution in the hard and a few tens of meV in the soft X-ray range [82,88,89]. Considering the most recent developments at the SIX beamline at NSLS-II, they now reach a $\Delta E = 14$meV at an energy of $E = 1$ keV, translating to a $E/\Delta E \approx 71500$ [90]. The downside of the WDX based detection is that each (crystal) configuration covers a relatively small energy range, say a few hundred eV in the soft energy range to a few keV in the hard energy range. Another aspect is that due to the $\cot(\theta_B)$ relation the resolving power decreases notably for measurements at low Bragg angles θ_B [91,92]. For example comparing a measurement at $\theta_B = 80^\circ$ with a measurement at $\theta_B = 65^\circ$ means the resolution at $\theta_B = 65^\circ$ is approximately 2.6 times lower ($\frac{\cot(65)}{\cot(80)} \approx 2.64$) than the resolution at $\theta_B = 80^\circ$.

A flat crystal spectrometer employed in a scanning approach provides the highest resolution, because curved crystals suffer from geometrical aberrations related to imperfections in the crystal when it is bent. Though, the strain in the crystal can be reduced with the 'strip-bent' method [93]. The spherically bent crystals (SBC) used in Johann and Johansson Rowland circle geometry give a luminosity enhancement of the order of 10^2–10^3 due to an increased solid angle, but at the cost of some losses in the resolution due to the geometrical aberrations [94]. For both types of crystals, flat and curved, two types of spectrometer exists: Laue type (transmission) and Bragg type (reflection) instruments. Most reflection type instruments using curved crystal spectrometers are either operated in the Johann/Johansson geometry where the crystal is aligned in Rowland geometry, or in the slightly different von Hamos geometry. The transmission type instruments are most commonly using curved crystals employed in the DuMond and Cauchois geometry [94].

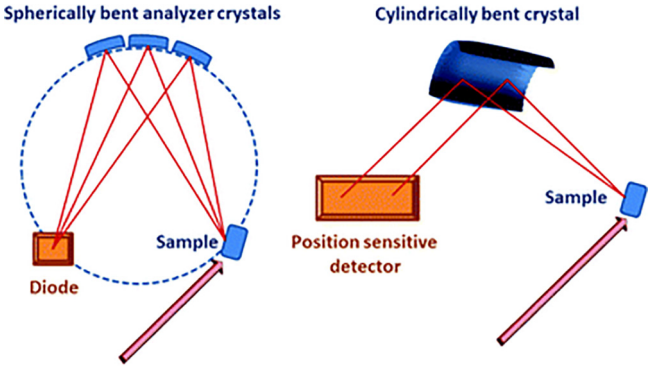

Fig. 3. Johansson and von Hamos geometry: Point to point focussing Johansson geometry, and point to line focussing in the von Hamos geometry. (Image reused from Bauer [100] published under CC3.0).

A reflection type spectrometer essentially consists of three parts:

1. **Source** of the emission, e.g. X-ray tube or illuminated sample.
2. **Crystal** as the wavelength dispersive element.
3. **Detector**, to measure the X-ray intensity.

The Johann and Johansson geometries are almost identical, the main difference being the different crystals. Johansson crystals are bent to twice the radius of curvature of the spectrometer circle, and the inner surface is then ground away to match the radius equal to that of the spectrometer circle. The effect is that the angle of incidence equals the angle of reflection while the Bragg angle remains constant over the entire surface of the crystal. This leads essentially to a perfect focus with a high diffraction intensity (Fig. 2). Therefore, a Johansson crystal gives a better resolution over the entire spectrometer range than the Johann crystals [95].

While Johansson crystals must be bent and ground, the Johann crystal is just bent. Hence Johansson crystals are typically more expensive due to additional difficulties in the manufacturing process. More details on the differences between Johann and Johans-

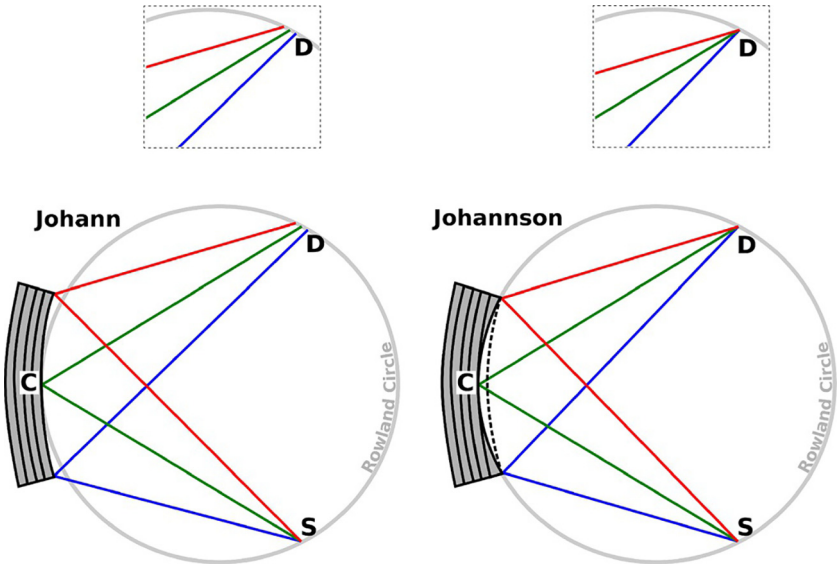

Fig. 2. Johann vs Johansson crystal illustrating that the focus does not lie exactly on the detector in Johann geometry. (Image reused from Kowalska [96] with permission from Wiley).

son are discussed in more detail by Kowalska [96] and Kvashnina [97].

One important attribute in WDX spectroscopy is the effective solid angle. A larger solid angle directly translates into a higher intensity due to the collection of more photons. Hence, a common approach is to combine a number of crystals for a larger effective solid angle of detection. The first multi-crystal experimental setup used six crystals and was developed by Wang in 1997 [98]. Today there are several experimental setups operating at synchrotron facilities using an arrangement of multiple SBC to increase the solid angle [99–101]. Alonso-Mori [101] mentions for example the ESRF (beamline BM30B/CRG-FAME XAS, 5 analysers [102], and beamline ID26, 5 analyzers [103]), SSRL (beamline 6–2 using 14 analyzers [4]) the SLS (SuperXAS beamline uses 5 crystals) [104], and NSLS (beamline X21, uses 9 crystals) [105].

While the detectable countrate can be increased with multiple crystals, it typically also reduces the resolution due to small misalignments between each crystal. Furthermore, not all emissions from the sample are necessarily isotropic. Fluorescence emission is typically assumed to be isotropic, but especially resonant techniques or experiments with polarised light can show a strong angular dependence [106–108]. In other words, increasing the solid angle with multiple crystals comes at the cost of potentially loosing information of the angle of emission, which can be relevant for polarisation dependent experiments or resonant techniques [10,11,13,106–108].

Another approach, of particular importance for time-resolved measurements, is the von Hamos geometry. It is based on a cylindrically bent crystal (CBC) which disperses the polychromatic light on a spatially resolving pixel detector (see Fig. 3, right) [3,101,100].

As such, the von Hamos setup enables one to acquire a spectrum without any moving components, implying a significant reduction of the measurement time per spectrum [101]. According to Bauer this comes at the cost of reduced energy resolution and lower signal intensities [100], while Alonso-Mori reports the signal to background ratio to be lower when compared with the one obtained in a Rowland based spectrometer [101]. However, this could be due to an insufficiently optimised setup, as Szlachetko states that the von Hamos setup provides a good energy resolution often below 1 eV at relatively large Bragg angles [3]. Furthermore, a von Hamos spectrometer can be built relatively compact due to the use of short curvature radiuses without loss on energy resolution. Importantly, both von Hamos and the Johansson geometries, can yield an absolute energy resolution significantly below the lifetime of characteristic emission lines, which is crucial for a detailed analysis of spectral features [3]. Something of more practical relevance is, that for the Johann/Johansson geometry one does not need a very tightly focused beam, because slits can be used to optimise the resolution of the instrument. For example, the Johann/Johansson type spectrometer works well with a source spot-size of approximately 0.5–1 mm, while the von Hamos geometry requires a good focus in the dispersion direction of approximately 50 μm.

Table 1
Comparison of three experimental XES setups with different sources and WDX spectrometers. a) refers to a laboratory von Hamos setup with a Ga metal-jet source [5] and b) refers to a commercial laboratory Johann setup from EasyXAFS using an X-ray tube as source, [123,125] and c) refers to a von Hamos setup installed at the PINK beamline at BESSY II. Most notable are the different acquisition times, where the synchrotron light source allows for much faster measurement due to the higher brilliance and better signal-to-noise ratio.

	a) LabXES at TUB/MPI	b) EasyXES100 at MPI	c) PINK XES at BESSY II
Source			
Brand	Excillium	Varex VF80-JM	–
Type	MetalJet	X-ray tube	Synchrotron
Target/source	Ga target	W and Pd anode	U17 cryo undulator
Max Power	250 W	100 W ($I_{max} = 4$ mA, $U_{max} = 35$ kV)	–
Energies	Ga Kα 9.2 keV	W Lα 8.3 keV Pd Kα 21 keV, Lα 2.8 keV	2—10 keV (tunable)
Photons/s	ca. $2.0 \cdot 10^9$	$10^{11} - 10^{12}$ (total counts)	$10^{13} - 10^{16}$, 10^{14} at 6 keV
Optics	50μm Be window focussing polycapillary	0.5—2mm (source slit in XES mode)	multilayer DCM ($E/\Delta E = 10 - 100$)
Spotsize	30×30 μm^2	10×10 mm^2 (without slits)	20 (V) $\times$ 500 (H)μm^2
Spectrometer			
Type	von Hamos circular	Johann	von Hamossegment
Mode	spatially dispersive	scanning mode	spatially dispersive
Crystal	cylindrical HAPG (Highly Annealed Pyrolytic Graphite)	SBCA Ge110, Ge211, Ge310, Si110, Si551, Si553	cylindrical, dised Si100, Si110, Si111, Si310, Ge100, Ge110, Ge111, Quartz ($10\bar{1}2$)
Crystal radius	$R = 30$ cm (full cylinder)	$R = 1$ m	$R = 25$ cm and $R = 30$ cm
Dimension	radius $r = 30$ cm, width $d = 30$ mm	radius $r = 5$ cm	50×100 mm^2
Solid angle	1 . . . 3 msr	$\pi r^2/R^2 \approx 8$ msr	0.005 . . . 0.1 msr
Energy range	2.6 . . . 9 keV (Cl Kα - Zn Kα)	5.5 . . . 12 keV (Ti Kβ - Pb Lα)	2.1 . . . 9.5 keV (e.g. P Kβ . . . Cu Kβ)
Resolution ΔE	1 . . . 2eV, $E/\Delta E \approx 4000$	0.5 . . . 1.5 eV	0.2 . . . 0.9 eV
Spectral window	20 . . . 100 eV	100 . . . 200 eV	20 . . . 100 eV
pressure	10^{-6} mbar	He chamber (up to 1 bar)	He bag, 10^{-5} mbar
Detector	25×25 mm^2 Princeton Instruments CCD	Silicon Drift Detector	7×26 mm^2 CCD (2—5 keV), Mythen (5.5—10 keV), Eiger (4—10 keV)
Sample-Environment	GloveBox, RT, 70 K Cryo	solid samples, RT	1 . . . 10 mbar, RT, He, 15 K Cryo
Distance to	polycapillary: 22.5 mm	exit window: 3 . . . 5 mm	exit window: 16 mm
Typical acquisition times	P K$\beta_{1,3}$ (KH_2PO_4): 30 h K K$\beta_{1,3}$ (KCl): 7 h Ca VtC ($CaCO_3$): 18 h	Co K$\beta_{1,3}$ (CoO): 30 min Co VtC (CoO): 3–10 h Cu VtC (CuI acetat): 12–24 h	P K$\beta_{1,3}$ (KH_2PO_4): 3 min Pd L$\alpha_{1,2}$ (Pd foil): 10 s Ru L$\beta_{1,2}$ (Ru(bpy) FP_6): 2 h K K$\beta_{1,3}$ (KCl): 1 min

Comparing the two geometries in terms of efficiency, the Johann approach is essentially always wasting a large fraction of photons, because it is always just looking at one energy at a time determined by the slit in front of the detector. Thus, though it introduces other limitations, the von Hamos approach appears to be the better choice in regard to the detection efficiency and acquisition times as it does not require scanning the spatially dispersed spectrum, but instead it simultaneously collects the photons of all energies.

In Table 1 we compare three examples of wavelength dispersive X-ray (WDX) setups. The table contains the specifications of two laboratory setups, a von Hamos setup with a metal-jet source and a commercial Johann setup from EasyXAFS using an X-ray tube as source, and another von Hamos setup installed at the PINK beamline at BESSY II. The table gives an overview of the differences in the configuration, and compares the countrates and energy ranges covered by the different sources and spectrometers. At the bottom of the table a few selected examples of typical acquisition times are given to enable for a rough comparison of lab-based measurements versus measurements using a synchrotron light source.

More details on the different geometries can also be found in the *Handbook of Practical X-ray Fluorescence Analysis* (page 296ff) [19]. Focussing on the various detection methods Heald [109] is comparing different detector techniques. He discusses crystal analysers and solid state detectors, as well as the combination of the two, and the application of filters to improve signal quality.

Since the initial original publications by Johann [110], Johansson [111] and von Hamos [112], there have been many publications [5,2,82,94,100–102,113–124] discussing and illustrating variations and improvements, though some articles describe setups at large scale facilities such as a free electron laser or synchrotron. This list, however, is just meant to be a starting point for the interested reader with no claim to be complete or exhaustive.

1.2. X-ray absorption and emission spectroscopy

Before going into more detail regarding in-house X-ray spectrometers, we first introduce the basics of *X-ray Absorption Spectroscopy* (XAS) and *X-ray Emission Spectroscopy* (XES), and the nomenclature used in this field.

In XAS the absorption of energy, typically carried by a photon, promotes an electron from a core-level to an empty orbital, thus one usually says that *"XAS probes the empty levels*". In XES on the other hand, one observes the decay of a previously created core–hole via a radiative decay process from an occupied upper shell, thus one says that *"XES probes the occupied levels*". This may appear trivial but it emphasises the complementary nature of the two spectroscopies. In other words, the two spectroscopies yield complementary information about the local electronic structure as we will discuss below.

Some recommended sources for those looking for more detailed information on XAS and XES going beyond our summary, we refer for example to the textbooks *X-ray Absorption and X-ray Emission Spectroscopy* [2] and *Core-Level Spectroscopy* [32], the article *High-Resolution X-ray Emission and X-ray Absorption Spectroscopy* [126] and with a more specific focus on X-ray Absorption Fine Structure (XAFS) spectroscopy we recommend the two books *XAFS for Everyone* [127] and *Introduction to XAFS: A Practical Guide to X-ray Absorption Fine Structure Spectroscopy* [128]. And, with a focus on catalysis but highly recommended *Reactivity of Surface Species in Heterogeneous Catalysts Probed by In Situ X-ray Absorption Techniques* [129].

1.2.1. XAS background

XAS is a well-established technique which can provide information on the oxidation state, site symmetry, and coordination environment of a selected analyte in the gas, liquid or solid phase [2,6,8,3–5,7,32,33,126,128,127,129,130]. Transmission XAS experiments are the most direct way to measure the absorption as it does not suffer from self-absorption effects, where the latter is the case in most fluorescence yield detected XAS (FY-XAS) experiments [33,131,132]. However, transmission experiments can suffer from other effects, for example the pinhole effect caused by inhomogeneous concentrations or densities. Thus they require careful sample preparation and relatively concentrated samples, ideally in a light matrix. In contrast dilute samples, or systems with heavy matrices are better measured with fluorescence yield detected methods. Transmission XAS is a one-step process which can be modelled using Fermi's Golden Rule [133]. Most XAS experiments are performed at large scale synchrotron facilities acting as a highly brilliant (low divergence, highly monochromatic, high intensity) tunable source of photons.

While XAS is a more general term referring to the absorption of photons, we are focussing here on the specific case where the XAS is used to study the X-ray Absorption Fine Structure (XAFS). Hence, in our review the two terms may be used interchangeably unless specific differences are emphasised. In a typical XAFS experiment, the incident beam is usually monochromatic and the energy is scanned through an absorption edge of interest to selectively probe the unoccupied levels. The importance of the monochromatic excitation in XAFS measurements becomes clear when considering incident energies E_0 above the ionisation level E_{ion}, which leads to the emission of photoelectrons with a well defined kinetic energy $E_{kin} = E_0 - E_{ion} = \frac{p^2}{2m_e}$ and hence a well defined de Broglie wavelength $\lambda_B = \frac{h}{p}$. In solids the de Broglie wave of the photoelectron is then coherently scattered by the atoms around the analyte, typically the first few coordination shells around the analyte. These coherently scattered photoelectron waves are then – dependent on their energy E_{kin} - constructively and destructively interfering and thus modulating the effective absorption cross section of the absorbing site (XAFS scattering model) [53,33,127,128,134]. This modulation of the effective absorption cross section creates the typical oscillations of the intensity often visible in XAFS spectra which then yield information on the local atomic structure around the analyte.[134].

However, there are exceptions to this monochromatic incident beam approach where XAFS spectra can also be acquired when the incident beam is not monochromatic. The approach is often called *Energy Dispersive XAS* (EDXAS), which should not be confused with the 'energy dispersive' detection using solid-state detectors. In fact, one uses a wavelength dispersive curved crystal polychromator to spatially disperse the polychromatic X-ray beam and focus it onto the sample (see Fig. 4). In other words, the polychromatic beam is spatially dispersed in such a way that photons of different energies are passing through the sample at different angles [8,129,130,135–138].

Hence, perhaps *Polychromatic Dispersive XAS* (PDXAS) would be a better name, as it avoids the confusion with the EDX based detection, while it emphasizes that the polychromatic incident beam is sent through the sample in a spatially dispersed manner. Such experiments are especially useful for fast time-resolved XAS experiments where one is interested in the dynamics of a system, because it enables one to acquire a complete spectrum in a single shot as the time consuming energy scan of the incident beam is not required [138,139]. An implicit requirement, for all XAFS measurements but in particular in PDXAS (because the polychromatic focussing leads to a higher intensity) is that absorbing sites must be well separated, such that there is no overlap between the photo

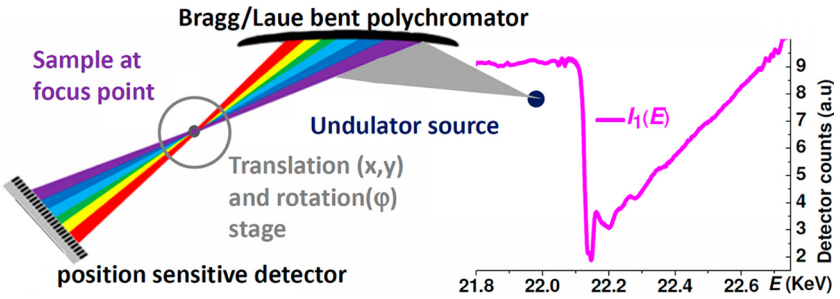

Fig. 4. Scheme illustrating the Polychromatic Dispersive XAS approach. (Image reprinted from Bordiga [129] with permission from American Chemical Society.).

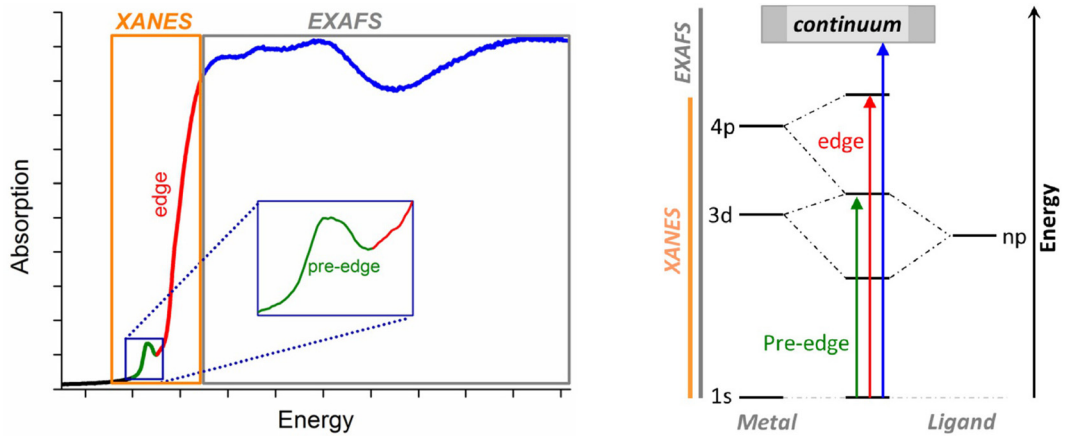

Fig. 5. Illustration of the XAFS energy range: On the left an example XAFS spectrum and its separation into the XANES and EXAFS range. And on the right the corresponding energy level diagram with the associated transitions. (Image reused from Kowalska [96] with permission from Wiley.).

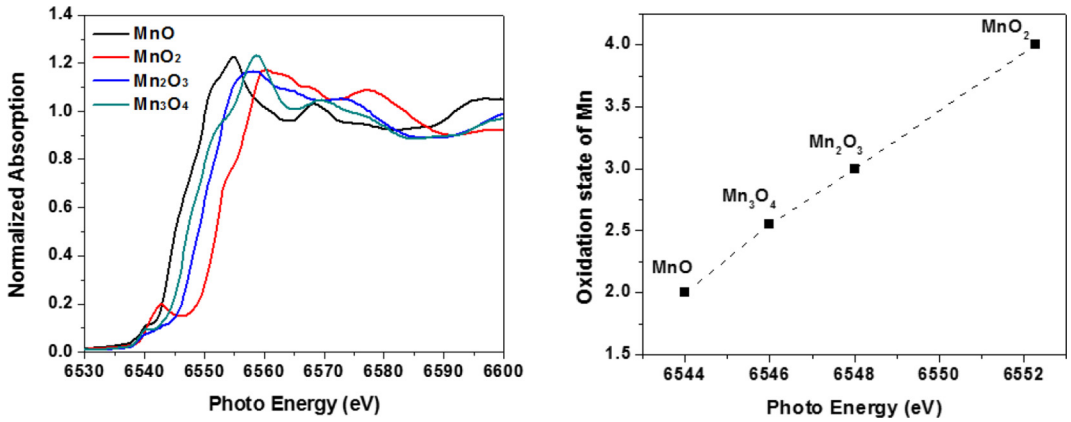

Fig. 6. K-edge XANES of manganese oxides illustrating the almost linear correlation between the oxidation state and the edge position, where an increase of the oxidation state shifts the absorption edge to a higher energy. (Image republished from Kuo [143] with permission of Royal Society of Chemistry.).

electron scattering spheres of each site. For example, if the incident photon density (intensity) would be so high that neighbouring sites each absorb a photon of different energy, then the photo electron scattering spheres would overlap and the XAFS structure would be altered due to the local interferences being disturbed by the interaction between the de Broglie waves of the neighbouring sites. However, such high intensities are typically only achievable at Free Electron Lasers (FELs) and certainly not (yet) achievable in the laboratory; this could explain why this aspect is usually not discussed at all.

XAFS spectra are commonly separated into the *X-ray Absorption Near Edge Structure* (XANES) covering the energy range approximately from 50 eV below to 100 eV above the main absorption edge, and the *Extended X-ray Absorption Fine Structure* (EXAFS) starting above the XANES region reaching up to several hundreds of eV above the main edge (see Fig. 5).

XANES spectra can be further split into the pre-edge region and the main edge. The K pre-edge for 3d transition metals corresponds to the promotion of an electron from the 1s orbital (K-shell) into a 3d orbital (M-shell). Thus, neglecting non-local and local pd-mixing, it rigorously refers to the local 1s → 3d quadrupole transition. In reality, however, local pd- and non-local orbital mixing between the metal and the ligand can be significant and thus allows the pre-edge to serve as a sensitive probe of the electronic

structure of the system [12,14,140,141]. This is not only, but specifically interesting in coordination chemistry and catalysis as the electronic structure and occupation of the valence shells is characteristic for these systems [134]. For studies focussing on the investigation of the pre-edge structure, often resonant techniques such as RIXS or HERFD are used (see Section 1.3).

The K main edge of 3d transition metals refers to the local 1s → 4p dipole transition and for higher photon energies ($E_{ph} > E_{ion}$) also to transitions into the continuum as mentioned above [7,32,128,134,141]. Typical applications of XANES include *"fingerprint analysis"* and the determination of the oxidation state of the analyte. Fingerprinting essentially means that one measures the XANES of known reference samples and subsequently compares the shape and structure of the spectrum with the XANES of an unknown system [142]. Using a more advanced analytic approach one can also perform a fit with a linear-combination of known references to derive the relative contributions in mixed systems. The determination of the oxidation state, or the change thereof, on the other hand typically refers to a shift of the main absorption edge (see Fig. 6) [7,127,128,143–145,134,141]. We want to point out that there are various ways to determine the "edge position", the most common is to use the maximum of the first derivative of the XANES spectrum.

Another nice example illustrating the relation between the oxidation and the energy position of various edge features is shown in a publication from Wong et al. (Fig. 5 therein) [141]. This shift of the absorption edge can be understood when considering that a change of the oxidation state implies the addition (chemical reduction, anionic) or the removal (chemical oxidation, cationic) of an electron, which means that the local charge changes with respect to the neutral metal state. The shift of the absorption edge occurs due to the change of the *effective* charge Z_{eff} of the nucleus. In other words, changing a neutral atom to a positive ion notably increases the binding energy of the core electrons[146]. Hence the energy required to promote an electron from a core-level into an empty orbital results in a shift of the absorption edge to higher (oxidation) or lower (reduction) energy [146,147]. This appears especially conclusive when considering that the frontier orbitals (HOMO,LUMO) lie for the 3d transition metals typically in the 3d shell, while the K-main edge typically arises from the 1s → 4p dipole transition. Hence, in a simple picture the edge position in K-edge XANES can be a direct measure of the analytes valence state [33,146,148]. Although XANES and EXAFS are part of same experiment, their respective analyses provide complementary information. While XANES is sensitive to oxidation state and geometrical structure around the central atom, EXAFS provides quantitative information on the local structure defined by bond distances, coordination numbers, and disorder around the probed atom.

1.2.2. XES background

A XES measurement refers to the observation of radiative decays after the creation of a core–hole, which is complementary to the non-radiative decay spectroscopies such as Photo-Electron Spectroscopy (PES) or Auger Electron Spectroscopy (AES). It is a second order process as it requires the creation of a core–hole first before the decay as second step can occur [149]. In general XES includes many decay processes covering the hard X-ray energy range filling the lowest core-levels, as well as the soft X-ray range filling vacancies in shells close to the valence levels. To distinguish the transitions we shortly introduce the labels and notations used.

In 1911 Barkla was the first to introduce labels for X-ray emission lines. Assuming that future discoveries would reveal *'more absorbing and more penetrating'* radiation he wanted to leave alphabetically some space in either direction, hence he started with the letter K for the - as we know today – innermost shell [150]. Subsequently the higher shells where then labelled alphabetically, and these labels are relating to the principle quantum number n as we use them today, where $n = 1, 2, 3, 4\ldots$ corresponds to the K,L, M,N,. . .atomic shells. If Barkla would have known already that there is no lower level, the 1*s* orbital would have the letter A instead of K [150]. The most common notations in X-ray spectroscopy are the Siegbahn notation [151,152] (first introduced by Moseley in 1913 [153]) and the IUPAC notation [154]. In Table 2 we summarise some of the transitions in K-edge XES.

However, we want to emphasise that spin–orbit coupling (SOC) as well as local Coulomb interactions and exchange coupling usually lead to an orbital mixing, such that their nature is not pure anymore. Thus the assignment of the orbitals involved in each transition typically refers to the dominant contribution only [32,155]. The true contributions strongly depend on the particular system such that the Kβ XES can also have significant metal 4p contributions as discussed by Tsutsumi et al. [156].

IUPAC explicitly recommends to use the hyphen to separate the initial and final state levels (indicating the vacancy/electron hole), thus one should always write for example K-$L_{2,3}$ or K-L_2L_3 instead of $KL_{2,3}$ or KL_2L_3. It is furthermore suggested to use K-$L_{2,3}$ instead of K-L_2L_3 in cases where the experimental resolution is not sufficient to distinguish the K-L_2 transition from the K-L_3 transition.[154] In the following we will continue to use the Siegbahn notation as it allows also for a distinct assignment of non-diagram transitions involving the molecular orbitals which relate to the so-called *satellites*.

The Kα_1 and Kα_2 lines, often just called Kα lines, refer to the radiative decay of a K-shell (1s orbital) vacancy being filled with an electron from the L_2L_3-shells (2p orbitals) [157]. Thus, it is dipole allowed having the highest transition probability for a 1s vacancy, leading the brightest emission in K-edge XES [154]. The

Table 2
K-edge XES transitions in the Siegbahn and IUPAC notations [154]. The bottom part of the table lists 'non-diagram' transitions relating to the 3p3d-exchange interaction and metal–ligand hybridised molecular orbitals (MO). The transitions with the comment VtC XES refer to *Valence-to-Core* decays, also called Kβ satellite emissions (see also Fig. 7).

Electron Transitions		X-ray Notations		
Shells	Orbitals	Siegbahn	IUPAC	Comment
$L_3 \rightarrow K$	$2p_{3/2} \rightarrow 1s$	Kα_1	K-L_3	brightest emission line in K-edge XES
$L_2 \rightarrow K$	$2p_{1/2} \rightarrow 1s$	Kα_2	K-L_2	spin–orbit split from Kα_1
$M_3 \rightarrow K$	$3p_{3/2} \rightarrow 1s$	Kβ_1	K-M_3	approx 5-10x weaker than Kα_1
$M_2 \rightarrow K$	$3p_{1/2} \rightarrow 1s$	Kβ_3	K-M_2	approx 100x weaker than Kα_1
$M_5 \rightarrow K$	$3d_{3/2} \rightarrow 1s$	Kβ'_5	K-M_5	weak quadrupole, part of VtC XES
$M_4 \rightarrow K$	$3d_{5/2} \rightarrow 1s$	Kβ''_5	K-M_4	weak quadrupole, part of VtC XES
	3p3d → 1s	Kβ'		K$\beta_{1,3}$ low-energy shoulder, pd exchange
	3dL2s → 1s	Kβ''		VtC XES, MO with ligand 2s orbitals
	3dL2p → 1s	K$\beta_{2,5}$		VtC XES, MO with ligand 2p orbitals

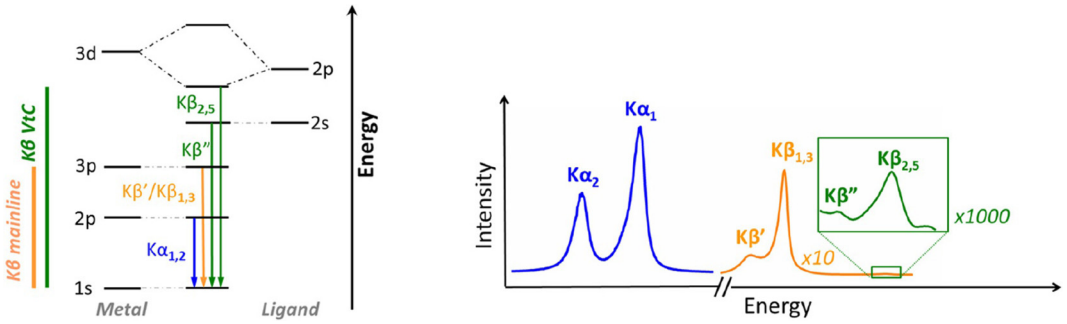

Fig. 7. Energy level diagram with the associated transitions and illustration of relative intensities of the K emission lines. (Image reused from Kowalska [96] with permission from Wiley.).

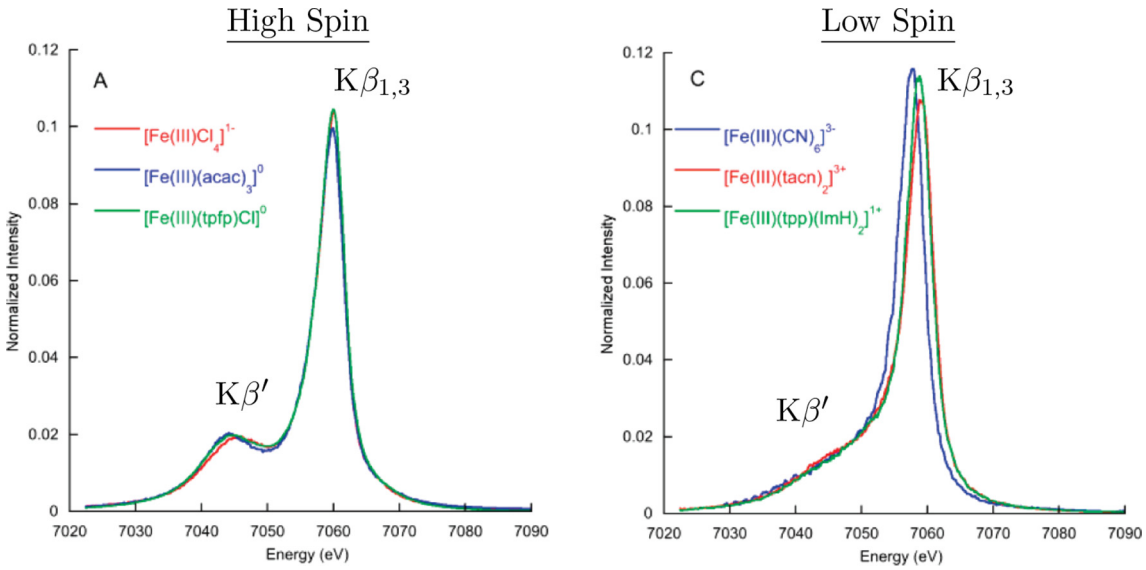

Fig. 8. Kβ main lines: $K\beta_{1,3}$ with the Kβ′ shoulder in iron compounds illustrate the spin sensitivity due to the local exchange interaction in the M-shell. The shoulder Kβ′ is almost absent in low-spin, while it is pronounced as separate peak on the low-energy side in high-spin compounds. (Image reprinted with permission from Lee [163]. Copyright American Chemical Society.).

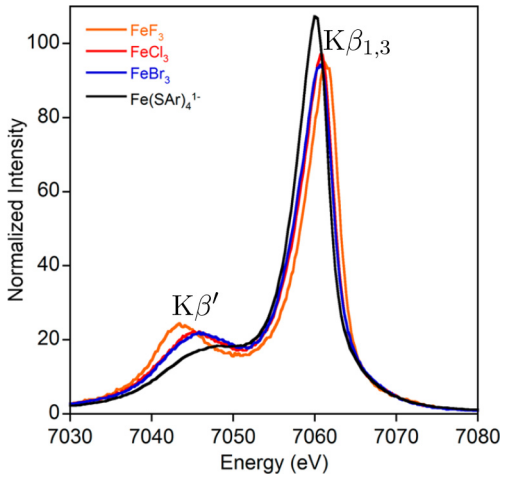

Fig. 9. Kβ main line spectra of iron compounds demonstrating significant differences in the appearance of the Kβ′ shoulder, despite all compounds being high spin Fe(III). (Image reprinted with permission from Pollock [159]. Copyright American Chemical Society.).

Kα emission is dominated by the 2p spin–orbit interaction, separating the $K\alpha_1$ and $K\alpha_2$ lines [158–160]. The Kβ main emission results when an electron from a 3p orbital refills a 1s core hole. The transition is dipole allowed, but with a notably smaller transition probability with respect to the Kα emission. The Kβ main line consists of the $K\beta_{1,3}$ main peak and a Kβ′ shoulder on the low-energy side as shown in Fig. 7 (right) and Fig. 8. The $K\beta_{1,3}$ doublet typically appears as a single peak due to the small spin–orbit interaction in the 3p valence shell (see Table 2) [158,159,161,162]. The separation between the $K\beta_{1,3}$ and Kβ′ feature is dominated by pd-exchange coupling, while further perturbation of the spectra results from a 3p SOC contribution being typically an order of magnitude smaller that the pd-exchange.

A comparison of some iron compounds in high-spin and low-spin (see Fig. 8) suggests that the appearance of the Kβ′ shoulder could be used as a fingerprint for the spin-state of a system [163,161,162,96,159,158].

The apparent difference of the Kβ′ shoulder between high-spin and low-spin complexes shown in Fig. 8 can be explained with the 3p3d exchange coupling in the valence shell, which typically dominates the other intra-atomic interactions in the valence shell. This creates a large energy splitting between an unpaired 3p elec-

tron with the spin parallel to the 3d electrons ($K\beta_{1,3}$ line) and the states arising from the 3p electrons with anti-parallel spin ($K\beta'$ line) [96,149,160,159,158,162]. Furthermore, through a systematic analysis of the energy splitting between the $K\beta_{1,3}$ and $K\beta'$ lines one can acquire information on the number of unpaired electrons and metal–ligand covalency [96,159].

As illustrated by Pollock et al. [159] with a series of high-spin iron compounds, the Kβ main line, and especially the Kβ' shoulder, can notably be modulated by the covalency of the ligand (see Fig. 9). This contradicts the common picture of the pure atomic nature of the Kβ main line, where the Kβ main emission is assigned to local intra-atomic transitions. In fact this shows that one must consider both, exchange coupling and covalency, when modelling and analysing the Kβ main emission comprising the $K\beta_{1,3}$ and Kβ' lines [159,162].

From a theoretical point of view it has been found that the Kβ main lines can be modelled within a crystal field multiplet approach, though its empirical nature limits the information one can extract. Whereas the non-empirical nature of DFT based calculations offers a significant advantage over the multiplet methodology, but it can get computationally more expensive [159].

The Kα and Kβ main emissions are nowadays commonly known and measured routinely. One can extend the transition rules to include also the molecular orbitals which are created by the hybridisation between the local atomic orbitals and the ligand's orbitals (see Table 2 bottom) [164]. These inter-atomic transitions will then yield information about the molecular electronic structure and the ligands involved [100,149,155,157,165,162]. Therefore we will in the following shortly introduce the so-called *satellite emissions*, which have first been reported by Sommerfeld and Wentzel in the early 1920s as *spark lines in the X-ray spectrum [45,52,166,167]*.

We do not want to omit that also the Kα decays can show satellites, however, we will focus here on the Kβ satellites as they involve the valence orbitals which are usually of greater interest. For more information on the Kα satellites we refer to Torres-Deluigi et al. [157]. The Kβ satellite emission lines are the $K\beta_{2,5}$ and Kβ'', which appear on the high-energy side of the $K\beta_{1,3}$ main line (see Table 2 and Fig. 7). Their relative intensity is usually only 10^{-2} to 10^{-3} with respect to the $K\beta_{1,3}$ main line. Hence the term *'satellite'*, as they are weak lines in the vicinity of a strong parent emission [157]. These satellites carry ligand information via the molecular orbitals created by the hybridisation between the metal and the ligand [76,96,149,155,161,164,168,163,169,162]. In other words, the satellite emission lines do not correspond to the energy difference of two energy levels of the same atom, instead they are transitions involving metal–ligand mixed molecular orbitals (see Fig. 7 and Table 2).[96] The measurement of these satellite emissions is sometimes also summarised under the term *Valence-to-Core XES* (VtC-XES) [100,149,155,165]. However, where appropriate we use the Siegbahn labels $K\beta_{2,5}$ and Kβ'' to clearly distinguish the two.

It has been found that the Kβ'' line typically involves the molecular orbitals with ligand *n*s-type atomic orbitals (e.g. ligand 2s → metal 1s), while the $K\beta_{2,5}$ line is particularly sensitive to valence changes of the orbitals and primarily related to molecular orbitals with ligand *n*p-type atomic character (e.g. ligand 2p → metal 1s, see also Fig. 7) [170,96,160,163,164,171,172,149,161,168,173,174]. To be more clear, it is only ligand 2s/2p for the ligand elements with atomic number $Z = 5$ to 9 (B,C,N,O,F), hence, to be more general we refer above to ligand *n*s/*n*p orbitals. As Joe et al. [76] discuss, the centroid position of the $K\beta_{2,5}$ feature for example relates to the oxidation state and spin state of the analyte. The centroid and the intensity of the weak Kβ'' feature can be used to identify bond lengths and the element species of the ligands, which can be understood via the characteristic energy of the ligand's 2s level. Though entirely based on different mechanisms, VtC-XES is somewhat related to EXAFS in the sense that both spectroscopies yield information on the local atomic structure around the absorbing atom [157,171]. However, while difficult with EXAFS, as discussed in several publications VtC-XES enables to distinguish different ligands with similar atomic numbers *Z* such as carbon (C, $Z = 6$), nitrogen (N, $Z = 7$), oxygen (O, $Z = 8$) and fluorine (F, $Z = 9$) as the example shown in Fig. 10 nicely illustrates [149,157,160,163,171,175,176].

Other recent studies have shown that the XES satellites can reveal even more detailed information on the ligand-based valence molecular orbitals. It has been shown for manganese complexes that the VtC region (Kβ'' and $K\beta_{2,5}$) is sensitive to the relative contributions of the donor orbitals [170]. Another recommended study on copper complexes shows the sensitivity for the oxygen ligand O-O bondlengths [173]. A similar study on iron complexes shows the sensitivity to the nitrogen ligand N-N bondlengths [174].

And finally, although we will not discuss here in detail we also want to mention that for some elements with higher atomic numbers ($Z > 28$) [177], also the Lα and Lβ emission lines, which fill a vacancy in the L-shell, can show satellites. This has been already reported for Tantalum (Ta, $Z = 73$), Osmium (Os, $Z = 76$), Iridium (Ir, $Z = 77$), Gold (Au, $Z = 79$) and Uranium (U, $Z = 92$) by Richtmyer et al. in the 1930s.[177–179] Especially for those L-satellites also the *Coster-Kronig transitions* play an important role, which refer in an over-simplified way to an intra-shell electron reordering process [180].

Altogether, XES can provide valuable information on the absorbing species as well as information about the ligand environment and covalency, and even discriminate between different dimers with different protonation states [76,145,162,126,181,100,155,96,149,157].

Considering that XES often aims at the detection of very weak signals (satellites), which are often having a relative intensity of 10^{-12} with respect to the incident flux, it is understandable that XES came into broader use only with the advent of highly brilliant synchrotron light sources [5,2]. Therefor most publications on XES and especially VtC-XES are based on synchrotron experiments.

An overview of XES measurements, although focussing on synchrotron experiments, including an overview of different spectrometers can be found in chapter 6 of the textbook *X-ray Absorption and X-ray Emission Spectroscopy* [182]. Another good

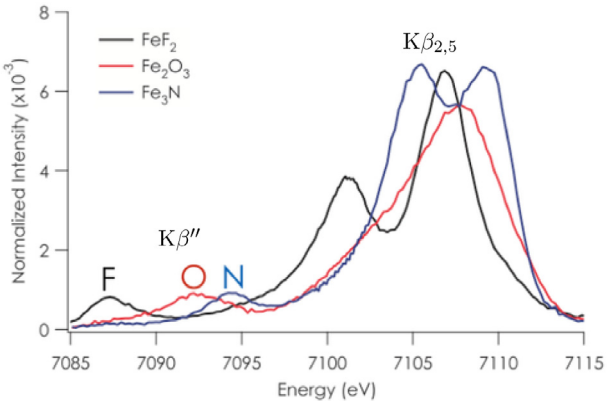

Fig. 10. Iron Kβ satellites: The different ligands appear with notable differences in the ligand 2p to metal 1s transitions ($K\beta_{2,5}$). The ligand 2s to metal 1s transitions (Kβ'') are shifting by approximately 8 eV for F, O and N ligation. (Image adapted with permission from Lancaster [175] and Lee[163].).

article on Kβ XES (including satellites) of various iron compounds discussing high-spin and low-spin states was published by Lee et al.[163] More details on the analysis of VtC-XES based on synchrotron measurements is discussed by Delgado-Jaime et al. [155] Two other highly recommendable publications by Pollock et al. [174,169], also focussing on synchrotron VtC-XES, discuss its use to better understand the underlying mechanisms via the study of the chemical structure based on a molecular orbital picture. While often difficult to obtain with other methods, VtC-XES allows to (i) assess the identity and number of ligands bound to a metal center, (ii) quantify the degree of bond activation, and (iii) get information about the protonation state of donor atoms [169].

Yet another interesting publication is an article from Torres-Deluigi et al. [157] While most articles refer only to the Kβ satellite emission, they also discuss the Kα satellites. Focussing on chemistry Kawai et al. [183] discuss *Chemical effects in the satellites of X-ray emission spectra*. And finally the review by Kowalska et al. [96] on X-ray absorption and emission spectroscopy is comparing also high resolution XAS and *Total Fluorescence Yield* (TFY) measurements, as well as applications for non-resonant XES measurements. A dedicated section gives insights into the different spectrometer geometries with some illustrations.

1.3. High-Resolution WDX Spectroscopies

Typically WDX techniques are associated with high-resolution photon-in/photon-out spectroscopies, such as for example *High Energy Resolution Fluorescence Detected X-ray Absorption Spectroscopy* (HERFD-XAS), or *Resonant X-ray Emission Spectroscopy* (RXES) and *Resonant Inelastic X-ray Scattering* (RIXS).

All these spectroscopies require a monochromatic incident beam for the excitation of the system, combined with a high-resolution detection of the subsequent radiative decays. In other words, a combination of two WDX monochromators is required, one for the incident beam, and one for the photons emitted from the sample. And, as one trades in any WDX approach intensity for resolution, each of the two monochromators leads a notable reduction of the available flux. Additionally, intrinsic effects such as the photo absorption cross-section in the first step, and the photon yield in the second step further reduce the detectable count-rate. This altogether emphasizes why resonant photon-in/photon-out spectroscopies are very photon–hungry, making an intense source necessary for such measurements. Although in principle also possible in the lab, to the best of our knowledge, RXES/RIXS and HERFD-XAS experiments can to date only be performed at synchrotron facilities where insertion devices deliver a sufficiently intense incident beam [76,184].

In *non-resonant XES*, however, one can use a 'white light excitation' such as an X-ray tube spectrum for example, hence the term *'non-resonant'*. The polychromatic excitation makes the absorption step more efficient, and only one WDX spectrometer is required to enable for a high-resolution detection of the XES. This makes non-resonant XES a suitable method for laboratory measurements. However, as shown by Kopelent et al. [185] there can be substantial differences between *non-resonant XES* and *resonant XES* (RXES).

In *resonant XES* (RXES), as well as in RIXS, the excitation energy is tuned to be in and around a resonance of a specific feature in the region of interest. This resonant excitation can make quantum mechanical interference effects relevant (→ Kramers-Heisenberg [13]). But because elucidating resonant techniques in detail goes far beyond the scope of this review, we would like to refer to other publications discussing HERFD-XAS and RXES/RIXS in more detail [9,12,14,15,32,140,186–190,184,103,100,13,185,76,96,162].

Before we focus in the following on laboratory experiments only, we want to clarify that high-resolution laboratory spectroscopy is to date mainly limited by the low intensities of available laboratory sources. Therefore transmission XAS and non-resonant XES are the most common WDX techniques in the laboratory. Nonetheless, recent developments show that at least total and partial fluorescence yield XAS experiments, using an energy dispersive Silicon Drift Detector (SDD), are becoming feasible in the lab [191]

1.4. Opportunities with laboratory-based WDX spectrometers

Laboratory WDX setups enable one to perform *non-resonant XES* with white light excitation and transmission XAS experiments in the laboratory. Therefor a single dispersive element (crystal) is used to monochromatise either the incident beam for transmission XAS experiments or the emitted light in non-resonant XES experiments (see Fig. 11).

Being intrinsically element specific the detection of the *X-ray Absorption Fine Structure* (XAFS) and XES has found many applications in the natural sciences. Due to its ability to penetrate materials it is especially useful in catalysis for in situ and operando studies [63]. As discussed above XAFS can give direct information on the oxidation state, symmetry and coordination

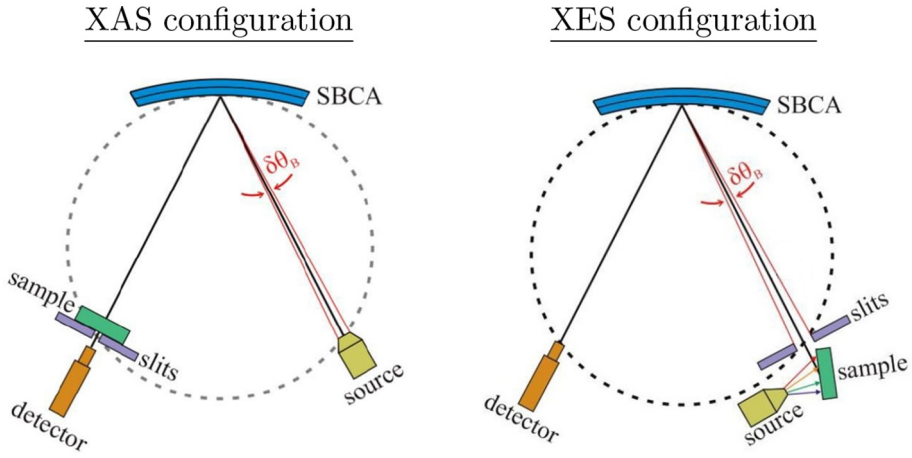

Fig. 11. Comparison of transmission XAS and non-resonant XES experiments using a WDX spectrometer and an X-ray tube as source. In the XAS configuration (left) the SBCA is used to disperse the polychromatic emission from the source for the monochromatic excitation. In non-resonant XES (right) the SBCA is used to disperse the X-ray emission spectrum from the sample. (Image reused from Mortensen [125], Published in the Journal of Physics under CC3.0).

of the analyte. XES, namely the shape of the Kβ lines and its satellites (i.e. Kβ'', K$\beta_{2,5}$) can reveal ligand information [162,100,192,183,96,157,2]. Due to the low photon yield such measurements are usually performed at a synchrotron to take advantage of the highly brilliant and intense incident beam.

However, the limited availability of measurement time and the competition for the few large scale facilities, makes it very appealing to bring the gained knowledge back to the lab. This is especially interesting for experiments on dangerous or toxic materials such as the actinides for example, which are only allowed at very few selected beamlines around the globe. Additionally, long time stability tests over weeks or even months are virtually impossible to be realised at a synchrotron.

Assuming a stable source and stable sample, and neglecting non-linear effects, repeating and averaging several measurements is equal to a measurement with an increased intensity. Thus one can counter a lower flux by extending the measurement time when using a lab-based setup. For example, to reduce the statistical error by a factor of $\sqrt{N}$ one has to do N repetitive measurements. Because noise reduction goes with $\sqrt{N}$, i.e. averaging four identical measurements gives an SNR twice as good; 100 measurements yield a 10× better SNR. In other words, this quickly becomes *very* time consuming and it shall be clear that this requires a stable and reliable source.

While the acquisition times in the lab can be expected to be notably higher, the application to solids and liquids is especially interesting for the study of materials and reactions in homogeneous and heterogeneous catalysis. Either in order to do long-term in situ measurements, or simply to perform preliminary measurements in preparation of and to optimise a measurement at a synchrotron.

Conventional energy-dispersive X-ray (EDX) spectroscopy using Silicon-Drift-Detectors (SDDs), typically referred to as *X-ray Fluorescence* (XRF) spectroscopy, is already for many years a well established lab technique for elemental analysis. In recent years the employment of wavelength-dispersive X-ray (WDX) spectrometers has become more common in laboratory setups making nowadays also high-resolution spectroscopies accessible in the lab. The main limitation are typically the photon sources available in the laboratory, as their intensity and especially their brilliance is usually several orders of magnitude less with respect to the highly brilliant synchrotron light sources.[19,193].

The most accessible high-resolution spectroscopy in the laboratory is *non-resonant XES*. The three main reasons are 1.) one can use the entire white-light spectrum of an X-ray tube for the excitation implying that no photons are wasted by monochromatizing the incident beam, 2.) it does not require a normalisation to the energy dependent incident flux (I_0 normalisation) and 3.) it can be used to measure virtually any kind of sample, including optically thick samples.

XAS experiments on the other hand, here we are focussing on XAFS (XANES and EXAFS), are typically performed in transmission to avoid spectral deformations due to self-absorption [33,131,194]. To realise a transmission XAS measurement an optically thin sample is required, where a reduction of the intensity to $1/e \approx 37\%$ at the main absorption edge is considered to be optimal. For highly concentrated liquid or powder samples the transmission can in many cases be adjusted by dilution (i.e. powders are often diluted with cellulose or boron-nitride, BN). But this is not always possible, i.e. solid samples such as single crystals, and ordered or multilayered structures cannot be diluted in this way. Furthermore, one must ensure that the sample does not undergo any reaction with the diluting substance which could result in an altered sample, i.e. cellulose can be burnt in high temperature in situ experiments, and though BN has a low reactivity, several reaction paths exist with salts. And BN also reacts at high temperatures (800 °C) with water forming boron trioxide and ammonia [195].

For low concentration samples ($\leqslant$ 3% analyte) on the other hand the contrast at the absorption edge (height of the step) can be too small. For samples with a light matrix the sample thickness can be increased, but the scattering background of the matrix of low-concentration analyte samples can reduce the signal-noise ratio (SNR) below an acceptable level. In other words, there are practical limits to increasing the thickness of such low concentration samples. Overall this means, that for transmission XAS experiments very specific sample conditions must be met.

Furthermore, all XAS experiments require an accurate measurement of the incident flux to compute the absorption of the sample using the Lambert–Beer relation:

$$\begin{aligned} I_T &= I_0 \cdot \exp(-\epsilon) \\ \Rightarrow \quad \epsilon &= -\ln\left(\tfrac{I_T}{I_0}\right) \end{aligned}$$

I_0 and I_T are the incident and transmitted intensity respectively and ϵ in the extinction of the sample for the energy (or wavelength) dependent transmission $T = \frac{I_T}{I_0}$. To avoid confusion, we empathise that in this form ϵ includes not only the photo-absorption cross section τ, but also the elastic and inelastic scattering cross section, σ_{ela} and σ_{inela} respectively [19].

An accurate I_0 measurement and subsequent normalisation is a crucial aspect especially when X-ray tubes are used as a source. Because in contrast to synchrotron sources the intensity of X-ray tubes has an intrinsic spectral shape, leading to intensity changes by several orders of magnitude due to the characteristic lines from the anode material. In other words, whenever possible one should choose an anode material where the characteristic lines do not lie in the energy range where the measurements will be performed (*region of interest*, ROI). This does of course still not allow to omit the I_0 normalisation, but on the one hand this helps to avoid saturation effects of the detector (i.e. when a characteristic line of the anode lies in the ROI) and on the other hand a rather constant incident flux improves the overall quality of the measured spectrum.

Fluorescence yield (FY) detected measurements (i.e. *Total Fluorescence Yield* (TFY) or *Partial Fluorescence Yield* (PFY) using an SDD) enables to perform XAFS experiments on optically thick samples, but this requires a sufficiently intense source. Mostly because the incident beam has to be monochromatic, and the two-step process (photon-in/photon-out) with its intrinsic competition between radiative and non-radiative decays (→ photon yield) further reduces the detectable intensity. However, as Honkanen et al. [191] demonstrate, with a sufficiently intense photon source, FY-XAS experiments are now becoming also accessible in the laboratory. And, though often ignored, it has been shown that FY detected spectra can differ from the real cross section measured in transmission XAS. Apart from saturation effects and self-absorption, there are also intrinsic mechanisms related to the fluorescence decay process which are altering the spectra [132]. This is why transmission XAS experiments are considered to be the most direct way to measure the real absorption.

Altogether, this makes nowadays non-resonant XES and transmission XAS experiments the most commonly performed high-resolution X-ray spectroscopies using an in-house laboratory setup [134]. As already emphasised above, one major limitation is certainly the limited incident flux when compared to synchrotron sources, but also the tunability while maintaining a high intensity, and hence the lack of brilliance of in-house sources, is a relevant factor. The lack of photons is also the main reason why photon–hungry experiments such as HERFD-XAS and RIXS/RXES experiments have still to be performed as large scale synchrotron facilities.

2. Recent advancement in laboratory spectrometers setups

Since the last quarter of the 20th century, several attempts have been made to bring wavelength dispersive X-ray spectroscopy via advanced techniques back into the lab. Some reports from Stern et al. in 1980 [196], Williams in 1982 [124] and an interesting scanning-free approach is reported by Lecante et al. in 1994 [121], all discussing laboratory XAFS spectrometer using the Rowland approach.

In this section we summarise and comment on the recent experimental developments using in-house laboratory setups. We separate the discussion into two parts: One for the von Hamos geometry and one for the Johann/Johansson geometry. Though some of the cited publications originate from the same research group, we present them in each part in a chronological order. An overview is given in Table 3.

2.1. Laboratory based von Hamos type spectrometers

Recent publications about laboratory von Hamos spectrometers are from Legall et al. in 2009 [197], Anklamm et al. in 2014 [113] and Schlesiger et al. in 2015 [198]. Those three all discuss setups using thin mosaic crystals as dispersive element developed in the same group. Nemeth et al. in 2016 [199] and Malzer et al. in 2018 [5] are reporting on a scanning-free von Hamos spectrometer to perform XAFS and XES measurements in the laboratory, where Malzer specifically emphasises the application of XES in catalysis research. More details on the last references are given in the following.

Legall et al. [197] investigate the performance of thin mosaic crystals for different spectroscopic methods and three different sources. As X-ray sources they used i) a low-power micro-focus X-ray tube with an Ag anode (iMOXS MFR; IfG GmbH), ii) the mySpot beamline at BESSY II and iii) an ultrafast laser plasma source (LPS) emitting femtosecond X-ray pulses at the Max-Born-Institut. For the detection they use 100 µm thick HAPG (Highly Annealed Pyrolytic Graphite) mosaic crystal films in the von Hamos geometry to achieve a large solid angle of acceptance. For thicker crystals they report an increase of the mosaic spread leading to an increase of the acceptance angle of the spectrometer, which is favourable in polychromatic single shot spectroscopy. They compare the EXAFS of a Ti foil measured with their lab setup to synchrotron measurements emphasising that the flux in the lab is about two orders of magnitude lower when compared to the synchrotron measurement. However, this can be an advantage when beam damage is an issue. Furthermore they compare measurements from other authors with their own and show the Kβ XES spectra for a Ti foil and a TiO_2 pellet, both fitted with the underlying peak structure formed by the various contributions (e.g. Kβ_5, K$\beta_{1,3}$, Kβ', Kβ'').

In a dedicated section for Plasma Emission Spectroscopy they discuss the feasibility of ps and fs timeresolved experiments as lab sources yield a notably lower flux when compared to synchrotron measurement. Additionally they compare the achieved intensities of their LPS with that of a 24 W (40 kV/0.6 mA) X-ray tube. For EXAFS measurements they report an acquisition time of about 10 h, when using a fs LPS utilising a Ti:Sa laser ($\lambda = 815$ nm) having pulse length of $t = 40$ fs, a pulse energy of $E > 1$ Joule after compression and a repetition rate of $f = 10$ Hz.

Anklamm et al. [113] describe their novel full-cylinder von Hamos approach with a low power X-ray tube as source. The reported parameters are: $R_{sag} = 150$ mm, HAPG (Highly Annealed Pyrolytic Graphite) thickness $d = 40$ µm with a mosaic spread of 0.1° FWHM and a crystal length of $l = 30$ mm. The image shown in Fig. 12 illustrates their variation of the typical von Hamos geometry where a full circle of a cylindrically bend crystal is used as dispersive element. Subsequently the orientation of the detector is perpendicular with respect to the rotation axis and thus the spectra appear as circles which can be integrated to obtain the usual $I(E)$ spectrum.

Using a full-cylinder instead of just a segment increases the solid angle and makes it a highly efficient spectrometer. It covers the energy range from 2.5 keV to 15 keV and thus allows for chemical speciation including all Kβ emission lines for the 3d transition

Table 3
Summary of the setups and experiments discussed in this section.

Authors	Experiment	Source	Spectrometer
Legall et al.[197]	XAS & XES	X-ray tube, LPS	HAPG vHamos
Anklamm et al.[113]	XES	X-ray tube	HAPG vHamos
Schlesiger et al.[198]	XAS	X-ray tube	HOPG vHamos
Nemeth et al.[199]	XAS & XES	X-ray tube	vHamos
Malzer et al.[5]	XES	Ga Jet	HAPG vHamos
Taguchi et al.[200]	XAS	X-ray tube	Johann
Seidler et al.[123]	XAS & XES	X-ray tube	Johann
Mortensen et al.[125]	XAS & XES	X-ray tube	Johann
Mundy et al.[201]	XAS	X-ray tube	Johann
Holden et al.[192]	XES	X-ray tube	Johann
Bes et al.[64]	XAS	X-ray tube	Johann
Hokanen et al.[191]	XAS, FY-XAS, imaging	X-ray tube	Johann
Jahrman et al.[202]	XAS & XES	X-ray tube	Johann
Bi et al.[203]	XAS & XES	X-ray tube	Johann
Joe et al.[76]	TR-XES	LPS	calorimeter
Mantouvalou et al. [204]	TR-XAS	LPS	eliptical grating
Sato et al.[205]	XES	X-ray tube	flat crystal
Limandri et al.[206]	XES	X-ray tube	Johann
Anwar et al.[207]	TR-XAS	LPS	HAPG vHamos
Moya-Cancino et al. [208]	In situ XAS	X-ray tube	Johann
Moya-Cancino et al. [209]	In-situ XAS	X-ray tube	Johann
Blachucki et al.[92]	Simultaneous XAS & XES	X-ray tube	vHamos

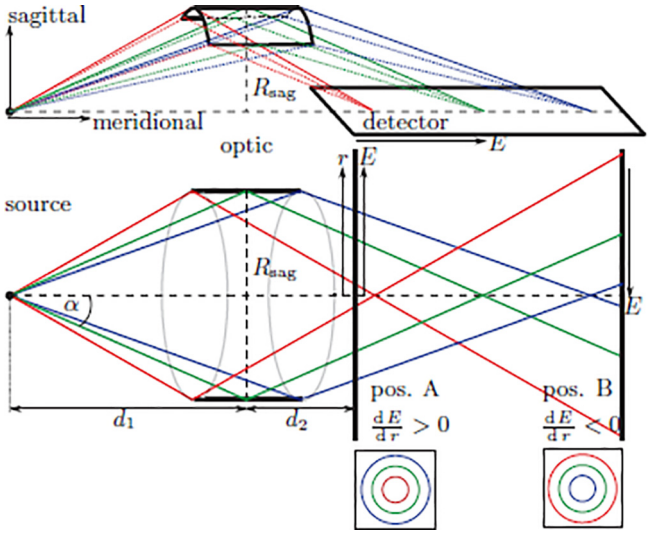

Fig. 12. Full cyclinder von Hamos setup: The conventional (top) and the novel full-cylinder von Hamos geometry (bottom) as described by Anklamm et al. [113] (Reprinted from Anklamm [113], with the permission of AIP Publishing.).

metal series. At an energy of 8 keV they report a resolving power of $E/\Delta E = 2000$, corresponding to a $\Delta E = 4$eV at 8 keV. For the measurement of the Kβ multiplet spectrum they report typical acquisition times of about 10 min for bulk materials, and hours for thin samples with a thickness of less than 1 μm. This shows that the increased solid angle enables for an excellent performance and relatively short acquisition times when compared to standard Rowland circle setups.

They have measured several iron Kβ spectra of samples with varying thicknesses (bulk to 0.3 μm) and different acquisition times (10 min to 180 min). And they demonstrate the spectrometers ability for chemical speciation by measuring the Kβ XES for several titan compounds such as Ti, TiO, Ti_2O_3 and TiO_2. For all measured samples the K$\beta_{1,3}$ mainline appears virtually noise free, and also the K$\beta_{2,5}$ can be clearly distinguished. For the TiO_2 the Kβ'' line can be observed as a high energy shoulder of the K$\beta_{1,3}$ mainline. The differences between the TiO and the Ti_2O_3 appear to be very small in the K$\beta_{2,5}$ region.

Note, the article from Malzer et al. [5] summarised below is basically the next generation of the Anklamm spectrometer, which provides a higher resolution by using a larger cylinder.

Schlesiger et al. [198] reports XAFS measurements also using the von Hamos approach and a novel type of HOPG (Highly Oriented Pyrolitic Graphite) as mosaic crystal. They use HAPG, Highly Annealed Pyrolitic Graphite, which is a recently developed type of pyrolitic graphite, but with lower mosaicity needed for high spectral resolving power. This configuration is compared to the results from other authors [94,123,210–214] and they find the HAPG spectrometer to have a higher efficiency and better resolving power. They report a resolving power of $E/\Delta E \approx 2000$, being significantly lower that what can be achieved with synchrotron based techniques. However, the standard low power X-ray tube as a source and a standard Peltier cooled X-ray CCD as detector give this laboratory setup the capability to perform XANES and EXAFS measurements in the lab. (More details on HOPG crystals can be found in the *Handbook of Practical X-ray Fluorescence Analysis* [19, p. 143ff].).

For a qualitative comparison they measured the XANES of a 6 μm thick Ni foil comparing it to synchrotron measurements. All features are distinguishable but the synchrotron data show better statistics and some spectral features are more pronounced. Furthermore they measured different concentrations of iron (pure Fe, 50% Fe, pure Fe_2O_3) showing that the spectra can be well distinguished, and thus they demonstrate that their spectrometer is well suited for the determination of mass fractions of chemical species in mixtures.

Nemeth et al. [199] propose a laboratory von Hamos type X-ray spectrometer as alternative to synchrotron based measurements. It allows for rapid transmission XAS experiments, but it is also capable to measure X-ray emission spectra. They use a cylindrically bent analyser crystal to build a flexible low-cost alternative with synchrotron grade S/N ratio at reasonable measurements times. The source is a water cooled X-ray tube with a copper anode operating at 10 kV and 40 mA, or 40 Watt respectively for XAS and 60 mA or 60 Watt for XES measurements. The data acquisition is realised with a position sensitive MYTHEN detector (1280 lines with 50 μm pitch), alternatively an Amptek SDD is used which shows a significantly lower resolution. The difference is clearly demonstrated with the XANES of a NiO sample for an approximate acquisition time of 2*h*. To test the chemical sensitivity they measured the K-edge XANES of several Ni compounds: metallic Ni foil, divalent NiO and $NiCl_2$, trivalent $YNiO_3$, tetravalent K_2NiF_6. The spectra are clearly distinguishable allowing to distinguish the oxidation states of nickel similar to synchrotron based measurements. A similar procedure is applied to a series of cobalt compounds: metallic Co foil, divalent CoO, mixed valent Co_3O_4 and trivalent $PrCoO_3$. The cobalt K-edge XANES, measured in the order of minutes to hours, allows to clearly distinguish the oxidation states of the different compounds. For both cases the differences in the oxidation state are nicely illustrated via the first derivative of the spectrum allowing a sufficient determination of the edge position. Furthermore, the Kα XES is measured for a Ni foil, and the Kα and Kβ XES is recorded for a CoO sample taking 70 min for the Kα and 19*h* for the Kβ.

Malzer et al. [5] did high resolution Kα and Kβ measurements using a Gallium-jet X-ray source and a von Hamos full cylinder optic with *Highly Annealed Pyrolytic Graphite* (HAPG) as a dispersive element allowing for the analysis of dilute samples. This can be considered as the next generation of the Anklamm spectrometer [113] cited above, providing a higher resolution by the employment of a larger cylinder. They cover the energy range of $E \approx 2.3 \ldots 10$ keV and report a resolving power of $E/\Delta E = 4000$, corresponding to a resolution of $\Delta E = 2$ eV at an energy of $E = 8$ keV. Their setup is specifically employed for catalysis research. They illustrate and discuss the power of this configuration by measurements of the sulphur Kα emission in FeS. The spectrum, ranging from 2295 eV to 2340 eV, took 1 h for the main lines and 5 h for the satellite lines above 2317 eV. Furthermore they illustrate the very notable improvements between the current setup and the prototype setup they have used earlier, by comparing spectra of the copper Kα and iron Kβ multiplet including the satellites in FeS for both setups. Emphasising the relevance of the sample characteristics on XES resolution, they compare the K$\alpha_{1,2}$ lines for thick and thin iron samples, Fe_2O_3 and Fe(TPP), which is of particular interest for dilute and low weight-percent (wt%) samples as they appear in catalysis. A notable difference between thick and thin samples is that with thin samples one can achieve the highest possible resolution, while this of course reduces the count rates. A pure Fe_2O_3 sample reaches $2 \cdot 10^6$ counts per second at the Kα_1, compared to the dilute iron oxide the count rates are one order of magnitude below that. In other words, going from thick to thin samples reduces the intensity by one order of magnitude. And going from the Kα_1 to the Kβ main emission line they predict a reduction of three orders of magnitude. Overall their approach looks very promising, as the high sensitivity allows for measurements on dilute samples with typical acquisition times of 5 to 10 hours.

2.2. Laboratory based Johann/Johansson type spectrometers

Recent developments using the Rowland configuration SBCA's are from Taguchi et al. in 2005 [200], Seidler et al. in 2014 [123] and Mortensen et al. in 2016 [125]. Where Seidler and Mortensen are promising *"Turn-key XAFS and non-resonant XES"* to be commercially available via their spectrometers sold under the EasyXAFS brand. Holden et al. in 2017 [215] describe a very compact emission spectrometer. Bes et al. in 2018 [64] describe a setup very similar to the one from Seidler et al. And Honkanen et al. in 2018 [191] describe a versatile setup which can be used in transmission, fluorescence and imaging mode. More details on these most recent developments are given in the following.

Taguchi et al. [200] describe the improvements of a Rowland circle lab spectrometer to measure the K-edge of low Z elements ($Z \leq 20$), such as calcium (Ca), potassium (K), aluminium (Al) and sulphur (S). They achieve this by replacing the path in air, by vacuum or helium which significantly increases the number of photons reaching the detector. Helium makes Ca K-edge (4038 eV) measurements fairly easy they report, but K K-edge (3607 eV) remains difficult. Hence, they set the limit for laboratory measurements to Ti under air, and to Ca when the beam path is under helium. They find, to be able to measure the K-edges of Al

(1559 eV) or Si (1838 eV), the entire beam path, including the sample and detector must be put in vacuum.

Seidler et al. [123] discuss the configuration of the now commercially available laboratory XAS/XES instrument sold under their EasyXAFS brand. The used source is a gold (Au) target (more precisely: a gold-coated copper anode) with 50 kV and 0.2 mA, respectively 10 W, and a SBCA with a radius of 1 m. The publication is mostly discussing and illustrating some of the details of their commercially available spectrometer. As example application they show the Co K-edge XANES of a cobalt metal foil and the Kβ XES of a CoO powder sample. In spite of the relatively low-power X-ray source with 10 W, they report a respectable total flux of the order of 10^3 to 10^4 photons/s and a resolution of about $\Delta E = 1$ eV.

Mortensen et al. [125], also from EasyXAFS, report on non-resonant XES measurements with white light excitation realised with a laboratory setup which they compare with synchrotron data being additionally broadened by 0.8 eV. The setup uses a Ge(444) SBCA with a 1 m radius of curvature and an X-ray tube with a gold (Au) anode operated at 40 kV/200 μA, or 8 W respectively.

They claim to do a critical evaluation of the setup via Co Kβ XES measurements of Co_3O_4 and $LiCoO_2$ reporting peak count rates of approximately 5000cts/s for concentrated samples for the K$\beta_{1,3}$ emission with a reproducibility of the measurements within 25 meV or better. They are advertising the instrument for the determination of the spin and oxidation state using K$\beta_{1,3}$ XES, though energy shifts due to different sample positions can hinder an exact analysis. Also the VtC-XES (Kβ'' and K$\beta_{2,5}$) appears in good agreement for these systems with a high Co concentration. Perhaps one of the most surprising claims is that the low distance to the X-ray tube source would allow excitation with count rates between those possible for a monochromatised bending magnet and an insertion device. Instead of placing source and sample exactly on the Rowland circle a slit is placed on the Rowland circle, and the source and sample are moved around 10 mm behind the slit. Two reasons are given for that, one being that the slit enables to tune the energy resolution by adjusting the slit's aperture, and the other is that a slit is easier to position exactly compared to placing the source and sample at the exact position on the Rowland circle. In spite of this reasoning EasyXAFS delivers their spectrometers without adjustable slits. Instead, in XAS mode just the tube's and detector's aperture ($d \approx 10$ mm) are used as 'slits'. For XES measurements three slits for the source end with fixed apertures of 0.5 mm, 1 mm and 2 mm are supplied.

The first EasyXAFS spectrometers have been delivered throughout 2018/2019 and first publications can be expected soon to show if they can in real use-cases successfully complement or even replace synchrotron measurements.

Mundy et al. [201] used the setup from Seidler [123] to measure the cobalt (Co) K-edge XANES of some synthesized CoP and Co_2P, $CoCl_2$ and Co metal commercial standards. The measurements are then used to determine the oxidation state of the cobalt, confirming sufficient resolution for such fingerprint analysis, which is nowadays a routine task.

Holden et al. [192] report on sulphur Kα XES measurements using a benchtop high resolution WDX spectrometer. They find good agreement with synchrotron based measurements, with low sulphur concentrations of 150 ppm, leading to the conclusion that their setup is well suitable for characterizations in sulphur chemistry.

Bes et al. [64] describe a setup *similar* to the one from Seidler et al. It is also using the Johann geometry and a comparable mechanical arrangement, but they use a different source and a different Rowland radius: The setup uses a source with a silver (Ag) anode operating with 30 kV and 10 mA, translating to a peak power of 300 W, using a Ge(111) SBCA from XRStech in Johann geometry with radius of $R = 0.5$ m.

They report on laboratory-scale uranium (U) L-edge XANES measurements of UO_2, KUO_3 and β-UO_3, which they consider to be an *efficient and affordable alternative* to synchrotron measurements due to the excellent agreement with studies using synchrotron radiation. They discuss three different geometries and some of the improvements made to the setups and the cylindrically and spherically bent crystal analysers (CBCA, SBCA), stating that SBCA's have a larger solid angle and a better resolution in the hard X-ray energy range. Apart from the satisfying agreement with synchrotron experiments, they in particular highlight that the possibility to do such measurement in the laboratory is a huge advantage for studies on actinides due to the additional challenges arising from safety concerns of active materials as well as the low number of synchrotrons/beamline which are prepared for measurements on active samples.

Honkanen et al.[191] describe their Johann-type X-ray absorption spectrometer using an X-ray tube with a peak power of 1.5 kW as source. It covers an energy range of 4–20 keV allowing to measure the K-edges of all 3d transition metals and the L-edges of all 5d transition metals and actinides. The SBCA Johann crystal, which they obtained from the ESRF, has a bending radius of $R = 0.5$ m and a surface diameter of $d = 100$ mm. The device can be configured in three different modes: Transmission, **fluorescence** and imaging. Respectively, the detector is either a scintillator or an Amptek FastSDD, and for imaging a Advacam Modupix detector with 256×256 pixel (each 55×55 μm). They report an energy resolutions typically in the range of 1–5 eV at 10 keV.

As example they show a K-edge XANES of a cobalt metal foil measured in transmission being almost identical to a spectrum obtained at a synchrotron. Furthermore an Ni K-edge EXAFS spectrum is shown being also very similar to a synchrotron spectrum. A Kα fluorescence spectrum of a cobalt (Co) foil was measured and corrected for self-absorption effects, both showing more noise in comparison to the transmission spectrum. In addition to the Co foil, also the K-edges of 100 nm thick CoO and Co_3O_4 films were measured in fluorescence which are more noisy in comparison to the powder reference spectra measured in transmission mode. Each measured at 20 kV and 40 mA, or 800 Watt respectively. To illustrate the imaging capabilities they depose powders of NiO, NiO_2 and Co_3O_4 on a potato starch and take pictures at photon energies below and above the edge, yielding a contrast-rich image for the corresponding powder.

This setup is particularly interesting, because it uses a high power X-ray tube as source, which enables for fluorescence yield detected XAS (FY-XAS) experiments.

Jahrman et al. [202] are reporting on improvements made to the above mentioned XAS/XES setup from Seidler [123]. Though the general conceptual design is essentially the same, they report some design and performance improvements. They specifically mention reduced degrees of freedom, an increased flux and an wider Bragg angle to enable measurements of the EXAFS region. In a dedicated table they compare the acquisitions times of XANES, EXAFS and XES measurements using different X-ray tubes, with palladium (Pd) and tungsten (W) anodes, and different powers of 50 and 100 Watts, combined with various cuts of silicon (Si) and germanium (Ge) based SBCAs. The results are illustrated with various measurements, such as for example XANES and XES measurements of battery electrode materials (Li-Mn spinel, Vanadyl phosphate (ϵ-$VOPO_4$), nickel-manganese-cobalt (NMC) laminates) and ceria (Ce) based samples, and EXAFS measurements of a Nickel foil which are partially compared to synchrotron data. Furthermore some valance-to-core XES for Vanadium (V) and Zinc (Zn), as well as some XANES and XES spectra of different uranium oxides are presented.

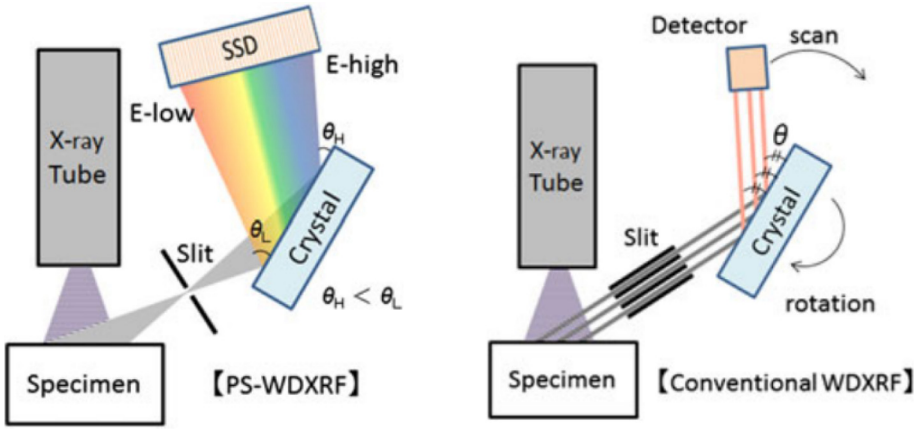

Fig. 13. (Left) Polychromatic Simultaneous Wavelength-Dispersive X-ray Fluorescence (PS-WDXRF) and (right) conventional scanning Wavelength-Dispersive X-ray Fluorescence (WDXRF). It uses a flat crystal with a slit for a non-scanning configuration. (Image reprinted from Sato [205] with permission from Wiley.).

Bi et al. [203] are presenting vanadium (V) K-edge XANES spectra which they apparently measured with the setup from Jahrman [202]. The paper does not give any details on the experimental setup, however, for the analysis they have combined the results from surface sensitive XPS measurements with bulk sensitive vanadium K-edge XANES to study oxygen vacancies in vanadium pentoxide (V_2O_5).

2.3. Notable in-house XAS and XES experiments

In this section we discuss some notable XAS and XES experiments, and the combination of the two, in various contexts. Complementing the previous section in here we discuss for example in situ experiments in chemistry as well as time resolved experiments to illustrate the status quo and what is already possible with in-house experimental setups.

Joe et al.[76] discuss *"photon-starved XES"* experiments using a tabletop picosecond laser-driven plasma as X-ray source for in-laboratory XES. They are illustrating the performance via example measurements detecting the spin-state of 3d electrons in iron (Fe_2O_3, FeS_2). The presented results do not include any time-resolved dynamics, but their results demonstrate the potential to perform time-resolved in-laboratory XES.

The setup they use is very interesting due to their unusual Laser-Plasma Source (LPS), consisting of a commercial Ti:Sapphire laser with a repetition rate of $f = 1$ kHz producing pulses with a wavelength $\lambda = 800$ nm and temporal length $t = 40$ fs (spatial length $l \approx \frac{40\text{ fs}}{c_0} \approx 12$ μm). The laser in then focussed onto a cylindrical **water jet** creating a plasma which in turn results in a broadband Bremsstrahlung X-ray spectrum covering approximately the energy range from 1 keV up to 14 keV, with its peak at 7 keV. The flux on the sample in this configuration is given with approximately $4 \cdot 10^6$ photons/s. Furthermore they use a poly-capillary lense to refocus the X-rays onto a 75 μm diameter circular spot. The X-ray source is designed for optical pump/X-ray probe experiments, for which the Laser beam is split prior to the interaction with the water-jet. While the presented experiment does not make use of the time-structure, it illustrates general feasibility of such measurements. Moreover, it shows the combination of such pulses from a LPS and a micro-calorimeter (*superconducting TES*) for the detection which can be used to measure X-ray spectra with sufficient resolution and statistics to reveal low-spin (LS) high-spin (HS) transitions.

Mantouvalou et al. [204] report on another good example promoting time-resolved XAFS measurements in the lab. They have successfully employed a laser plasma source (LPS) to measure the C and N K-edge XAFS structure with a single shot approach in the soft X-ray energy range using a $t = 1.2$ ns long X-ray pulse. With a reported resolving power of $E/\Delta E \approx 950$ at the respective K-edges, they confirm the feasibility of time-resolved measurements independent of large scale research facilities such as a synchrotron.

Sato et al. [205] describe a very notable flat-crystal setup without the need for mechanical scanning as shown in Fig. 13 (left). Sato calls it Polychromatic Simultaneous Wavelength-Dispersive X-ray Fluorescence (PS-WDXRF), emphasising that several wavelengths are measured at once.

The PS-WDXRF spectrometer uses an X-ray tube as source and a flat crystal dispersing the emission onto a Silicon Strip Detector (SSD). The notable difference is, that a measurement is performed without any moving parts and a spectrum can be acquired in 'a single shot'. The SSD is a `MYTHEN 1 K` from DECTRIS with 1,280 strips of dimensions 8 mm × 50 μm. The slit width G was set to 0.1mm. It is noteworthy, that a point source (e.g. very local excitation of the sample) would reduce the solid angle of the dispersed beam. In other words, a sufficiently large footprint of the excitation on the sample is important and this requires a homogeneous sample.

To illustrate the quality of the spectra they performed several Kβ measurements of reference compounds (e.g. Mn(II) vs Mn(IV), Cr vs Cr(III) vs Cr(VI)) and a simple analysis comparing the peak intensity ratios and shifts as indicators.

Limandri et al. [206] did a chemical study and quantitative analysis based on high-resolution Mn Kβ XES measurements using a Johann type lab spectrometer with a Si(110) crystal (in 440 reflection) with a Rowland circle $r = 41$ cm and an X-ray tube with a cobalt (Co) anode running at $U = 37$ kV and $I = 40$ mA ($P = 1480$ Watt). The reported energy resolution near backscattering at $\theta_B \approx 84°$ is given as $\Delta E = 2$ eV at the Mn $K\beta_{1,3}$ main line ($E \approx 6490$ eV), translating to a resolving power of $E/\Delta E = 3245$. They measured the Mn Kβ main line and the satellites ($K\beta'', K\beta_{2,5}$) where the satellites shape in nicely resolved and used for a subsequent analysis. The complete setup (sample, analyzer and detector is enclosed in an evacuated chamber, confirming that under these conditions even the weak satellites can be studied without the need for a synchrotron light source. Especially the combination of a high powered source and enclosing the setup in an evacuated environment appears to be the key for such an experimental success using an in-house setup.

Anwar et al. [207] used a laboratory femtosecond Laser Plasma X-ray Source (fs-LPXS) to perform ultrafast IR pump/X-ray probe experiments in the laboratory. The measurement was performed

in transmission mode using a Ti:Sapphire laser with a wavelength of $\lambda = 800$ nm, a repetition rate of $f = 1$ kHz, and a pulse length of $t = 50$ fs with each pulse having 5–8 mJ hitting a copper (Cu) target to create Bremstrahlung which is then acting as the X-ray source. The transmitted beam is dispersed using a highly annealed pyrolytic graphite (HAPG) being then sent to either an energy-dispersive X-ray PIN detector (AMPTEK, XR100CR or an X-ray CCD camera). The setup is described in more detail in a publication by Iqbal et al. [216]. They measured the Fe K-edge XANES of a magnetite (Fe_3O_4) film observing a 12 eV shift upon IR excitation attributing the shift to charge transfer effects between the Fe ions. The spectral shapes are noisy but the shift can be clearly observed. Especially for fs time-resolved XANES measurements laboratory setups are very appealing because the experiments are often difficult to perform at the synchrotron (synchrotron slicing [217–222]) and the limited time to execute the measurements is often a crucial factor in femtosecond synchrotron measurements.

Moya-Cancino et al. [208] reported in January 2019 the **first laboratory-based in situ XANES** of a solid Fischer–Tropsch synthesis catalyst (Co/TiO_2). This very exciting experiment is using the setup described above by Honkanen et al. [191]. The measurements are performed in transmission using a capillary cell with controlled temperature and pressure ($T = 523$ K, $p = 5$ bar). Their setup uses an X-ray tube with a silver (Ag) anode as source, operated at $P = 800$ W, $U = 20$ kV and $I = 40$ mA respectively, and a Si (533) SBCA with a radius of $R = 0.5$ m. A comparison of the Co K-edge XANES with synchrotron experiments shows an excellent agreement for the ex-situ and a very good agreement for the in situ measurements of several Co-based compounds.

This is an important step forward towards lab-based in situ and operando studies, which is not only relevant for chemistry, but many applications in research often require studies under in situ or operando conditions to understand the dynamics of the process.

Yet another article from **Moya-Cancino et al.** [209] is *Elucidating the K-Edge X-ray Absorption Near-Edge Structure of Cobalt Carbide* under in situ conditions. The laboratory setup uses an X-ray tube with a silver (Ag) anode operating at $U = 20$ kV and $I = 40$ mA ($P = 800$ Watt) as source, while the spectrometer employs a Si(533) SBCA with a bending radius of $R = 50$ cm in Johann geometry and a Nal scintillator detector (Details described by Honkanen et al. [191]). They measured different steps of the carburization at elevated temperatures. Activation (reduction of Co_3O_4 to metal Co) was done at $T = 623$ K and 1 bar in pure H_2 flow and the carburization reaction at $T = 523$ K, with 1 and 5 bar in pure CO flow. They combined short term (1–5 hours) synchrotron based measurements, with longer (up to 75 h) experiments from the laboratory with satisfying resolution, where subsequently the difference with the reduced (metallic) state Co K-edge XANES was derived. The difference spectra show a notably higher noise level for the lab-based measurements but the shapes are over all sufficient for a subsequent analysis. The main features of the XANES enable to elucidate the activation and deactivation process of the Fischer–Tropsch synthesis catalyst.

Błachucki et al. [92] are reporting on a very interesting setup for simultaneous XAS and XES measurements using a double von Hamos spectrometer. The X-ray source is an XOS X-beam Superflux PF X-ray tube with a Molybdenum (Mo) anode and integrated focussing optics. It can be operated at a maximum voltage of $U = 50$ kV and maximum current of $I = 1$ mA (max power $P = 50$ Watt) with a divergence of $\theta \approx 3°$.

Two identical crystals are used, one crystal is dispersing the transmitted beam to acquire a XAS, and another crystal is dispersing the emission from the sample acquiring a XES. Both crystals used are cylindrically bent Si(440) with a curvature radius of $R = 25$ cm and the 2D detectors are two Andor Newton DO920P cameras with 1024×256 pixels (size: 26 μm) equipped with a $d = 250$ μm thick Beryllium (Be) window to decrease the pressure in the sensors' proximity to $p = 10^{-7}$ bar at a temperature of $T = -10$ °C. The setup itself is enclosed in a box with ambient conditions. The noteworthy aspect of this geometry is that it does not require any moving components, hence it can be operated without any motors (see Fig. 14).

The setup can perform measurements on solids, powders and liquids, and it is due to the ability to tightly focus the beam (micrometer size) compatible with very small amounts of samples (micro- to milligrams) as well as liquid jets and flow-through cells.

To demonstrate the performance of the setup they have simultaneously measured the K-edge XAS and Kβ XES of Iron (Fe), Nickel (Ni) and Copper (Cu) metal foils with a thickness of $d = 5$ μm each. For I_0 normalisation they measure the incident flux without a sample for 10 h, while the actual measurements of the samples yield good spectra after about 2 h, however, increasing the measurement time to 20 h improved the spectra by a factor of 3 allowing also to extract detailed information of the valence-to-core region (Kβ satellites).

3. Applications of laboratory-scale XAS and XES and their relevance in materials chemistry and catalysis research

Laboratory based XAS-XES has the potential for application in a large number of research fields including e.g. energy, catalysis, photonics, geology, archaeology, biology and environmental

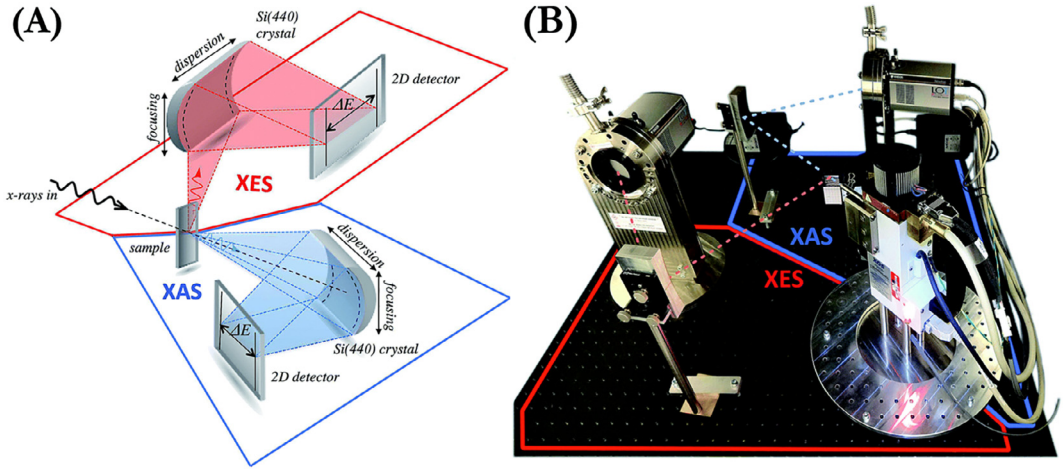

Fig. 14. (A) Schematic view of the double von Hamos spectrometer. (B) View of the developed experimental setup without shielding. (Image reprinted from Błachucki [92], Published by The Royal Society of Chemistry under CC3.0.).

sciences. In this review we summarise the applications of the currently available instrumentation in the fields of catalysts and materials chemistry.

3.1. Obtaining a fundamental understanding of the functionality of materials at the atomic level

Catalysis and materials chemistry are cross-cutting disciplines that plays a pivotal role in the chemical and energy conversion industries. Indeed, at least one catalytic step is involved in the production of more than 85% of the chemical products [223,224]. Key global challenges such as increasing the sustainability of the chemical industry and energy sector rely heavily on the development of innovative processes that produce less toxic (side) products and utilise, convert or store renewable energy. As a consequence, considerable efforts are currently undertaken to develop novel, more effective catalytic or electro-catalytic processes, providing a key step for cleaner and more sustainable economies. Prominent examples of current developments are the catalytic conversion of CO_2 into value-added chemicals or fuels (such as methanol synthesis or the dry reforming of methane), the production of olefins and aromatics from a synthesis gas (Fischer–Tropsch), alkane dehydrogenation, methane oxidation (partial oxidation of methane to syngas or methanol) and the electrochemical production of H_2, to name a few [225]. A key step towards the development of more effective (electro-) catalysts is an in-depth understanding of the relationship between a catalysts structure and its activity to avoid a cumbersome trial and error approach for their improvement.

To formulate such structure–function relationships, the identification and characterisation of a catalyst's active sites (and deactivation pathways) is critical, allowing in turn the possibility to design more effective catalytic materials yielding higher activities and selectivities towards the desired product(s). However, the role of the individual features of typically multi-component industrial catalysts remains elusive, mainly due to their intrinsic complexity and difficulties in determining in detail their structure and electronic properties under operating conditions.

Heterogeneous (electro-) catalysts are complex and dynamic systems, typically composed of different phases and sites that exhibit different functionalities. A catalyst's structure can thereby range from crystalline, nano-crystalline and amorphous phases to single sites. Yet, all of these structural features are susceptible to undergo changes during reaction (and activation) [226]. To characterise such complex and dynamic systems, X-ray absorption spectroscopy has been shown to be a very valuable tool since it provides element-specific information of the local structure, geometry and oxidation state of a target element. Specifically, using EXAFS analysis the atomic structure within the range of approximately 1–6 Å can be probed allowing inter-atomic distances, coordination number, and identity of neighbour species around the absorbing atom to be determined. XANES analysis provides information on the oxidation state and coordination geometry of the species probed [2]. Hence, XAS can shed light on both active or spectator species, as well as the support or promoters that are present in a multi-component catalytic material. Moreover, XAS can provide information on the local structure of a target element in a crystalline material with intrinsic local disorder.

3.2. Characterisation opportunities in laboratories to allow for a more efficient synchrotron beam time usage

XAS measurements are mostly carried out at synchrotron beamlines due to the high photon flux and tunable energy available. However, the limited access to these facilities restricts the number of materials and systems that can be studied by XAS and potentially hinders the more rapid development of new catalyst formulations and synthesis procedures. The availability of XAS as a routine characterisation tool for materials holds great potential for the advancement of (electro-) catalytic materials and the synthesis routes to yield the desired structural features. The availability of XAS and XES at laboratories has the potential to increase the efficiency of the synchrotron experiments, by performing detailed, yet routine characterisations on lab-based equipment, while experiments that require high photon flux such as time resolved in situ experiments or the study of materials with a low content of the element of interest, will be studied at the large scale facilities.

Recently, the availability of laboratory scale XAS and XES systems has accelerated, ameliorating to some extent the limited access to synchrotron based instruments. In the last decade, several reports using commercial or in-house built lab-based XAS and XES spectrometers have been published. These works have demonstrated the usefulness of lab-based XAS instrumentation for studying catalytic systems, in particular when complemented by other laboratory techniques or in certain cases with XAS data collected at synchrotron facilities [208,209,227–245].

3.3. XAS analysis to determine the local structure using laboratory-based equipment

An excellent illustration of lab-based XAS experimentation has been the characterisation of iron-based zeolites (Fe-TNU-9, Fe-TNU-10, and Fe-IM-5), containing both Fe and Al in framework positions and their steam-activated forms as catalysts for N_2O decomposition [238]. For comparison an isomorphously substituted Fe-ZSM-5 with a similar Fe content was also studied. The goal of this work was to examine the effect of the structure of the zeolite on the nature and distribution of extra-framework iron species and in turn on their N_2O decomposition activity. The specific activity (per mole of iron) was found to follow the following order: Fe-TNU-10 < Fe-IM-5 < Fe-TNU-9 < Fe-ZSM-5. A combination of extra-framework Fe and Al species has been proposed to be the active sites for N_2O decomposition. In addition, steam activation is required to obtain a highly homogeneous distribution of oxidic iron species upon Fe extraction from the zeolite framework, giving steam-activated iron zeolites. Lee et al. [238] were able to perform EXAFS analysis at the Fe K-edge (range of 2.0–12 Å) of the as synthesised materials and after steam activation at a relatively low iron loading (1.3–1.7 wt% Fe) using a laboratory XAS instrument (Rigaku, R-XAS Looper) in transmission mode. The EXAFS data of steam-activated zeolites revealed that the degree of extraction of framework Fe atoms depends on the structure type of the zeolites (Fig. 15).

As-synthesised zeolites, made by a hydrothermal synthesis, exhibit Fe in the framework. After steam activation, the relative intensity of the Fe-O peak at $R = 2.0$ Å, due to framework Fe atoms, in the Fourier transform becomes higher in the order Fe-TNU-9 $\ll$Fe-ZSM-5 $\sim$ Fe-IM- 5 < Fe-TNU-10. These EXAFS results were correlated with the poor N_2O decomposition activity of Fe-TNU-10, since Fe atoms in the zeolite framework are not catalytically active for this reaction. The results were also compared with Fe-TNU-9 and Fe-ZSM-5 zeolites prepared by a sublimation method, showing the presence of Fe_2O_3 particles in the as prepared material. For this class of materials, steam treatment resulted in the further sintering of Fe_2O_3 nanoparticles, which correlates well with the lower activity of the materials prepared by the sublimation method. In line with these observations, TEM showed that the materials prepared by sublimation were characterised by larger particles that are inactive for N_2O decomposition. Combining the result of EXAFS modelling with TEM, UV–vis spectroscopy and electron paramagnetic resonance, which provided further evidence of the Fe species and their dispersion, allowed the authors to con-

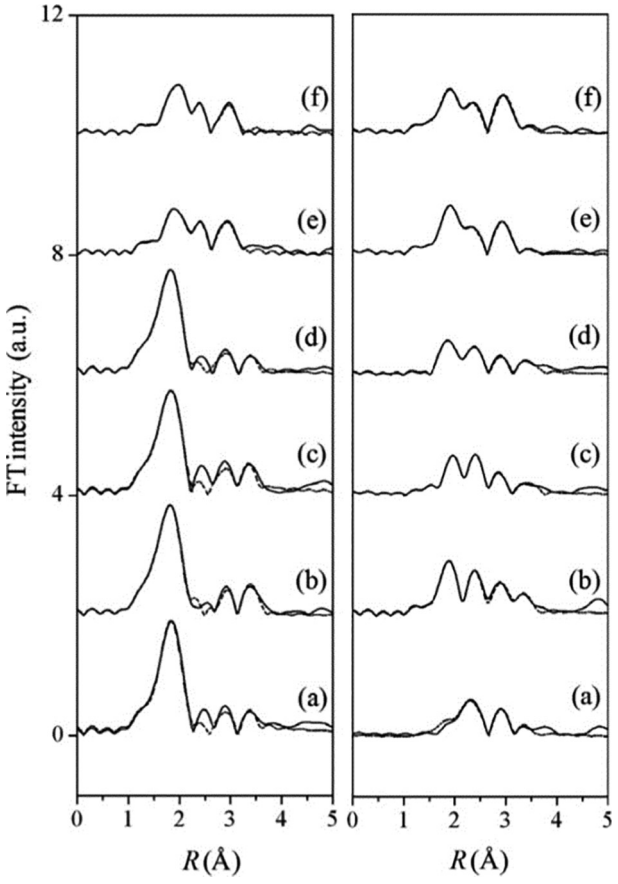

Fig. 15. EXAFS Fourier transform data of as-synthesised (left), and steam-activated (right): (a) Fe-TNU-9(HS), (b) Fe-TNU-10(HS), (c) Fe-IM-5(HS), (d) Fe-ZSM-5(HS), (e) Fe-TNU-9(S), and (f) Fe-ZSM-5(S). HS stands for hydrothermal synthesis and (S) for sublimation method. (Figure adapted from Lee [238] with permission from Elsevier.).

clude that the zeolite structure determines the nature and distribution of extra-framework iron species formed during the calcination and steaming steps, controlling in turn the N_2O decomposition activity of the material.

Another study that highlights the usefulness of lab-based XAS was reported by Yamamoto and co-workers. The study focused on elucidating the structure of tungsten oxide, supported on zirconium oxide doped with yttrium- or ytterbium (WO_x/Y(Yb)-ZrO_2), to investigate the mechanism responsible for the strong solid acidity in these materials [233]. To probe the effect of the quantity of dopant added, on the crystalline phases, acidity and the type of tungsten species, WO_x/Y(Yb)-ZrO_2 materials with varying concentrations of Y or Yb (xY(Yb)-$ZrO_2, x = 0 - 40$) while maintaining the tungsten loading (15 wt% WO_3) were prepared. The materials were probed for catalytic reactions that require strong acidic catalysts, namely n-butane skeletal isomerisation, alkylation of anisole with benzyl alcohol and 2-butanol decomposition. Structural insight into the catalysts was obtained using XANES (W L_1-edge) and EXAFS (W L_3-edge and Yb L_3-edge) complemented by XRD and UV–vis. XRD showed an increasing fraction of the tetragonal zirconia phase with increasing Y (Yb) doping. Assessment of the local environment around Yb by EXAFS confirmed the incorporation of Yb into the tetragonal ZrO_2 lattice forming a substitutional solid solution. W L_1-edge XANES and pre-edge analysis indicated that the tungsten species in the samples were in a distorted WO_6 octahedral geometry and a quantitative component analysis of the (W L_3-edge) EXAFS spectra by a least-squares method allowed to determine the relative amounts of tree different tungsten species depending on the Y (or Yb) loading: WO_3-like species, $Y_2(WO_4)_3$ and Y_2WO_6.The EXAFS results (Fig. 16) showed that the fraction of WO_3-like species was ~ 70% in WO_x/4Y-ZrO_2, which was the most active catalyst.

The combination of EXAFS, XRD and UV–vis allowed for the following conclusions to be drawn: i) monoclinic ZrO_2 with Y (Yb)-doping of less than 2 mol% led to large WO_3 particles. ii) Y (Yb) stabilised tetragonal zirconia effectively stabilised small clusters of WO_3 and provided strong acidity which is critical to effectively catalyse reactions that require strong acidic catalysts, such as alkane skeletal isomerisation and the Friedel–Crafts alkylation and iii) inactive mixed oxides ($(WO_4)_3$ and Y_2WO_6) were formed when the Y (Yb) doping level exceeded 10 mol%.

3.4. Recent advances in the in situ characterisation using laboratory instruments for long time-scale dynamics

More recently, lab-based XAS has been extended to in situ studies [208,209,246]. As already mentioned above, Moya-Cancino et al.

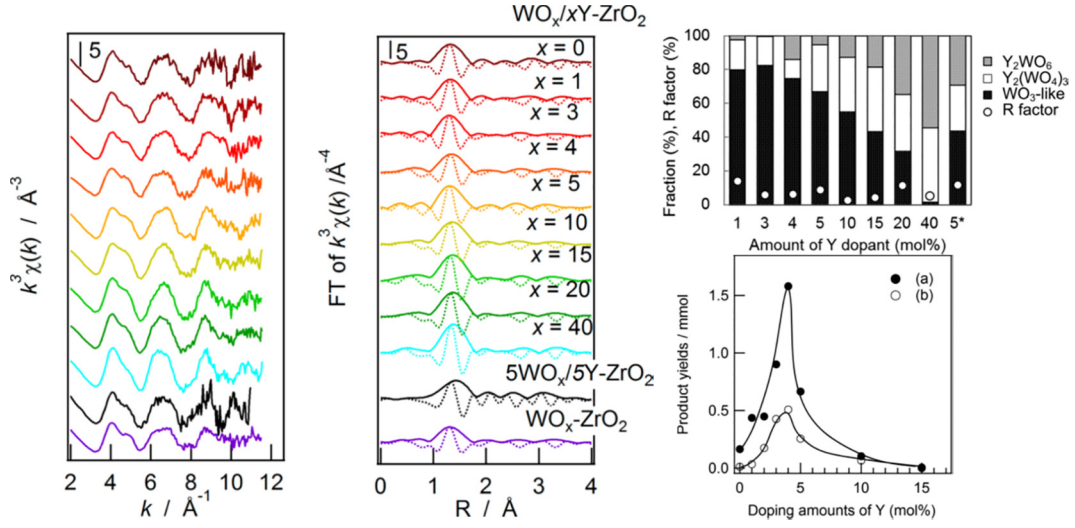

Fig. 16. (Left): Tungsten (W) L_3-edge EXAFS spectra and their Fourier transforms of WO_x/xY-ZrO_2 catalysts (k range: 2.5–11.0 $Å^{-1}$). (Right top): Tungsten species in WO_x/Y-ZrO_2 determined by EXAFS as a function of Y doping. (Right bottom): Product yields of the alkylation of anisole with benzyl alcohol as a function of the amount of WO_x/Y-ZrO_2: (a) benzyl anisole and (b) dibenzyl ether. (Adapted from Yamamoto [233] with permission from American Chemical Society.).

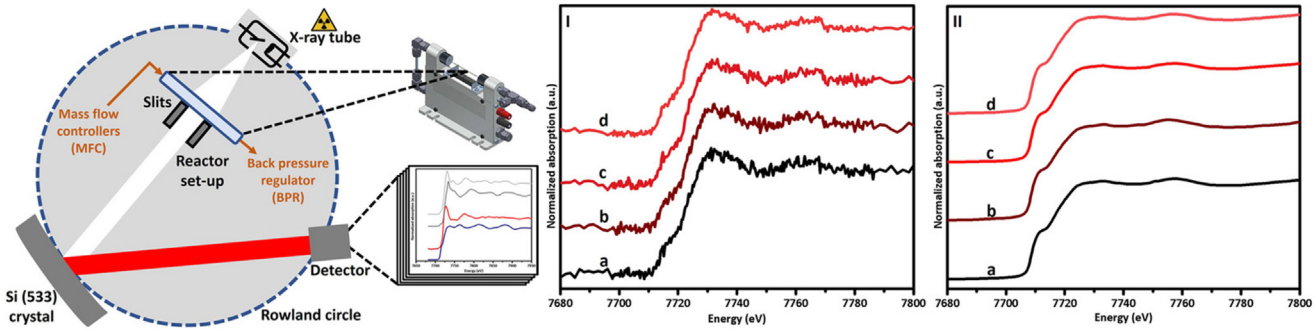

Fig. 17. In situ XANES spectra during FTS over a Co/TiO_2 catalyst (523 K 1 bar and a H_2/CO ratio = 0.5) measured I) with a laboratory-based set-up: a) 8.75 h, b) 17.5 h, c) 26.25 h and d) 35 h, and II) at BM26, ESRF at a) 6 h, b) 10 h, c) 12 h and d) 15 h. (Figure adapted from MoyaCancino [208] with permission from Wiley).

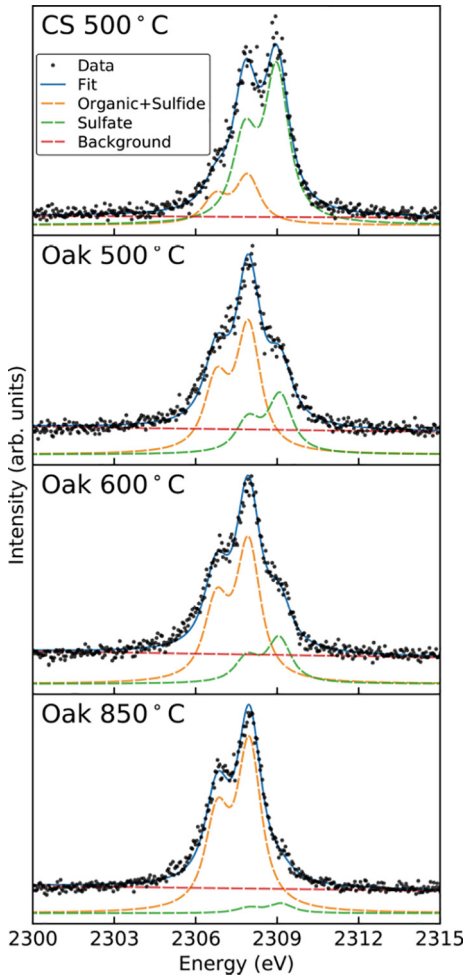

Fig. 18. Kα XES spectra obtained from four different biochar samples and linear combination fits to determine the sulphur speciation of the biochar samples. The lower energy doublet component represents S with a lower oxidation state (both organic and sulphidic species) and the higher energy doublet represents sulphur in a higher oxidation state (sulphate). (Reprinted from Holden [192] with permission from American Chemical Society.).

described the development of an in situ setup based on a laboratory based X-ray spectrometer, and demonstrated its application for the study of an industrial Co/TiO_2 based catalysts for Fischer–Tropsch (FTS) at 523 K and 5 bar for 200 h time on stream using a quartz capillary plug-flow reactor [208]. Analysis of the acquired in situ Co K-edge XANES data by linear combination fitting (using reference spectra) indicated that cobalt is maintained in its metallic form under reactive conditions. Only a very small fraction of inactive $CoTiO_3$ phase was detected under FTS conditions. This observation allowed to rule out the oxidation of cobalt as the main deactivation pathway. The XANES spectra collected in the laboratory set-up were validated by comparison with results obtained using synchrotron radiation XANES (BM26 beamline, ESRF). However, the lower signal-to-noise ratio obtain in the laboratory experiment (when compared to the synchrotron data) limited the time-resolution to 7.8 h per averaged spectra (Fig. 17). The poorer signal to noise ratio that is achieved using lab-based XAS instruments means that dynamic features of catalyst restructuring may be better assessed by performing experiments at synchrotron based facilities. However, long-term stability tests of catalysts may readily be explored using laboratory-based equipment, providing the concentration of the photo-absorber is sufficiently high.

A follow-up work by Moya-Cancino et al., based on the same setup as described above, studied the Co K-edge spectrum of cobalt carbide (Co_2C) during the in situ carburisation of pure metallic cobalt and by applying a non-negative matrix factorisation (NNMF) method [209]. The spectrum of pure Co_2C was further corroborated by theoretical calculations. The applied methodology allowed to provide the reference spectrum of the elusive cobalt carbide phase formed under in situ FTS conditions. Overall, this work contributes to the further understanding of the role of cobalt carbides in FTS that remains highly debated. Moreover, these studies demonstrate the usefulness of the laboratory based XAS experiments to study catalysts at relevant conditions.

3.5. XES studies providing information about speciation and coordination chemistry

XES studies, which can be carried out as well in laboratory-based instruments, can provide information about speciation and coordination chemistry that is complementary to XAS [202,192,5,247,159,2]. An example of such application, published by Holden et al.[192], is the determination of the sulphur speciation in biochars. The distribution of the oxidation states of sulphur (S) in different biochar samples was performed by fitting XES spectra using two $K\alpha_{1,2}$ doublet components (each doublet is composed of $K\alpha_1$ and $K\alpha_2$ with a fixed intensity ratio) representing two oxidation states (Fig. 18).

One of the fitted components of the XES spectra has a $K\alpha_1$ at 2309.15 eV and represents sulphate species; the second sulphur component has a $K\alpha_1$ at 2307.97 eV and represents sulphur (S) with a lower oxidation state (attributed to both organic and sulphidic species). Using this approach the distribution of the oxidation states of sulphur in the different biochar samples was quantified. The results were validated by comparison with sulphur (S) K-edge XANES data (previously acquired at beamline 4–3 of the

Stanford Synchrotron Radiation Lightsource [248]) and good agreement between the XES and XANES results were reported. Although XES was not able to resolve between organic and sulphidic species it proved to be very useful to distinguish sulphur species of lower and a higher oxidation states and to quantify their distribution.

3.6. Scientific opportunities of laboratory scale XAS-XES and further developments needed

The studies described in this section showcase the potential of laboratory-based XAS and XES instrumentation for characterisation in material chemistry, catalysts and environmental science. The potential applications are much broader than the examples covered in this review. Presumably due to the limited number of laboratory-based equipment, the number of studies are limited, but they are expected to growth with the increasing number of available instrumentation and a continuous improvements of their capabilities. A general limitation of laboratory-based equipment is the relatively low signal to noise ratio which has to be compensated by long acquisition times. This limits to some extent the study of very low concentration samples. Nonetheless it is important to remark that the use of low X-ray doses can also be an advantage for samples that are very prone to radiation damage. Moreover, recent developments have shown the usefulness of these instruments for in situ studies of processes that occur over a longer timescale (for instance the structural evolution of catalysts that occurs over days or weeks). Importantly, laboratory-based spectrometers will not replace synchrotron studies, but they can complement them, allowing for better sample screening and, thus, leading to an optimisation of the relatively scarce beamtime at synchrotrons. This is a key aspect since in many cases there are no other available techniques to characterise certain materials aspect (for instance doping) and an efficient use of synchrotron time will profit enormously by a thorough preliminary assessment of the samples under study in readily available laboratory-based instrumentation. Further advances in the field of laboratory based XAS and XES may include the integration of more powerful X-ray sources and the implementation of highly efficient detectors, which can lead to a reduction of the acquisition times.

4. Conclusion and outlook

We have summarized the details of several laboratory setups and presented examples showing that X-ray spectroscopy in the laboratory is, for certain applications, becoming a realistic alternative to the large scale synchrotron facilities.

Various laboratory setups exist already which are employed for in-house XAS and non-resonant XES experiments. Transmission XAS experiments are for a broad range of systems feasible in the lab as long as their optical thickness fulfils the requirements. Non-resonant XES experiments are possible even on optically thick samples and they are already widely used for complementary experimental studies. The relatively low costs of laboratory setups and the broad range of possible applications makes them an useful alternative to synchrotron experiments. Either as preliminary study to strengthen an application for measurement time at a synchrotron, or even for full research quality studies. Also worth to mention in the fact that laboratory setups are a very nice teaching instrument, i.e. to explain students the methodology.

Standard XAS and XES measurements on reference compounds and model systems under ex-situ conditions can routinely be realised in the laboratory [249]. Though limited to larger time-scales, the most recent developments prove that also experiments under in situ and operando conditions can now be realised in the laboratory [208]. This will be especially useful in the field of chemistry and catalysis, but laboratory X-ray spectroscopy can be expected to soon cover a broad range of fields, similar to the ones mentioned in the introduction. The applications are often limited to certain types of samples and sufficiently powerful sources are needed to deliver the required flux to perform the experiments with reasonable acquisition times and acceptable SNR. Measurements on samples with an analyte fraction down to approximately 3 wt% can now be routinely realised in the laboratory. Highly diluted samples with a small analyte fraction ($\leq$ 3 wt%) make in-house experiments still challenging, but with a sufficiently stable source these difficulties can to some degree be overcome by longer acquisition times. Low analyte concentrations in a heavy matrix, however, typically require a fluorescence yield approach, which was until recently only possible at the synchrotron. But the recent developments and the employment of high-power X-ray tubes show that also in-house fluorescence yield experiments are becoming feasible now [191]. This also illustrates that the limiting factor is in most cases the source of X-rays, as typical in-house sources cannot offer the unique capabilities such as the tunability while maintaining high intensities as they are available at a synchrotron.

Considering sources covering the soft and hard X-ray energy range, the employment of high intensity laser plasma sources, the new micro-structured anode materials for better heat-dissipation, and the Line Focus X-ray Tubes appear to be among of the most promising developments regarding X-ray sources. In particular the improvements in modern laser plasma sources suggest that for example spin-state studies using time-resolved XES can soon be realised routinely in the laboratory [76]. Further, the interesting development of a compact light source by Lyncean could fill the gap between X-ray tubes and large scale synchrotrons [67].

However, the very photon–hungry techniques such as high energy fluorescence detected (HERFD) XAS, resonant XES and resonant inelastic X-ray scattering (RIXS) appear to be still beyond the practical limits of in-house experiments and therefore still have to be performed at a synchrotron offering the highest brilliances. Although, to be optimistic, with modern detectors such as a *Transition Edge Sensor* (TES) [250,251] some systems with a large photon-yield and sufficient stability could in principle be measured in the laboratory if a sufficiently efficient source is available and long acquisition times can be accepted.

Altogether we conclude that in the next years an increased number of X-ray experiments will be moving back into the laboratory, as in-house X-ray instruments are for certain applications indeed a valuable alternative to measurements at large scale synchrotrons.

Declaration of Competing Interest

The authors declare that they have no known competing financial interests or personal relationships that could have appeared to influence the work reported in this paper.

Acknowledgements

Patric Zimmermann and Jeroen A. van Bokhoven acknowledge the ESI platform at the Paul Scherrer Institute for funding. Serena DeBeer and Sergey Peredkov acknowledge the Max Planck Society for funding. Moniek Tromp acknowledges the NWO for a VIDI 723.014.010. Paula M. Abdala and Christoph Müller acknowledge ETH SEED-02 17–2 and SNF grant (CRSII5_183495) for funding.

Appendix A. Supplementary data

Supplementary data associated with this article can be found, in the online version, at https://doi.org/10.1016/j.ccr.2020.213466.

References

[1] G.R. Lachance, F. Claisse, Quantitative X-ray Fluorescence Analysis: Theory and Application, Gerald R. Fernand Claisse, Wiley Chichester; New York, 1995, ISBN 0471951676, URL:https://nla.gov.au/nla.cat-vn2021539.

[2] Jeroen A. Van Bokhoven, Carlo Lamberti, X-Ray Absorption and X-Ray Emission Spectroscopy, John Wiley & Sons Ltd (2016), https://doi.org/10.1002/9781118844243, ISBN 9781118844243.

[3] Jakub Szlachetko, Jacinto Sá, Chapter 1: X-Ray Spectroscopy – The Driving Force to Understand and Develop Catalysis. In Advanced Catalytic Materials - Photocatalysis and Other Current Trends. 2016. ISBN 9789537619800. DOI: 10.5772/61940. URL:http://www.intechopen.com/books/advanced-catalytic-materials-photocatalysis-and-other-current-trends/x-ray-spectroscopy-the-driving-force-to-understand-and-develop-catalysis.

[4] Yulia Pushkar, Xi Long, Pieter Glatzel, Gary W. Brudvig, G. Charles Dismukes, Terrence J. Collins, Vittal K. Yachandra, Junko Yano, Uwe Bergmann, Direct detection of oxygen ligation to the mn4ca cluster of photosystem ii by x-ray emission spectroscopy, Angewandte Chemie International Edition 49 (4) (2010) 800–803, DOI: 10.1002/anie.20090536. URL:https://onlinelibrary.wiley.com/doi/abs/10.1002/anie.200905366.

[5] Wolfgang Malzer, Daniel Grötzsch, Richard Gnewkow, Christopher Schlesiger, Fabian Kowalewski, Benjamin Van Kuiken, Serena DeBeer, Birgit Kanngießer, A laboratory spectrometer for high throughput X-ray emission spectroscopy in catalysis research. Review of Scientific Instruments, 89 (11) (2018). ISSN 10897623. DOI: 10.1063/1.5035171. doi: 10.1063/1.5035171.

[6] Moniek Tromp, Jeroen A. van Bokhoven, Anne M. Arink, Johannes H. Bitter, Gerard van Koten, Diederik C. Koningsberger, Cu k-edge exafs characterisation of copper(i) arenethiolate complexes in both the solid and liquid state: Detection of cu-cu coordination, Chemistry - A European Journal 8 (24) (2002) 5667–5678, https://doi.org/10.1002/1521-3765(20021216)8:24<5667::AID-CHEM5667>3.0.CO;2-O, URL:https://onlinelibrary.wiley.com/doi/abs/10.1002/1521-3765.

[7] Moniek Tromp, Jerome Moulin, Gillian Reid, John Evans, Cr k-edge xanes spectroscopy: Ligand and oxidation state dependence - what is oxidation state?, AIP Conference Proceedings 882 (1) (2007) 699–701, https://doiorg/10.1063/1.2644637, URL:https://aip.scitation.org/doi/abs/10.1063/1.2644637.

[8] Moniek Tromp, Catalysis seen in action, Philosophical Transactions of the Royal Society A: Mathematical, Physical and Engineering Sciences 373 (2036) (2015) 20130152, https://doi.org/10.1098/rsta.2013.0152, URL:https://royalsocietypublishing.org/doi/abs/10.1098/rsta.2013.0152.

[9] Luuk J.P. Ament, Michel van Veenendaal, Thomas P. Devereaux, John P. Hill, Jeroen van den Brink. Resonant inelastic x-ray scattering studies of elementary excitations. Reviews of Modern Physics, 83, 705–767, Jun 2011. DOI: 10.1103/RevModPhys.83.705. URL:https://link.aps.org/doi/10.1103/RevModPhys.83.705.

[10] Elke Arenholz, Gerrit van der Laan, Rajesh V. Chopdekar, Yuri Suzuki, Anisotropic x-ray magnetic linear dichroism at the fe $L_{2,3}$ edges in fe_3 o_4, Physical Review B 74 (Sep 2006) , https://doi.org/10.1103/PhysRevB.74.094407, URL:https://link.aps.org/doi/10.1103/PhysRevB.74.094407 094407.

[11] Elke Arenholz, Gerrit van der Laan, Rajesh V. Chopdekar, Yuri Suzuki, Angle-dependent ni^{2+} x-ray magnetic linear dichroism: Interfacial coupling revisited, Physical Review Letters 98 (May 2007) , https://doi.org/10.1103/PhysRevLett.98.197201, URL:https://link.aps.org/doi/10.1103/PhysRevLett.98.197201 197201.

[12] Frank de Groot, György Vankó, Pieter Glatzel, The 1s x-ray absorption pre-edge structures in transition metal oxides, Journal of Physics: Condensed Matter 21 (10) (Feb 2009) , https://doi.org/10.1088/0953-8984/21/10/104207, URL: https://doi.org/10.1088 104207.

[13] M. Rovezzi, P. Glatzel, Hard x-ray emission spectroscopy: a powerful tool for the characterization of magnetic semiconductors, Semiconductor Science and Technology 29 (2) (Jan 2014) , https://doi.org/10.1088/0268-1242/29/2/023002, URL: https://doi.org/10.1088 023002.

[14] Patric Zimmermann, Nadejda Bouldi, M. Hunault, Marcin Sikora, James M. Ablett, Jean-Pascal Rueff, Blair Lebert, Philippe Sainctavit, Frank M.F. de Groot, Amélie Juhin. 1s2p resonant inelastic x-ray scattering magnetic circular dichroism as a probe for the local and non-local orbitals in cro2. Journal of Electron Spectroscopy and Related Phenomena, 222, 74–87, 2018a. ISSN 0368–2048. doi: 10.1016/j.elspec.2017.08.004. URL:http://www.sciencedirect.com/science/article/pii/S0368204816301682.

[15] Patric Zimmermann, M. Hunault, Frank M.F. de Groot. 1s2p rixs calculations for 3d transition metal ions in octahedral symmetry. Journal of Spectroscopy, 2018: 50pages, 2018b. doi: 10.1155/2018/3618463. URL: https://doi.org/10.1155/2018/3618463. Article ID 3618463.

[16] Federico Boscherini. Applications of XAFS to Nanostructures and Materials Science, pages 485–498. Springer, Berlin Heidelberg, Berlin, Heidelberg, 2015. ISBN 978-3-642-55315-8. DOI: 10.1007/978-3-642-55315-8_17. URL: https://doi.org/10.1007/978-3-642-55315-8_17.

[17] Zhentang Zhao, Tetsuya Ishikawa, Renzhong Tai, Jianhua He, Yuying Huang, Jie Wang, Xingyu Gao, Tiqiao Xiao, Jingyuan Ma, Tsun-Kong Sham, Liang Cao, Xing-Yu Gao, AndrewT.S. Wee, Dong-Chen Qi, Renzhong Tai, Kazumichi Namikawa, PeterMüller-Buschbaum, Gang Xiong, Oussama Moutanabbir, Manfred Reiche, Ross Harder, Ian Robinson, Jun Zhong, Hui Zhang, Xuhui Sun, Shuit-tong Lee, Catalin Miron, Minna Patanen, Safia Benkoula, Yanan Fu, Honglan Xie, Biao Deng, Guohao Du, Tiqiao Xiao. Synchrotron Radiation in Materials Science: Light Sources, Techniques, and Applications, Wiley-VCH, 2018. ISBN 9783527339860.

[18] M. J dos Anjos, R. T Lopes, E.F. O de Jesus, J. T Assis, R Cesareo, C.A. A Barradas, Quantitative analysis of metals in soil using x-ray fluorescence, Spectrochimica Acta Part B: Atomic Spectroscopy 55 (7) (2000) 1189–1194, ISSN 0584–8547. doi: 10.1016/S0584-8547(00)00165-8. URL:http://www.sciencedirect.com/science/article/pii/S0584854700001658.

[19] Burkhard Beckhoff, Birgit Kanngießer, Norbert Langhoff, Reiner Wedell, and Helmut Wolff, editors. Handbook of Practical X-Ray Fluorescence Analysis. Springer, Berlin, Heidelberg, 2006. ISBN 9783540286035. 10.1007/978-3-540-36722-2. URL: https://doi.org/10.1007/978-3-540-36722-2.

[20] Chen Zhao, Yiwen Zhang, Chong-Chen Wang, Miaole Hou, Aiqun Li, Recent progress in instrumental techniques for architectural heritage materials, Heritage Science 7 (1) (2019) 36, ISSN 2050-7445. DOI: 10.1186/s40494-019-0280-z. URL: 10.1186/s40494-019-0280-z..

[21] Birgit Kanngießer, Wolfgang Malzer, Alexis Fuentes Rodriguez, Ina Reiche, Three-dimensional micro-xrf investigations of paint layers with a tabletop setup, Spectrochimica Acta Part B: Atomic Spectroscopy 60 (1) (2005) 41–47, ISSN 0584–8547. doi: 10.1016/j.sab.2004.10.012. URL:http://www.sciencedirect.com/science/article/pii/S0584854704003027..

[22] Lino Piotto, Roger Gent, Giovanni Bibbo, Myth busting - in the world of x-rays, Radiographer 54 (1) (2007) 3–5, https://doi.org/10.1002/j.2051-3909.2007.tb00060.x, URL:https://onlinelibrary.wiley.com/doi/abs/10.1002/j.2051-3909.2007.tb00060.x.

[23] Birgit Kanngießer, Wolfgang Malzer, Ina Reiche, A new 3d micro x-ray fluorescence analysis set-up - first archaeometric applications, Nuclear Instruments and Methods in Physics Research Section B: Beam Interactions with Materials and Atoms 211 (2) (2003) 259–264, ISSN 0168–583X. doi: 10.1016/S0168-583X(03)01321-1. URL:http://www.sciencedirect.com/science/article/pii/S0168583X03013211..

[24] B. Kanngießer, I. Mantouvalou, W. Malzer, T. Wolff, O. Hahn, Non-destructive, depth resolved investigation of corrosion layers of historical glass objects by 3d micro x-ray fluorescence analysis, Journal of Analytical Atomic Spectrometry 23 (2008) 814–819, https://doi.org/10.1039/B717286A.

[25] Ioanna Mantouvalou, Timo Wolff, Oliver Hahn, Ira Rabin, Lars Lühl, Marcel Pagels, Wolfgang Malzer, Birgit Kanngiesser, 3d micro-xrf for cultural heritage objects: New analysis strategies for the investigation of the dead sea scrolls, Analytical Chemistry 83 (16) (2011) 6308–6315, https://doi.org/10.1021/ac2011262, PMID:21711051.

[26] G. Zentai, X-ray imaging for homeland security, in: 2008 IEEE International Workshop on Imaging Systems and Techniques, 2008, pp. 1–6, https://doi.org/10.1109/IST.2008.4659929.

[27] Richard D.R. Macdonald, Design and implementation of a dual-energy x-ray imaging system for organic material detection in an airport security application. Proc. SPIE 4301, Machine, Vision Applications in Industrial Inspection IX (2001), https://doi.org/10.1117/12.420922.

[28] Lia Corrales, Lynne Valencic, Elisa Costantini, Javier Garcia, Efrain Gatuzz, Tim Kallman, Julia Lee, Norbert Schulz, Sascha Zeegers, Claude Canizares, Bruce Draine, Sebastian Wisconsin, Edmund Hodges-Kluck, Edward B. Jenkins, Frits Paerels, Randall K. Smith, Tea Temim, Joern Wilms, Daniel Wolf Savin. Astromineralogy of interstellar dust with X-ray spectroscopy. Bulletin of the American Astronomical Society, 51 (3) (2019), 264. URL:https://ui.adsabs.harvard.edu/abs/2019BAAS...51c.264C.

[29] Jonathan W. Woo, EXAFS and XANES: New astrophysical tools to study the solid state structure of interstellar grains, The Astrophysical Journal 447 (2) (1995). DOI: 10.1086/309571. https://doi.org/10.1086.

[30] Alan Owens, Michael Denby, Alan Wells, Adam Keay, Dale E. Graessle, Richard L. Blake, The effect of x-ray absorption fine structure in soft x-ray astronomical telescopes, The Astrophysical Journal 476 (2) (1997) 924–931, https://doi.org/10.1086/303628, URL: https://doi.org/10.1086.

[31] K. Ishibashi, M.F. Davidson, K. Corcoran, S.A. Drake, J.H. Swank, R. Petre, Resolving X-ray Temporal Variations in ηCarinae, in: Jon A. Morse, Roberta M. Humphreys, Augusto Damineli (Eds.), Eta Carinae at The Millennium, volume 179 of Astronomical Society of the Pacific Conference Series, 1999, p. 266, URL:https://ui.adsabs.harvard.edu/abs/1999ASPC..179..266I.

[32] Frank de Groot, A. Kotani, Core level spectroscopy of solids. CRC Press, 01 2008. ISBN 9780429195792. DOI: 10.1201/9781420008425.

[33] A.J. Achkar, T.Z. Regier, H. Wadati, Y.-J. Kim, H. Zhang, D.G. Hawthorn, Bulk sensitive x-ray absorption spectroscopy free of self-absorption effects, Physical Review B 83 (Feb 2011) , https://doi.org/10.1103/PhysRevB.83.081106, URL: https://link.aps.org/doi/10.1103/PhysRevB.83.081106 081106.

[34] R Van Grieken, A. Markowicz, Handbook of X-Ray Spectrometry, second ed., CRC Press, 11 2001, ISBN 9780824706005.

[35] W.C. Roentgen, Uber eine neue art von strahlen, Sitzungsberichte der Physikalisch-Medizinischen Gesellschaftzu Wurtzburg 9 (1895) 132–141, URL:https://ci.nii.ac.jp/naid/10026412199/en/.

[36] W.C. Rontgen, Ueber eine neue art von strahlen (2 mitteilung), Sitzungsberichte der Phikalisch-medizinischen Gesellschaft zu Wurzburg 2 (1896) 11–17, URL:https://ci.nii.ac.jp/naid/10027056924/en/.

[37] NobelPrize.org. Nobel Media AB 2019. The nobel prize in physics 1901. URL: https://www.nobelprize.org/prizes/physics/1901/summary/.

[38] Manuel Lederman, The early history of radiotherapy: 1895–1939, International Journal of Radiation Oncology*Biology*Physics 7 (5) (1981) 639–648, ISSN 0360-3016. doi: 10.1016/0360-3016(81)90379-5. URL:http://www.sciencedirect.com/science/article/pii/0360301681903795..

[39] Emil H. Grubbé, Priority in the therapeutic use of x-rays, Radiology 21 (2) (1933) 156–162, https://doi.org/10.1148/21.2.156.
[40] M. Plücker. I. observations on the electric discharge. The London, Edinburgh, and Dublin Philosophical Magazine and Journal of Science, 18 (117) (1859a) 1–7. DOI: 10.1080/14786445908642710. doi: 10.1080/14786445908642710.
[41] M. Plücker. Ii. observations on the electric discharge. The London, Edinburgh, and Dublin Philosophical Magazine and Journal of Science, 18 (117) (1859b) 7–20. DOI: 10.1080/14786445908642711. doi: 10.1080/14786445908642711.
[42] John Stachel, Bohr and the Photon, Springer, Netherlands, Dordrecht, 2009, ISBN 978-1-4020-9107-0, DOI: 10.1007/978-1-4020-9107-0_5.
[43] M. Born, W. Heisenberg, Zur quantentheorie der molekeln, Annalen der Physik 379 (9) (1924) 1–31, https://doi.org/10.1002/andp.19243790902, URL:https://onlinelibrary.wiley.com/doi/abs/10.1002/andp.19243790902.
[44] M. Born, W. Heisenberg, P. Jordan, Zur quantenmechanik ii, Zeitschrift für Physik 35 (8) (1926) 557–615, ISSN 0044-3328. DOI: 10.1007/BF01379806. doi: 10.1007/BF01379806..
[45] A. Sommerfeld, G. Wentzel, Über reguläre und irreguläre dubletts, Zeitschrift für Physik 7 (1) (1921) 86–92, ISSN 0044-3328. DOI: 10.1007/BF01332778. doi: 10.1007/BF01332778..
[46] A. Sommerfeld, W. Heisenberg, Eine bemerkung über relativistische röntgendubletts und linienschärfe, Zeitschrift für Physik 10 (1) (1922) 393–398, ISSN 0044-3328. DOI: 10.1007/BF01332582. doi: 10.1007/BF01332582..
[47] Finn Aaserud, Niels Bohr Collected Works – Volume 11: The Political Arena (1934–1961). North Holland, 2005. ISBN 9780444513366.
[48] William Henry Bragg, William Lawrence Bragg, The reflection of x-rays by crystals, Proceedings of the Royal Society of London Series A Containing Papers of a Mathematical and Physical Character 88 (605) (1913) 428–438, DOI: 10.1098/rspa.1913.0040. URL:https://royalsocietypublishing.org/doi/abs/10.1098/rspa.1913.0040.
[49] M. de Broglie, Recherches sur la diffraction des rayons de röntgen par les milieux cristallins, Radium (Paris) 10 (8) (1913) 245–249, https://doi.org/10.1051/radium:01913001008024500.
[50] D. Coster, On the spectra of x-rays and the theory of atomic structure, The London, Edinburgh, and Dublin Philosophical Magazine and Journal of Science 44 (261) (1922) 546–573, https://doi.org/10.1080/14786440908565195.
[51] D. Coster, über die absorptionsspektren im röntgengebiet, Zeitschrift für Physik 25 (1924) 83–98, https://doi.org/10.1007/BF01327511.
[52] H.R. Robinson, Lxviii multiple ionization in x-ray levels, The London, Edinburgh, and Dublin Philosophical Magazine and Journal of Science 4 (23) (1927) 763–774, DOI: 10.1080/14786441008564379.
[53] R.deL. Kronig, Zur theorie der feinstruktur in den röntgenabsorptionsspektren, Zeitschrift für Physik 70 (1931) 317–323, DOI: 10.1007/BF01339581.
[54] Osvald Lundquist, Über die kβ-linien in den röntgenemissionsspektra der elemente phosphor und kalium, Zeitschrift für Physik 33 (1) (1925) 901–915, ISSN 0044-3328. DOI: 10.1007/BF01328379.
[55] T. Miyahara, H. Kitamura, T. Katayama, M. Watanabe, S. Sato, SOR-RING an electron storage ring dedicated to spectroscopy, Particle Accelerators 7 (1976) 163–175, URL:http://cds.cern.ch/record/1107944/files/p163.pdf.
[56] P.L. Hartman, Introductory remarks, Nuclear Instruments and Methods in Physics Research 195 (1) (1982) 1–6, ISSN 0167–5087. doi: 10.1016/0029-554X(82)90749-2. URL:http://www.sciencedirect.com/science/article/pii/0029554X82907492.
[57] G. Shen, Y. Wang, High-pressure apparatus integrated with synchrotron radiation, Reviews in Mineralogy and Geochemistry 78 (1) (2014) 745–777, ISSN 1529-6466. DOI: 10.2138/rmg.2014.78.18.
[58] M. Berndt, W. Brunk, R. Cronin, D. Jensen, R. Johnson, A. King, J. Spencer, T. Taylor, H. Winick, Initial operation of ssrl wiggler in spear, IEEE Transactions on Nuclear Science 26 (3) (1979) 3812–3815, ISSN 0018–9499. DOI: 10.1109/TNS.1979.4330617.
[59] Dennis M. Mills, Third-generation hard x-ray synchrotron radiation sources: Source properties, optics, and experimental techniques. Third-Generation Hard X-Ray Synchrotron Radiation Sources: Source Properties, Optics, and Experimental Techniques, by Dennis M. Mills (Editor), pp. 406. ISBN 0-471-31433-1. Wiley-VCH, March 2002, 03 2002.
[60] Pantaleo Raimondi, Esrf-ebs: The extremely brilliant source project, Synchrotron Radiation News 29 (6) (2016) 8–15, https://doi.org/10.1080/08940886.2016.1244462.
[61] Alexandre Loulergue. Baseline lattice for the upgrade of soleil, 2018. URL: http://accelconf.web.cern.ch/AccelConf/fls2018/talks/mop2wb03_talk.pdf.
[62] Andreas Streun, Terence Garvey, Lenny Rivkin, Volker Schlott, Thomas Schmidt, Philip Willmott, Albin Wrulich, SLS-2 – the upgrade of the Swiss Light Source, Journal of Synchrotron Radiation 25 (3) (May 2018) 631–641, https://doi.org/10.1107/S1600577518002722.
[63] Arno Bergmann and Beatriz Roldan Cuenya, Operando insights into nanoparticle transformations during catalysis. ACS Catalysis, 0 (ja): null, 0. DOI: 10.1021/acscatal.9b01831.
[64] R. Bès, T. Ahopelto, A.P. Honkanen, S. Huotari, G. Leinders, J. Pakarinen, K. Kvashnina, Laboratory-scale X-ray absorption spectroscopy approach for actinide research: Experiment at the uranium L3-edge, Journal of Nuclear Materials 507 (2018) 50–53, ISSN 00223115. DOI: 10.1016/j.jnucmat.2018.04.034.
[65] Michael Feser, The lyncean compact light source: x-ray synchrotron radiation for analytical and imaging applications (conference presentation), 2017. doi: 10.1117/12.2277898. Advances in Laboratory-based X-Ray Sources, Optics, and Applications VI.
[66] K. Achterhold, M. Bech, S. Schleede, G. Potdevin, R. Ruth, R. Loewen, F. Pfeiffer, Monochromatic computed tomography with a compact laser-driven X-ray source. Scientific Reports, 3: 3–6, 2013. ISSN 20452322. DOI: 10.1038/srep01313.
[67] Benjamin Hornberger, Jack Kasahara, Martin Gifford, Ronald Ruth, Rod Loewen, A compact light source providing high-flux, quasi-monochromatic, tunable X-rays in the laboratory. In Alex Murokh and Daniele Spiga, editors, Advances in Laboratory-based X-Ray Sources, Optics, and Applications VII, volume 11110, pages 1–13. International Society for Optics and Photonics, SPIE, 2019. DOI: 10.1117/12.2527356.
[68] E. Ammann and W. Kutschera. X-ray tubes - Continuous innovative technology. British Journal of Radiology, 70 (SPECIAL.ISSUE): 1–9, 1997. ISSN 00071285. DOI: 10.1259/bjr.1997.0002.
[69] G. Harding, A. Thran, B. David, Liquid metal anode X-ray tubes and their potential for high continuous power operation, Radiation Physics and Chemistry 67 (1) (2003) 7–14, ISSN 0969806X. DOI: 10.1016/S0969-806X(03)00007-0.
[70] M. Otendal, T. Tuohimaa, U. Vogt, H.M. Hertz, A 9kev electron-impact liquid-gallium-jet x-ray source, Review of Scientific Instruments 79 (1) (2008) , https://doi.org/10.1063/1.2833838 016102.
[71] G.R. Fisher, An x-ray source for a laboratory exafs facility, AIP Conference Proceedings 64 (1) (1980) 21–30, https://doi.org/10.1063/1.32239, URL: https://aip.scitation.org/doi/abs/10.1063/1.32239.
[72] T. Tuohimaa, J. Ewald, M. Schlie, J.M. Fernández-Varea, H.M. Hertz, U. Vogt, A microfocus x-ray source based on a nonmetal liquid-jet anode, Applied Physics Letters 92 (23) (2008) , https://doi.org/10.1063/1.2942379 233509.
[73] Stefan Bartzsch, Uwe Oelfke, Line focus x-ray tubes - a new concept to produce high brilliance x-rays, Physics in Medicine and Biology 62 (22) (2017) 8600–8615, ISSN 13616560. DOI: 10.1088/1361-6560/aa910b.
[74] S.H. Wenbing Yun, Benjamin Stripe Lau, Alan Lyon, David Reynolds, Sylvia JY Lewis, Sharon Chen, Vladimir Semenov, Richard Ian Spink, Novel high brightness x-ray source and high efficiency x-ray optic for development of x-ray instrumentation, Microscopy and Microanalysis 22 (S3) (2016) 118–119, https://doi.org/10.1017/S1431927616001446.
[75] Henryk Fiedorowicz, Inam Ul Ahad, Andrzej Bartnik, Tomasz Fok, Roman Jarocki, Barbara Korczyc, Jerzy Kostecki, Anna Szczurek, Miroslaw Szczurek, Przemyslaw Wachulak, Lukasz Wegrzynski, Laser plasma sources of soft X-rays and extreme ultraviolet (EUV) for application in science and technology. Proceedings - 2014 International Conference Laser Optics, LO 2014, page 14, 2014. ISSN 1996756X. 10.1109/LO.2014.6886335. URL https://doi.org/10.1109/LO.2014.6886335.
[76] Y.I. Joe, G.C. O'Neil, L. Miaja-Avila, J.W. Fowler, R. Jimenez, K.L. Silverman, D.S. Swetz, J.N. Ullom, Observation of iron spin-states using tabletop x-ray emission spectroscopy and microcalorimeter sensors. Journal of Physics B: Atomic, Molecular and Optical Physics, 49 (2) (2016). ISSN 13616455. DOI: 10.1088/0953-4075/49/2/024003.
[77] I. Mantouvalou, R. Jung, J. Tuemmler, H. Legall, T. Bidu, H. Stiel, W. Malzer, B. Kanngieer, W. Sandner, Note: Study of extreme ultraviolet and soft x-ray emission of metal targets produced by laser-plasma-interaction, Review of Scientific Instruments 82 (6) (2011) 10–13, ISSN 00346748. DOI: 10.1063/1.3600069..
[78] L. Miaja-Avila, G.C. O'Neil, J. Uhlig, C.L. Cromer, M.L. Dowell, R. Jimenez, A.S. Hoover, K.L. Silverman, and J.N. Ullom. Laser plasma x-ray source for ultrafast time-resolved x-ray absorption spectroscopy. Structural Dynamics, 2 (2) (2015). ISSN 23297778. DOI: 10.1063/1.4913585.
[79] Matthias Müller, Meike Schellhorn, Klaus Mann, Laboratory-scale near-edge x-ray absorption fine structure spectroscopy with a laser-induced plasma source, Journal of Analytical Atomic Spectrometry 34 (2019) 1779–1785, https://doi.org/10.1039/C9JA00140A.
[80] S.M. Gruner, E.F. Eikenberry, M.W. Tate. Comparison of x-ray detectors, in: M. G. Rossmann and E. Arnold, editors, International Tables for Crystallography Volume F: Crystallography ofbiological macromolecules, volume 1, chapter 7.1, pages 143–147. Springer, Netherlands, 2001. ISBN 978-1-4020-5416-7. DOI: 10.1107/9780955360206000667.
[81] U. Fano, Ionization yield of radiations. ii. the fluctuations of the umber of ions, Physical Review 72 (1947) 26–29, DOI: 10.1103/PhysRev.72.26. URL:https://link.aps.org/doi/10.1103/PhysRev.72.26.
[82] J. Uhlig, W.B. Doriese, J.W. Fowler, D.S. Swetz, C. Jaye, D.A. Fischer, C.D. Reintsema, D.A. Bennett, L.R. Vale, U. Mandal, G.C. O'Neil, L. Miaja-Avila, Y.I. Joe, A. El Nahhas, W. Fullagar, F. Parnefjord Gustafsson, V. Sundström, D. Kurunthu, G.C. Hilton, D.R. Schmidt, J.N. Ullom, High-resolution X-ray emission spectroscopy with transition-edge sensors: present performance and future potential, Journal of Synchrotron Radiation 22 (3) (2015) 766–775, DOI: 10.1107/S1600577515004312.
[83] Anna Bergamaschi, Antonio Cervellino, Roberto Dinapoli, Fabia Gozzo, Beat Henrich, Ian Johnson, Philipp Kraft, Aldo Mozzanica, Bernd Schmitt, Xintian Shi, The MYTHEN detector for X-ray powder diffraction experiments at the Swiss Light Source, Journal of Synchrotron Radiation 17 (5) (2010) 653–668, ISSN 09090495. DOI: 10.1107/S0909049510026051.
[84] B. Henrich, A. Bergamaschi, C. Broennimann, R. Dinapoli, E.F. Eikenberry, I. Johnson, M. Kobas, P. Kraft, A. Mozzanica, B. Schmitt, PILATUS: A single photon counting pixel detector for X-ray applications, Nuclear Instruments and Methods in, Physics Research, Section A: Accelerators, Spectrometers

Detectors and Associated Equipment 607 (1) (2009) 247–249, ISSN 01689002. DOI: 10.1016/j.nima.2009.03.200.
[85] Junji Miyahara, Kenji Takahashi, Yoshiyuki Amemiya, Nobuo Kamiya, Yoshinori Satow, A new type of X-ray area detector utilizing laser stimulated luminescence, Nuclear Instruments and Methods in Physics Research A 246 (1-3) (1986) 572–578, ISSN 01689002. 10.1016/0168-9002(86)90156-7. URL: https://doi.org/10.1016/0168-9002(86)90156-7..
[86] C. Ponchut, J.M. Rigal, J. Clément, E. Papillon, A. Homs, and S. Petitdemange. MAXIPIX, a fast readout photon-counting X-ray area detector for synchrotron applications. Journal of Instrumentation, 6 (1) (2011). ISSN 17480221. DOI: 10.1088/1748-0221/6/01/C01069.
[87] J.C. Russ, Quantitative results with x-ray fluorescence spectrometry using energy dispersive analysis of x-rays, X-Ray Spectrometry 1 (3) (1972) 119–123, https://doi.org/10.1002/xrs.1300010308, URL:https://onlinelibrary.wiley.com/doi/abs/10.1002/xrs.1300010308.
[88] V.N. Strocov, T. Schmitt, U. Flechsig, T. Schmidt, A. Imhof, Q. Chen, J. Raabe, R. Betemps, D. Zimoch, J. Krempasky, X. Wang, M. Grioni, A. Piazzalunga, L. Patthey, High-resolution soft X-ray beamline ADRESS at the Swiss Light Source for resonant inelastic X-ray scattering and angle-resolved photoelectron spectroscopies, Journal of Synchrotron Radiation 17 (5) (Sep 2010) 631–643, https://doi.org/10.1107/S0909049510019862.
[89] N.B. Brookes, F. Yakhou-Harris, K. Kummer, A. Fondacaro, J.C. Cezar, D. Betto, E. Velez-Fort, A. Amorese, G. Ghiringhelli, L. Braicovich, R. Barrett, G. Berruyer, F. Cianciosi, L. Eybert, P. Marion, P. van der Linden, L. Zhang, The beamline id32 at the esrf for soft x-ray high energy resolution resonant inelastic x-ray scattering and polarisation dependent x-ray absorption spectroscopy. Nuclear Instruments and Methods in Physics Research Section A: Accelerators, Spectrometers, Detectors and Associated Equipment, 903: 175–192, 2018a. ISSN 0168–9002. doi: 10.1016/j.nima.2018.07.001. URL: http://www.sciencedirect.com/science/article/pii/S0168900218308234.
[90] Ignace Jarrige, Valentina Bisogni, Yi Zhu, William Leonhardt, Joseph Dvorak, Paving the way to ultra-high-resolution resonant inelastic x-ray scattering with the six beamline at nsls-ii, Synchrotron Radiation News 31 (2) (2018) 7–13, https://doi.org/10.1080/08940886.2018.1435949.
[91] Uwe Bergmann, Stephen P. Cramer, High-resolution large-acceptance analyzer for x-ray fluorescence and Raman spectroscopy. in: Albert T. Macrander, Andreas K. Freund, Tetsuya Ishikawa, and Dennis M. Mills (Eds.), Crystal and Multilayer Optics, volume 3448, pages 198–209. International Society for Optics and Photonics, SPIE, 1998. DOI: 10.1117/12.332507.
[92] Wojciech Błachucki, Joanna Czapla-Masztafiak, Jacinto Sá, Jakub Szlachetko, A laboratory-based double x-ray spectrometer for simultaneous x-ray emission and x-ray absorption studies, Journal of Analytical Atomic Spectrometry 34 (2019) 1409–1415, https://doi.org/10.1039/C9JA00159J.
[93] Mauro Rovezzi, Christophe Lapras, Alain Manceau, Pieter Glatzel, Roberto Verbeni, High energy-resolution x-ray spectroscopy at ultra-high dilution with spherically bent crystal analyzers of 0. 5 m radius, Review of Scientific Instruments 88 (1) (2017) 013108, DOI: 10.1063/1.4974100.
[94] M. Szlachetko, M. Berset, J. Cl Dousse, J. Hoszowska, J. Szlachetko, High-resolution Laue-type DuMond curved crystal spectrometer, Review of Scientific Instruments 84 (9) (2013) 0–12, ISSN 00346748. DOI: 10.1063/1.4821621.
[95] V.D. Scott, G. Love, S.J.B. Reed, Quantitative Electron-Probe Microanalysis (second ed.), London and New York (Ellis Horwood), 1995, ISBN 0 13 104050 2.
[96] Joanna K. Kowalska, Frederico A. Lima, Christopher J. Pollock, Julian A. Rees, Serena DeBeer, A practical guide to high-resolution x-ray spectroscopic measurements and their applications in bioinorganic chemistry, Israel Journal of Chemistry 56 (9–10) (2016) 803–815, ISSN 18695868. DOI: 10.1002/ijch.201600037. doi: 10.1002/ijch.201600037..
[97] Kristina O. Kvashnina, Andreas C. Scheinost, A Johann-type X-ray emission spectrometer at the Rossendorf beamline, Journal of Synchrotron Radiation 23 (3) (2016) 836–841, ISSN 16005775. DOI: 10.1107/S1600577516004483..
[98] X. Wang, M.M. Grush, A.G. Froeschner, S.P. Cramer, High-resolution x-ray fluorescence and excitation spectroscopy of metalloproteins, Journal of Synchrotron Radiation 4 (4) (Jul 1997) 236–242, https://doi.org/10.1107/S0909049596015440.
[99] N.B. Brookes, G. Ghiringhelli, P. Glatzel, M. Moretti Sala, Resonant inelastic x-ray scattering at the esrf: An evolving portfolio for hard and soft x-rays, Synchrotron Radiation News 31 (2) (2018) 26–30, DOI: 10.1080/08940886.2018.1435953.
[100] Matthias Bauer, HERFD-XAS and valence-to-core-XES: New tools to push the limits in research with hard X-rays?, Physical Chemistry Chemical Physics 16 (27) (2014) 13827–13837, ISSN 14639076 DOI: 10.1039/c4cp00904e.
[101] Roberto Alonso-Mori, Jan Kern, Dimosthenis Sokaras, Tsu Chien Weng, Dennis Nordlund, Rosalie Tran, Paul Montanez, James Delor, Vittal K. Yachandra, Junko Yano, Uwe Bergmann, A multi-crystal wavelength dispersive x-ray spectrometer. Review of Scientific Instruments, 83 (7) (2012), ISSN 00346748. DOI: 10.1063/1.4737630.
[102] Isabelle Llorens, Eric Lahera, William Delnet, Olivier Proux, Aurélien Braillard, Jean Louis Hazemann, Alain Prat, Denis Testemale, Quentin Dermigny, Frederic Gelebart, Marc Morand, Abhay Shukla, Nathalie Bardou, Olivier Ulrich, Stéphan Arnaud, Jean Franois Berar, Nathalie Boudet, Bernard Caillot, Perrine Chaurand, Jérôme Rose, Emmanuel Doelsch, Philippe Martin, Pier Lorenzo Solari, High energy resolution five-crystal spectrometer for high quality fluorescence and absorption measurements on an x-ray absorption spectroscopy beamline. Review of Scientific Instruments, 83 (6) (2012), ISSN 00346748. DOI: 10.1063/1.4728414. doi: 10.1063/1.4728414.
[103] Pieter Glatzel, Frank M.F. de Groot, Uwe Bergmann, Hard x-ray photon-in photon-out spectroscopy, Synchrotron Radiation News 22 (2) (2009) 12–16, DOI: 10.1080/08940880902813725.
[104] Evgeny Kleymenov, Jeroen A. van Bokhoven, Christian David, Pieter Glatzel, Markus Janousch, Roberto Alonso-Mori, Marco Studer, Markus Willimann, Anna Bergamaschi, Beat Henrich, Maarten Nachtegaal, Five-element johann-type x-ray emission spectrometer with a single-photon-counting pixel detector, Review of Scientific Instruments 82 (6) (2011) , https://doi.org/10.1063/1.3600452 065107.
[105] Q. Qian, T.A. Tyson, W.A. Caliebe, and C.-C. Kao. High-efficiency high-energy-resolution spectrometer for inelastic x-ray scattering. Journal of Physics and Chemistry of Solids, 66 (12): 2295–2298, 2005. ISSN 0022-3697. 2004, doi: 10.1016/j.jpcs.2005.09.069.http://www.sciencedirect.com/science/article/pii/S0022369705003537. 5th International Conference on Inelastic X-ray Scattering (IXS 2004).
[106] Paolo Carra, Michele Fabrizio, B.T. Thole, High resolution x-ray resonant raman scattering, Physical Review Letters 74 (1995) 3700–3703, DOI: 10.1103/PhysRevLett.74.3700. URL:https://link.aps.org/doi/10.1103/PhysRevLett.74.3700.
[107] Amélie Juhin, Christian Brouder, Frank De Groot, Angular dependence of resonant inelastic x-ray scattering: a spherical tensor expansion General case The Kramers-Heisenberg formula, Central European Journal of Physics 12 (5) (2014) 323–340, https://doi.org/10.2478/s11534-014-0450-2.
[108] E. Goering, A. Bayer, S. Gold, G. Schütz, M. Rabe, U. Rüdiger, G. Güntherodt, Strong anisotropy of projected 3d moments in epitaxial cro_2 films, Physical Review Letters 88 (May 2002) , https://doi.org/10.1103/PhysRevLett.88.207203, URL:https://link.aps.org/doi/10.1103/PhysRevLett.88.207203 207203.
[109] Steve M. Heald, Strategies and limitations for fluorescence detection of XAFS at high flux beamlines, Journal of Synchrotron Radiation 22 (2) (2015) 436–445, ISSN 16005775. DOI: 10.1107/S1600577515001320.
[110] H.H. Johann, Die erzeugung lichtstarker röntgenspektren mit hilfe von konkavkristallen, Zeitschrift für Physik 69 (3) (1931) 185–206, ISSN 0044-3328. DOI: 10.1007/BF01798121.
[111] Tryggve Johansson, Über ein neuartiges genau fokussierendes röntgenspektrometer, Zeitschrift für Physik 82 (7) (1933) 507–528, ISSN 0044-3328. DOI: 10.1007/BF01342254.
[112] L. von Hámos, Röntgenspektroskopie und abbildung mittels gekrümmter kristallreflektoren, Naturwissenschaften 20 (38) (1932) 705–706, ISSN 1432-1904. DOI: 10.1007/BF01494468.
[113] Lars Anklamm, Christopher Schlesiger, Wolfgang Malzer, Daniel Grötzsch, Michael Neitzel, Birgit Kanngießer. A novel von Hamos spectrometer for efficient X-ray emission spectroscopy in the laboratory. Review of Scientific Instruments, 85 (5) (2014). ISSN 10897623. DOI: 10.1063/1.4875986.
[114] Ari Pekka Honkanen, Roberto Verbeni, Laura Simonelli, Marco Moretti Sala, Ali Al-Zein, Michael Krisch, Giulio Monaco, Simo Huotari, Improving the energy resolution of bent crystal X-ray spectrometers with position-sensitive detectors, Journal of Synchrotron Radiation 21 (4) (2014) 762–767, ISSN 16005775. DOI: 10.1107/S1600577514011163.
[115] Ari Pekka Honkanen, Roberto Verbeni, Laura Simonelli, Marco Moretti Sala, Giulio Monaco, Simo Huotari, Study on the reflectivity properties of spherically bent analyser crystals, Journal of Synchrotron Radiation 21 (1) (2014) 104–110, ISSN 09090495. DOI: 10.1107/S160057751302242X.
[116] J. Hoszowska, J. Cl Dousse, J. Kern, Ch Rhême, High-resolution von Hamos crystal X-ray spectrometer, Nuclear Instruments and Methods in Physics Research, Section A: Accelerators, Spectrometers, Detectors and Associated Equipment 376 (1) (1996) 129–138, ISSN 01689002. DOI: 10.1016/0168-9002(96)00262-8.
[117] J. Szlachetko, M. Cotte, J. Morse, M. Salome, P. Jagodzinski, J.-Cl. Dousse, J. Hoszowska, Y. Kaysere, J. Susini, Wavelength-dispersive spectrometer for X-ray microfluorescence analysis at the X-ray microscopy beamline ID21 (ESRF), Journal of Synchrotron Radiation 17 (3407) (2010) 400–408, ISSN 0909–0495. DOI: 10.1107/S0909049510010691. URL:https://onlinelibrary.wiley.com/doi/pdf/10.1107/S0909049510010691..
[118] Jens Rehanek, Christopher J. Milne, Jakub Szlachetko, Joanna Czapla-Masztafiak, Jörg Schneider, Thomas Huthwelker, Camelia N. Borca, Reto Wetter, Luc Patthey, Pavle Juranic, A compact and versatile tender X-ray single-shot spectrometer for online XFEL diagnostics. Journal of Synchrotron Radiation, 25 (1) (2018) 16–19. ISSN 16005775. DOI: 10.1107/S1600577517012796.
[119] M.M. Elena Baronova, Stepanenko, and Nino Pereira. Cauchois-johansson x-ray spectrograph for 1.5-400 kev energy range. Review of Scientific Instruments -, REV SCI INSTR 72 (2001) 02, https://doi.org/10.1063/1.1324754.
[120] Xing Gao, Songqi Gu, Qian Gao, Yang Zou, Zheng Jiang, Shuo Zhang, Xiangjun Wei, Haisheng Yu, Guodong Sheng, Peiquan Duan, and Yuying Huang. A high-resolution X-ray fluorescence spectrometer and its application at SSRF. X-Ray Spectrometry, 42 (6): 502–507, 2013. ISSN 00498246. DOI: 10.1002/xrs.2511. doi: 10.1002/xrs.2511.
[121] P. Lecante, J. Jaud, A. Mosset, J. Galy, A. Burian. A laboratory EXAFS spectrometer in transmission dispersive mode. Review of Scientific Instruments, 65 (4) (1994) 845–849. ISSN 00346748. DOI: 10.1063/1.1144909.

[122] Kozo Shinoda, Shigeru Suzuki, Masaru Kuribayashi, Takeyoshi Taguchi, Dimensional position sensitive XAFS by using in-house X-ray spectrometer, Journal of Physics: Conference Series 186 (2009), https://doi.org/10.1088/1742-6596/186/1/012036.

[123] G.T. Seidler, D.R. Mortensen, A.J. Remesnik, J.I. Pacold, N.A. Ball, N. Barry, M. Styczinski, O.R. Hoidn, A laboratory-based hard x-ray monochromator for high-resolution x-ray emission spectroscopy and x-ray absorption near edge structure measurements. Review of Scientific Instruments, 85 (11) (2014). ISSN 10897623. DOI: 10.1063/1.4901599.

[124] Arthur Williams, Laboratory x-ray spectrometer for EXAFS and XANES measurements. Review of Scientific Instruments, 54 (2) (1983) 193–197. ISSN 00346748. DOI: 10.1063/1.1137344.

[125] Devon R. Mortensen, Gerald T. Seidler, Alexander S. Ditter, Pieter Glatzel, Benchtop Nonresonant X-ray Emission Spectroscopy: Coming Soon to Laboratories and XAS Beamlines Near You? Journal of Physics: Conference Series, 712 (1) (2016). ISSN 17426596. DOI: 10.1088/1742-6596/712/1/012036.

[126] Frank de Groot, High-resolution x-ray emission and x-ray absorption spectroscopy, Chemical Reviews 101 (6) (2001) 1779–1808, https://doi.org/10.1021/cr9900681, PMID:11709999.

[127] Scott Calvin and Kirin Emlet Furst, XAFS for everyone. CRC Press, Boca Raton, FL, 2013. URL:http://cds.cern.ch/record/2631754.

[128] Grant Bunker, Introduction to XAFS: A Practical Guide to X-ray Absorption Fine Structure Spectroscopy, Cambridge University Press (2010), https://doi.org/10.1017/CBO9780511809194.

[129] Silvia Bordiga, Elena Groppo, Giovanni Agostini, Jeroen A. van Bokhoven, Carlo Lamberti, Reactivity of surface species in heterogeneous catalysts probed by in situ x-ray absorption techniques, Chemical Reviews 113 (3) (2013) 1736–1850, https://doi.org/10.1021/cr2000898, PMID:23444971.

[130] J.E. Penner-Hahn< 2.13 - x-ray absorption spectroscopy, in: Jon A. McCleverty and Thomas J. Meyer, editors, Comprehensive Coordination Chemistry II, pages 159–186. Pergamon, Oxford, 2003. ISBN 978-0-08-043748-4. doi: 10.1016/B0-08-043748-6/01063-X. URL:http://www.sciencedirect.com/science/article/pii/B008043748601063X.

[131] R.D. Cowan, G.H. Dieke, Self-absorption of spectrum lines, Reviews of Modern Physics 20 (Apr 1948) 418–455, https://doi.org/10.1103/RevModPhys.20.418, URL:https://link.aps.org/doi/10.1103/RevModPhys.20.418.

[132] Reshmi Kurian, Kristjan Kunnus, Philippe Wernet, Sergei M Butorin, Pieter Glatzel, and Frank M F de Groot. Intrinsic deviations in fluorescence yield detected x-ray absorption spectroscopy: the case of the transition metal $l_{2,3}$edges. Journal of Physics: Condensed Matter, 24 (45): 452201, Oct 2012. DOI: 10.1088/0953-8984/24/45/452201. https://doi.org/10.1088.

[133] J.J. Rehr, Theory and calculations of x-ray spectra: Xas, xes, xrs, and nrixs, Radiation Physics and Chemistry, 75 (11) (2006) 1547–1558. ISSN 0969-806X. https://doi.org/10.1016/j.radphyschem.2005.11.014. URL:http://www.sciencedirect.com/science/article/pii/S0969806X06002167. Proceedings of the 20th International Conference on X-ray and Inner-Shell Processes.

[134] Maoyu Wang, Líney Árnadóttir, Zhichuan J. Xu, and Zhenxing Feng. In situ x-ray absorption spectroscopy studies of nanoscale electrocatalysts. Nano-Micro Letters, 11 (1) (2019) 47. ISSN 2150-5551. DOI: 10.1007/s40820-019-0277-x.

[135] S. Pascarelli, T. Neisius, S. De Panfilis, Turbo-XAS: dispersive XAS using sequential acquisition, Journal of Synchrotron Radiation 6 (5) (Sep 1999) 1044–1050, https://doi.org/10.1107/S0909049599004513.

[136] Sakura Pascarelli, Olivier Mathon, Advances in high brilliance energy dispersive x-ray absorption spectroscopy, Phys. Chem. Chem. Phys. 12 (2010) 5535–5546, https://doi.org/10.1039/B926509K.

[137] Moniek Tromp, Andrew J. Dent, Jon Headspith, Timothy L. Easun, Xue-Zhong Sun, Michael W. George, Olivier Mathon, Grigory Smolentsev, Michelle L. Hamilton, John Evans, Energy dispersive xafs: Characterization of electronically excited states of copper(i) complexes, The Journal of Physical Chemistry B 117 (24) (2013) 7381–7387, https://doi.org/10.1021/jp4020355, PMID:23718738.

[138] J. Gerbrand Mesu, Ad M.J. van der Eerden, Frank M.F. de Groot, Bert M. Weckhuysen, Synchrotron radiation effects on catalytic systems as probed with a combined in-situ uv-vis/xafs spectroscopic setup, The Journal of Physical Chemistry B, 109 (9): 4042–4047, 2005. DOI: 10.1021/jp045206r.

[139] Mark A. Newton, Daryl G. Burnaby, Andrew J. Dent, Sofia Diaz-Moreno, John Evans, Steven G. Fiddy, Thomas Neisius, Sandra Turin, Energy dispersive extended x-ray absorption fine structure, mass spectrometric, and diffuse reflectance infrared studies of the interaction of al2o3-supported rhi(co)2cl species with no and re-formation under co, The Journal of Physical Chemistry B 106 (16) (2002) 4214–4222, https://doi.org/10.1021/jp013749k.

[140] Delphine Cabaret, Amélie Bordage, Amélie Juhin, Mounir Arfaoui, Emilie Gaudry, First-principles calculations of x-ray absorption spectra at the k-edge of 3d transition metals: an electronic structure analysis of the pre-edge, Phys. Chem. Chem. Phys. 12 (2010) 5619–5633, https://doi.org/10.1039/B926499J.

[141] J. Wong, F.W. Lytle, R.P. Messmer, D.H. Maylotte, k-edge absorption spectra of selected vanadium compounds, Physial Review B 30 (Nov 1984) 5596–5610, https://doi.org/10.1103/PhysRevB.30.5596, URL:https://link.aps.org/doi/10.1103/PhysRevB.30.5596.

[142] Frank E. Huggins, Mohammad Najih, Gerald P. Huffman, Direct speciation of chromium in coal combustion by-products by x-ray absorption fine-structure spectroscopy, Fuel 78 (2) (1999) 233–242, ISSN 0016-2361. doi: 10.1016/S0016-2361(98)00142-2. URL:http://www.sciencedirect.com/science/article/pii/S0016236198001422.

[143] Chung-Hao Kuo, Islam M. Mosa, Srinivas Thanneeru, Vinit Sharma, Lichun Zhang, Sourav Biswas, S. Mark Aindow, Pamir Alpay, James F. Rusling, Steven L. Suib, Jie He, Facet-dependent catalytic activity of mno electrocatalysts for oxygen reduction and oxygen evolution reactions, Chemical Communications 51 (2015) 5951–5954, https://doi.org/10.1039/C5CC01152C.

[144] A.N. Mansour, C.A. Melendres, M. Pankuch, R.A. Brizzolara, X-ray absorption fine structure spectra and the oxidation state of nickel in some of its oxycompounds, Journal of the Electrochemical Society 141 (6) (1994) L69–L71, https://doi.org/10.1149/1.2054990.

[145] Sandeep K. Padamati, Davide Angelone, Apparao Draksharapu, Gloria Primi, David J. Martin, Moniek Tromp, Marcel Swart, Wesley R. Browne, Transient Formation and Reactivity of a High-Valent Nickel(IV) Oxido Complex, Journal of the American Chemical Society 139 (25) (2017) 8718–8724, ISSN 15205126. DOI: 10.1021/jacs.7b04158.

[146] D. Joseph, A.K. Yadav, S.N. Jha, and D. BHATTACHARYYA. Chemical shift of mn and cr k-edges in x-ray absorption spectroscopy with synchrotron radiation. Bulletin of Materials Science, 36 (6) (2013) 1067–1072, Nov 2013. ISSN 0973–7669. DOI: 10.1007/s12034-013-0567-8. doi: 10.1007/s12034-013-0567-8.

[147] Markus Kubin, Meiyuan Guo, Thomas Kroll, Heike Löchel, Erik Källman, Michael L. Baker, Rolf Mitzner, Sheraz Gul, Jan Kern, Alexander Föhlisch, Alexei Erko, Uwe Bergmann, Vittal Yachandra, Junko Yano, Marcus Lundberg, Philippe Wernet, Probing the oxidation state of transition metal complexes: a case study on how charge and spin densities determine mn l-edge x-ray absorption energies, Chem. Sci. 9 (2018) 6813–6829, https://doi.org/10.1039/C8SC00550H.

[148] Bruce Ravel, Introduction to x-ray absorption spectroscopy, 2015.https://www.bnl.gov/ps/userguide/lectures/Lecture-4-Ravel.pdf.

[149] Benedikt Lassalle-Kaiser, Thaddeus T. Boron, Vera Krewald, Jan Kern, Martha A. Beckwith, Mario U. Delgado-Jaime, Henning Schroeder, Roberto Alonso-Mori, Dennis Nordlund, Tsu-Chien Weng, Dimosthenis Sokaras, Frank Neese, Uwe Bergmann, Vittal K. Yachandra, Serena DeBeer, Vincent L. Pecoraro, Junko Yano, Experimental and computational x-ray emission spectroscopy as a direct probe of protonation states in oxo-bridged mniv dimers relevant to redox-active metalloproteins, Inorganic Chemistry 52 (22) (2013) 12915–12922, https://doi.org/10.1021/ic400821g.

[150] Charles G. Barkla, Xxxix. the spectra of the fluorescent röntgen radiations. The London, Edinburgh, and Dublin Philosophical Magazine and Journal of Science, 22 (129) (1911) 396–412. DOI: 10.1080/14786440908637137.

[151] Manne Siegbahn, Relations between the K and L Series of the High-Frequency Spectra, Nature 96 (2416) (1916) 676, https://doi.org/10.1038/096676b0.

[152] Manne Siegbahn, The Spectroscopy of X-rays, London Oxford University Press, 1925.

[153] Henry Gwyn Jeffreys Moseley, Xciii. the high-frequency spectra of the elements, The London, Edinburgh, and Dublin Philosophical Magazine and Journal of Science, 26 (156) (1913) 1024–1034. DOI: 10.1080/14786441308635052.

[154] R. Jenkins, R. Manne, R. Robin, C. Senemaud, Iupac nomenclature system for x-ray spectroscopy, X-Ray Spectrometry 20 (3) (1991) 149–155, https://doi.org/10.1002/xrs.1300200308, URL:https://onlinelibrary.wiley.com/doi/abs/10.1002/xrs.1300200308.

[155] Mario Ulises Delgado-Jaime, Serena DeBeer, Matthias Bauer, Valence-to-core X-ray emission spectroscopy of iron-carbonyl complexes: Implications for the examination of catalytic intermediates. Chemistry - A European Journal, 19 (47) (2013) 15888–15897. ISSN 15213765. DOI: 10.1002/chem.201301913.

[156] Kenjiro Tsutsumi, Hiroo Nakamori, Kouichi Ichikawa, X-ray mn kβemission spectra of manganese oxides and manganates, Physical Review B 13 (Jan 1976) 929–933, https://doi.org/10.1103/PhysRevB.13.929.

[157] M. Torres Deluigi, J. Díaz-Luque, Analysis of the K Satellite Lines in X-Ray Emission Spectra, X-Ray Spectroscopy 2012) (2012) 65–80, https://doi.org/10.5772/28882.

[158] M. Deutsch, G. Hölzer, J. Härtwig, J. Wolf, M. Fritsch, E. Förster, K$\alpha$and kβx-ray emission spectra of copper, Physical Review A 51 (Jan 1995) 283–296, https://doi.org/10.1103/PhysRevA.51.283.

[159] Christopher J. Pollock, Mario Ulises Delgado-Jaime, Mihail Atanasov, Frank Neese, Serena DeBeer, Kβ) mainline x-ray emission spectroscopy as an experimental probe of metal-ligand covalency. Journal of the American Chemical Society, 136 (26) (2014) 9453–9463. DOI: 10.1021/ja504182n.

[160] U. Bergmann, C.R. Horne, T.J. Collins, J.M. Workman, S.P. Cramer, Chemical dependence of interatomic x-ray transition energies and intensities - a study of Mn Kβ" and K$\beta_{2,5}$ spectra. Chemical Physics Letters, 302 (1) (1999) 119–124. ISSN 0009–2614. doi: 10.1016/S0009-2614(99)00095-0. URL:http://www.sciencedirect.com/science/article/pii/S0009261499000950.

[161] Kyle M. Lancaster, Kenneth D. Finkelstein, Serena DeBeer, Kβx-ray emission spectroscopy offers unique chemical bonding insights: Revisiting the electronic structure of ferrocene, Inorganic Chemistry 50 (14) (2011) 6767–6774, https://doi.org/10.1021/ic200822b, PMID:21692497.

[162] Anuj Bhargava, Cindy Y. Chen, Kenneth D. Finkelstein, Matthew J. Ward, Richard D. Robinson, X-ray emission spectroscopy: an effective route to extract site occupation of cations, Physical Chemistry Chemical Physics 20 (2018) 28990–29000, https://doi.org/10.1039/C8CP04628J.

[163] Nicole Lee, Taras Petrenko, Uwe Bergmann, Frank Neese, Serena DeBeer, Probing valence orbital composition with iron kβx-ray emission spectroscopy, Journal of the American Chemical Society 132 (28) (2010) 9715–9727, https://doi.org/10.1021/ja101281e, PMID:20578760.

[164] Erik Gallo, Carlo Lamberti, Pieter Glatzel, Investigation of the valence electronic states of ti(iv) in ti silicalite-1 coupling x-ray emission spectroscopy and density functional calculations, Physical Chemistry Chemical Physics 13 (2011) 19409–19419, https://doi.org/10.1039/C1CP21556F.
[165] Erik Gallo, Pieter Glatzel, Valence to core x-ray emission spectroscopy, Advanced Materials 26 (46) (2014) 7730–7746, https://doi.org/10.1002/adma.201304994, https://onlinelibrary.wiley.com/doi/abs/10.1002/adma.201304994.
[166] Gregor Wentzel. Zur systematik der röntgenspektren. Zeitschrift für Physik, 6 (1): 84–99, Dec 1921. ISSN 0044–3328. DOI: 10.1007/BF01327967. doi: 10.1007/BF01327967.
[167] Gregor Wentzel, Funkenlinien im röntgenspektrum, Annalen der Physik 371 (23) (1922) 437–461, https://doi.org/10.1002/andp.19223712302, https://onlinelibrary.wiley.com/doi/abs/10.1002/andp.19223712302.
[168] Martha A. Beckwith, Michael Roemelt, Marie-Noëlle Collomb, Carole DuBoc, Tsu-Chien Weng, Uwe Bergmann, Pieter Glatzel, Frank Neese, Serena DeBeer, Manganese kβx-ray emission spectroscopy as a probe of metal-ligand interactions, Inorganic Chemistry 50 (17) (2011) 8397–8409, https://doi.org/10.1021/ic200970t, PMID:21805960.
[169] Christopher J. Pollock, Serena DeBeer, Insights into the geometric and electronic structure of transition metal centers from valence-to-core x-ray emission spectroscopy, Accounts of Chemical Research 48 (11) (2015) 2967–2975, https://doi.org/10.1021/acs.accounts.5b00309, PMID:26401686.
[170] Julian A. Rees, Vlad Martin-Diaconescu, Julie A. Kovacs, Serena DeBeer, X-ray absorption and emission study of dioxygen activation by a small-molecule manganese complex, Inorganic Chemistry 54 (13) (2015) 6410–6422, https://doi.org/10.1021/acs.inorgchem.5b00699, PMID:26061165.
[171] Erik Gallo, Modification of the electronic structure of catalytic active transition-metal centers upon molecular adsorption: an XAS/XES study. PhD thesis, Université de Rennes, April 2013. https://www.theses.fr/2013REN1S054.pdf.
[172] Grigory Smolentsev, Alexander V. Soldatov, Johannes Messinger, Kathrin Merz, Thomas Weyhermüller, Uwe Bergmann, Yulia Pushkar, Junko Yano, Vittal K. Yachandra, Pieter Glatzel, X-ray emission spectroscopy to study ligand valence orbitals in mn coordination complexes, Journal of the American Chemical Society 131 (36) (2009) 13161–13167, https://doi.org/10.1021/ja808526m, PMID:19663435.
[173] George E., Cutsail III, Nicole L. Gagnon, Andrew D. Spaeth, William B. Tolman, Serena DeBeer, Valence-to-core x-ray emission spectroscopy as a probe of o-o bond activation in cu_2)ø_2) complexes. Angewandte Chemie International Edition, 58 (27) (2019): 9114–9119. DOI: 10.1002/anie.201903749. https://onlinelibrary.wiley.com/doi/abs/10.1002/anie.201903749.
[174] Christopher J. Pollock, Katarzyna Grubel, Patrick L. Holland, Serena DeBeer, Experimentally quantifying small-molecule bond activation using valence-to-core x-ray emission spectroscopy, Journal of the American Chemical Society 135 (32) (2013) 11803–11808, https://doi.org/10.1021/ja3116247, PMID:23862983.
[175] Kyle M. Lancaster, Michael Roemelt, Patrick Ettenhuber, Yilin Hu, Markus W. Ribbe, Frank Neese, Uwe Bergmann, Serena DeBeer, X-ray emission spectroscopy evidences a central carbon in the nitrogenase iron-molybdenum cofactor. Science, 334 (6058) (2011b): 974–977. ISSN 0036–8075. DOI: 10.1126/science.1206445. https://science.sciencemag.org/content/334/6058/974.
[176] P. Chandrasekaran, Karen P. Chiang, Dennis Nordlund, Uwe Bergmann, Patrick L. Holland, Serena DeBeer, Sensitivity of x-ray core spectroscopy to changes in metal ligation: A systematic study of low-coordinate, high-spin ferrous complexes. Inorganic Chemistry, 52 (11) (2013): 6286–6298. 10.1021/ic3021723. URL https://doi.org/10.1021/ic3021723. PMID:23662855.
[177] F.K. Richtmyer and Sidney Kaufman. X-ray satellites of high atomic number elements. Phys. Rev., 44 (1933): 605–609. DOI: 10.1103/PhysRev.44.605. https://link.aps.org/doi/10.1103/PhysRev.44.605.
[178] F.R. Hirsh, F.K. Richtmyer, The relative intensities of certain l-series x-ray satellites in cathode-ray and in fluorescence excitation, Physical Review 44 (1933) 955–960, https://doi.org/10.1103/PhysRev.44.955, URL:https://link.aps.org/doi/10.1103/PhysRev.44.955.
[179] Robert D. Richtmyer, The probability of KL ionization and x-ray satellites, Physical Review 49 (1936) 1–8, https://doi.org/10.1103/PhysRev.49.1.
[180] D. Coster and R. De L. Kronig. New type of auger effect and its influence on the x-ray spectrum. Physica, 2 (1): 13–24, 1935. ISSN 0031–8914. doi: 10.1016/S0031-8914(35)90060-X. URL:http://www.sciencedirect.com/science/article/pii/S003189143590060X.
[181] Pieter Glatzel, Uwe Bergmann, High resolution 1s core hole X-ray spectroscopy in 3d transition metal complexes—electronic and structural information, Coordination Chemistry Reviews 249 (1–2) (2005) 65–95, https://doi.org/10.1016/j.ccr.2004.04.011.
[182] Pieter Glatzel, Roberto Alonso-Mori, Dimosthenis Sokaras, Hard x-ray photon-in/photon-out spectroscopy: Instrumentation, theory and applications. In X-Ray Absorption and X-Ray Emission Spectroscopy, chapter 6, pages 125–153. John Wiley & Sons Ltd, 2016. ISBN 9781118844243. DOI: 10.1002/9781118844243.ch6. URL:https://onlinelibrary.wiley.com/doi/abs/10.1002/9781118844243.ch6.
[183] Jun Kawai, Chemical effects in the satellites of X-ray emission spectra. Nuclear Inst. and Methods in Physics Research, B, 75 (1–4) (1993) 3–8. ISSN 0168583X. DOI: 10.1016/0168-583X(93)95599-Z.
[184] Alexander S. Ditter, William M. Holden, Samantha K. Cary, Veronika Mocko, Matthew J. Latimer, Erik J. Nelson, Stosh A. Kozimor, Gerald T. Seidler, Resonant inelastic X-ray scattering using a miniature dispersive Rowland refocusing spectrometer, Journal of Synchrotron Radiation 27 (2020), https://doi.org/10.1107/S1600577520001022.
[185] R. Kopelent, J.A. Van Bokhoven, M. Nachtegaal, J. Szlachetko, O.V. Safonova, X-ray emission spectroscopy: Highly sensitive techniques for time-resolved probing of cerium reactivity under catalytic conditions. Physical Chemistry Chemical Physics, 18 (47) (2016) 32486–32493. ISSN 14639076. DOI: 10.1039/c6cp05830b. doi: 10.1039/c6cp05830b.
[186] Stephen Best, Joan ribas gispert coordination chemistry wiley-vch, 2008, Applied Organometallic Chemistry 23 (11) (2009) 482–483, https://doi.org/10.1002/aoc.1550.
[187] Frank M.F. de Groot, Pieter Glatzel, Uwe Bergmann, Peter A. van Aken, Raul A. Barrea, Stephan Klemme, Michael HäMichael Roemelt, Marie-Novecker, Axel Knop-Gericke, Willem M. Heijboer, Bert M. Weckhuysen, 1s2p resonant inelastic x-ray scattering of iron oxides. The Journal of Physical Chemistry B, 109 (44) (2005) 20751–20762. DOI: 10.1021/jp054006s.
[188] F. Albert Cotton, I - ligand field theory. Journal of Chemical Education, 41 (9) (1964) 466. DOI: 10.1021/ed041p466.
[189] Joan Ribas Gispert, Coordination Chemistry. Wiley, May 2008. ISBN 978-3-527-31802-5. URL:https://www.wiley.com/en-us/Coordination+Chemistry-p-9783527318025.
[190] M.A. Korotin, V.I. Anisimov, D.I. Khomskii, G.A. Sawatzky, cro_2: A self-doped double exchange ferromagnet, Physical Review Letters 80 (May 1998) 4305–4308, https://doi.org/10.1103/PhysRevLett.80.4305.
[191] Ari-Pekka Honkanen, Sami Ollikkala, Taru Ahopelto, Antti-Jussi Kallio, Merja Blomberg, Simo Huotari. Johann-type laboratory-scale X-ray absorption spectrometer with versatile detection modes, arXiv, pages 1–10, 2018. http://arxiv.org/abs/1812.01075.
[192] William M. Holden, Gerald T. Seidler, Singfoong Cheah, Sulfur Speciation in Biochars by Very High Resolution Benchtop KαX-ray Emission Spectroscopy. Journal of Physical Chemistry A, 122 (23): 5153–5161, 2018. ISSN 15205215. DOI: 10.1021/acs.jpca.8b02816.
[193] C. Kunz, Synchrotron radiation: Third generation sources. Journal of Physics Condensed Matter, 13 (34) (2001) 7499–7510. ISSN 09538984. DOI: 10.1088/0953-8984/13/34/303.
[194] W. Frentrup, D. Schröder, R. Manzke, Correction of self absorption on xas measurements in fluorescence mode, J. Phys. IV France 7 (1997), https://doi.org/10.1051/jp4/1997073, C2-509-C2-510.
[195] F. Shimazu, C. Sterling, Effect of wet and dry heat on structure of cellulose, Journal of Food Science 31 (4) (1966) 548–551, https://doi.org/10.1111/j.1365-2621.1966.tb01902.x.
[196] Edward A. Stern, AIP conference proceedings: Laboratory EXAFS facilities 1980: University of Washington workshop, American Institute of Physics, 1980, ISBN 0883181630.
[197] Herbert Legall, Holger Stiel, Matthias Schnürer, Marcel Pagels, Birgit Kanngießer, Matthias Müller, Burkhard Beckhoff, Inna Grigorieva, Alexander Antonov, Vladimir Arkadiev, Aniouar Bjeoumikhov, An efficient X-ray spectrometer based on thin mosaic crystal films and its application in various fields of X-ray spectroscopy, Journal of Applied Crystallography 42 (4) (2009) 572–579, https://doi.org/10.1107/S0021889809006803.
[198] C. Schlesiger, L. Anklamm, H. Stiel, W. Malzer, and B. Kanngiesser. XAFS spectroscopy by an X-ray tube based spectrometer using a novel type of HOPG mosaic crystal and optimized image processing. Journal of Analytical Atomic Spectrometry, 30 (5): 1080–1085, 2015. ISSN 13645544. DOI: 10.1039/c4ja00303a. doi: 10.1039/c4ja00303a.
[199] Zoltán Németh, Jakub Szlachetko, Éva G. Bajnóczi, and György Vankó. Laboratory von Hámos X-ray spectroscopy for routine sample characterization. Review of Scientific Instruments, 87 (10) (2016) 103105-1-103105-10. ISSN 10897623. DOI: 10.1063/1.4964098.
[200] T. Taguchi, K. Shinoda, K. Tohji, Customization of an InHouse XAFS spectrometer for sulfur measurement. Physica Scripta, page 1017, 2005. DOI: 10.1238/physica.topical.115a01017. https://doi.org/10.1238.
[201] M Elizabeth Mundy, David Ung, Nathan L Lai, Evan P Jahrman, Gerald T Seidler, Brandi M. Cossairt, Aminophosphines as Versatile Precursors for the Synthesis of Metal Phosphide Nanocrystals. Chemistry of Materials, 30 (2018) 5373–5379. ISSN 0897-4756. DOI: 10.1021/acs.chemmater.8b02206. doi: 10.1021/acs.chemmater.8b02206.
[202] Evan P. Jahrman, William M. Holden, Alexander S. Ditter, Devon R. Mortensen, Gerald T. Seidler, Timothy T. Fister, Stosh A. Kozimor, Louis F.J. Piper, Jatinkumar Rana, Neil C. Hyatt, Martin C. Stennett, An improved laboratory-based x-ray absorption fine structure and x-ray emission spectrometer for analytical applications in materials chemistry research. Review of Scientific Instruments, 90 (2), 2019a. ISSN 10897623. DOI: 10.1063/1.5049383.
[203] Wenchao Bi, Evan P. Jahrman, Gerald T. Seidler, Jichao Wang, Guohua Gao, Guangming Wu, Muhammad Atif, M.S. AlSalhi, Guozhong Cao, Tailoring Energy and Power Density through Controlling the Concentration of Oxygen Vacancies in V_2 O_5/PEDOT Nanocable-Based Supercapacitors. ACS Applied Materials & Interfaces, page acsami.9b03830, 2019. ISSN 1944–8244. DOI: 10.1021/acsami.9b03830. URL:http://pubs.acs.org/doi/10.1021/acsami.9b03830.
[204] I. Mantouvalou, K. Witte, W. Martyanov, A. Jonas, D. Grötzsch, C. Streeck, H. Löchel, I. Rudolph, A. Erko, H. Stiel, B. Kanngießer, Single shot near edge x-ray

absorption fine structure spectroscopy in the laboratory. Applied Physics Letters, 108 (20) (2016). ISSN 00036951. DOI: 10.1063/1.4951000.
[205] Kenji Sato, Akihiro Nishimura, Masatomo Kaino, Susumu Adachi, Polychromatic simultaneous wdxrf for chemical state analysis using laboratory x-ray source, X-Ray Spectrometry 46 (5) (2017) 330–335, https://doi.org/10.1002/xrs.2797, URL:https://onlinelibrary.wiley.com/doi/abs/10.1002/xrs.2797.
[206] S Limandri, J Robledo, and G Tirao. Extracting chemical information from high-resolution Kβ) X-ray emission spectroscopy. Spectrochimica Acta Part B: Atomic Spectroscopy, 144: 29–37, 2018. ISSN 0584–8547. DOI: 10.1016/j.sab.2018.03.004. doi: 10.1016/j.sab.2018.03.004.
[207] M.I. Anwar, M. Iqbal, B.J. Hwang, M. Faiyaz, B.S. Mun, K.A. Janulewicz, D.Y. Noh, Ultrafast x-ray absorption near edge spectroscopy of fe3o4 using a laboratory based femtosecond x-ray source, Optics Express 27 (5) (2019) 6030–6036, https://doi.org/10.1364/OE.27.006030, URL:http://www.opticsexpress.org/abstract.cfm?URI=oe-27-5-6030.
[208] José G. Moya-Cancino, Ad.M.J. Ari-Pekka Honkanen, Herrick van der Eerden, Lieven Folkertsma Schaink, Mahnaz Ghiasi, Alessandro Longo, Frank M.F. de Groot, Florian Meirer, Simo Huotari, Bert M. Weckhuysen, In-situ X-Ray Absorption Near Edge Structure Spectroscopy of a Solid Catalyst using a Laboratory-Based Set-up, ChemCatChem ISSN (2019) 1–7, https://doi.org/10.1002/cctc.201801822.
[209] Jose G. Moya-Cancino, Ari-Pekka Honkanen, Ad M.J. van der Eerden, Herrick Schaink, Lieven Folkertsma, Mahnaz Ghiasi, Alessandro Longo, Florian Meirer, Frank M.F. de Groot, Simo Huotari, Bert M. Weckhuysen, Elucidating the k-edge x-ray absorption near-edge structure of cobalt carbide. ChemCatChem, 11 (13), 2019b. DOI: 10.1002/cctc.201900434. https://onlinelibrary.wiley.com/doi/abs/10.1002/cctc.201900434.
[210] Fuzhong Wei, Z W Chen, W.M. Gibson, Measurement of oxidation states for transition elements with a small spot tabletop XANES instrument. X-ray Spectrometry, (38): 382–385, February 2009. 10.1002/xrs.1185. URL https://doi.org/10.1002/xrs.1185.
[211] Hironobu Maeda, Hikaru Terauchi, Kazuhiro Tanabe, Nagao Kamijo, Moritaka Hida, Hajimu Kawamura, Development of a laboratory EXAFS facility and its application to amorphous GeSe semiconductors, Japanese Journal of Applied Physics 21 (Part 1, No. 9) (1982) 1342–1346, https://doi.org/10.1143/jjap.21.1342.
[212] Mitsuru Sano, Kazuo Taniguchi, Hideo Yamatera, The exafs study of cu(ii) aqueous solution using a position sensitive detector, Chemistry Letters 9 (10) (1980) 1285–1286, https://doi.org/10.1246/cl.1980.1285.
[213] Masaharu Nomura, Kiyotaka Asakura, Ukyo Kaminaga, Tadashi Matsushita, Kazutake Kohra, Haruo Kuroda, Exafs spectroscopy of some iron(iii) compounds by use of dispersive-type in-laboratory x-ray spectrometer, Bulletin of the Chemical Society of Japan 55 (12) (1982) 3911–3914, https://doi.org/10.1246/bcsj.55.3911.
[214] Ukyo Kaminaga, Tadashi Matsushita, Kazutake Kohra, A dispersive method of measuring extended x-ray absorption fine structure, Japanese Journal of Applied Physics 20 (5) (May 1981) L355–L358, https://doi.org/10.1143/jjap.20.l355.
[215] William M. Holden, Oliver R. Hoidn, Alexander S. Ditter, Gerald T. Seidler, Joshua Kas, Jennifer L. Stein, Brandi M. Cossairt, Stosh A. Kozimor, Jinghua Guo, Yifan Ye, Matthew A. Marcus, Sirine Fakra, A compact dispersive refocusing Rowland circle X-ray emission spectrometer for laboratory, synchrotron, and XFEL applications. Review of Scientific Instruments, 88 (7) (2017). ISSN 10897623. DOI: 10.1063/1.4994739.
[216] M. Iqbal, Z. Urrehman, H. Im, J.G. Son, O. Seo, H. Stiel, P.V. Nickles, D.Y. Noh, and K.A. Janulewicz, Performance improvement of a kαsource by a high-resolution thin-layer-graphite spectrometer and a polycapillary lens. Applied Physics B, 116 (2) (2014) 305–311. ISSN 1432–0649. DOI: 10.1007/s00340-013-5691-z.
[217] G. Ingold, A. Streun, B. Singh, R. Abela, P. Beaud, G. Knopp, L. Rivkin, V. Schlott, T. Schmidt, H. Sigg, J.F. van der Veen, A. Wrulich, S. Khan, Sub-picosecond optical pulses at the sls storage ring. In PACS2001. Proceedings of the 2001 Particle Accelerator Conference (Cat. No.01CH37268), volume 4, pages 2656–2658 vol 4, June 2001. DOI: 10.1109/PAC.2001.987863.
[218] G. Ingold, P. Beaud, S.L. Johnson, D. Grolimund, V. Schlott, T. Schmidt, A. Streun, Technical report: Femto: A sub-ps tunable hard x-ray undulator source for laser/x-ray pump-probe experiments at the sls, Synchrotron Radiation News 20 (5) (2007) 35–39, https://doi.org/10.1080/08940880701631377.
[219] R.W. Schoenlein, S. Chattopadhyay, H.H.W. Chong, T.E. Glover, P.A. Heimann, C.V. Shank, A.A. Zholents, M.S. Zolotorev, Generation of femtosecond pulses of synchrotron radiation. Science, 287 (5461): 2237–2240, 2000. ISSN 0036–8075. DOI: 10.1126/science.287.5461.2237. URL:https://science.sciencemag.org/content/287/5461/2237.
[220] A.A. Zholents, M.S. Zolotorev, Femtosecond x-ray pulses of synchrotron radiation, Physical Review Letters 76 (Feb 1996) 912–915, https://doi.org/10.1103/PhysRevLett.76.912.
[221] S. Khan, K. Holldack, T. Kachel, R. Mitzner, T. Quast, Femtosecond undulator radiation from sliced electron bunches, Physical Review Letters 97 (Aug 2006) , https://doi.org/10.1103/PhysRevLett.97.074801 074801.
[222] D.K. Kalantaryan, G.A. Amatuni, V.M. Tsakanov, P. Beaud, G. Ingold, A. Streun, Laser - Beam Interaction and Calculation of the Sliced Bunch Radiation Spectra for the SLS FEMTO Beam Line. Conf. Proc., C0806233: WEPC026, 2008. URL:https://accelconf.web.cern.ch/accelconf/e08/papers/wepc026.pdf.
[223] Manfred Baerns (Ed.), Basic Principles in Applied Catalysis. Springer Science & Business Media, 2013. ISBN 9783662059814. DOI: 10.1007/978-3-662-05981-4.
[224] I. Chorkendorff, J.W. Niemantsverdriet, Concepts of Modern Catalysis and Kinetics, Third. Wiley-VCH Verlag, 2017.
[225] Paola Lanzafame, Siglinda Perathoner, Gabriele Centi, Silvia Gross, E.J.M. Hensen, Grand challenges for catalysis in the science and technology roadmap on catalysis for europe: moving ahead for a sustainable future, Catalysis Science & Technology 7 (22) (2017) 5182–5194, DOI: 10.1039/C7CY01067B.
[226] José A. Rodríguez, Jonathan C. Hanson, Peter J. Chupas, In-situ Characterization of Heterogeneous Catalysts, volume 1. Wiley Online Library, 2013. 10.1002/9781118355923. URL https://doi.org/10.1002/9781118355923.
[227] Cynthia A Fuentes, María V Gallegos, Juan R García, Jorge Sambeth, Miguel A. Peluso, Catalytic glycolysis of poly (ethylene terephthalate) using zinc and cobalt oxides recycled from spent batteries. Waste and Biomass Valorization, pages 1–11, 2019. DOI: 10.1007/s12649-019-00807-6.
[228] Zoltán Németh, Éva G Bajnóczi, Bogdán Csilla, György Vankó, Laboratory exafs determined structure of the stable complexes in the ternary ni (ii)–edta–cn- system. Physical Chemistry Chemical Physics, 21 (18) (2019) 9239–9245. DOI: 10.1039/C9CP00982E.
[229] Ana Foi, Florencia Di Salvo, Fabio Doctorovich, Cristián Huck-Iriart, José Martín Ramallo-López, Maximilian Dürr, Ivana Ivanović-Burmazović, Kathrin Stirnat, Simon Garbe, Axel Klein, Synthesis and structural characterisation of unprecedented primary n-nitrosamines coordinated to iridium (iv). Dalton Transactions, 47 (33) (2018) 11445–11454. 10.1039/C8DT02549E. URL https://doi.org/10.1039/C8DT02549E.
[230] Vera V Butova, Andriy P Budnyk, Alexander A Guda, Kirill A Lomachenko, Aram L Bugaev, Alexander V Soldatov, Sachin M Chavan, Sigurd Øien-Ø degaard, Unni Olsbye, Karl Petter Lillerud, et al. Modulator effect in uio-66-ndc (1, 4-naphthalenedicarboxylic acid) synthesis and comparison with uio-67-ndc isoreticular metal–organic frameworks. Crystal Growth & Design, 17 (10): 5422–5431, 2017.
[231] Wenhai Wang, Long Kuai, Wei Cao, Marko Huttula, Sami Ollikkala, Taru Ahopelto, Ari Pekka Honkanen, Simo Huotari, Mengkang Yu, Baoyou Geng, Mass-Production of Mesoporous MnCo_2)Ø_4) Spinels with Manganese(IV)- and Cobalt(II)-Rich Surfaces for Superior Bifunctional Oxygen Electrocatalysis. Angewandte Chemie - International Edition, 56 (47) (2017) 14977–14981. ISSN 15213773. DOI: 10.1002/anie.201708765.
[232] Raghavendra Shavi, Vishwanath Hiremath, Aditya Sharma, Sung Ok Won, Jeong Gil Seo, Synergistic activating effect of promoter and oxidant in single step conversion of methane into methanol over a tailored polymer-ag coordination complex. RSC Advances, 7 (39) (2017) 24168–24176.
[233] Takashi Yamamoto, Aoi Teramachi, Akihiro Orita, Akihito Kurimoto, Takashi Motoi, Tsunehiro Tanaka, Generation of strong acid sites on yttrium-doped tetragonal zro2-supported tungsten oxides: Effects of dopant amounts on acidity, crystalline phase, kinds of tungsten species, and their dispersion, The Journal of Physical Chemistry C 120 (35) (2016) 19705–19713, https://doi.org/10.1021/acs.jpcc.6b05388.
[234] Baeck Choi, Woo-Hyun Nam, Dong Young Chung, In-Su Park, Sung Jong Yoo, Jae Chun Song, Yung-Eun Sung, Enhanced methanol tolerance of highly pd rich pd-pt cathode electrocatalysts in direct methanol fuel cells, Electrochimica Acta 164 (2015) 235–242, https://doi.org/10.1016/j.electacta.2015.02.203.
[235] Tae Hwan Lim, Sung June Cho, Hee Sung Yang, Mark H Engelhard, Do Heui Kim, Effect of co/ni ratios in cobalt nickel mixed oxide catalysts on methane combustion, Applied Catalysis A: General 505 (2015) 62–69.
[236] Kazuhide Kamiya, Ryo Kamai, Kazuhito Hashimoto, Shuji Nakanishi, Platinum-modified covalent triazine frameworks hybridized with carbon nanoparticles as methanol-tolerant oxygen reduction electrocatalysts, Nature Communications 5 (2014) 5040.
[237] Iunia Podolean, Victor Kuncser, Nicoleta Gheorghe, Dan Macovei, Vasile I Parvulescu, Simona M. Coman, Ru-based magnetic nanoparticles (mnp) for succinic acid synthesis from levulinic acid. Green Chemistry, 15 (11) (2013) 3077–3082.
[238] Jun Kyu Lee, Young Jin Kim, Heung-Ju Lee, Su Hyun Kim, Sung June Cho, In-Sik Nam, Suk Bong Hong, Iron-substituted tnu-9, tnu-10, and im-5 zeolites and their steam-activated analogs as catalysts for direct n2o decomposition. Journal of catalysis, 284 (1) (2011) 23–33. DOI: 10.1016/j.jcat.2011.08.012.
[239] Young Bae Jang, Tak Hee Kim, Min Ho Sun, Jun Lee, Sung June Cho, Preparation of iridium catalyst and its catalytic activity over hydrazine hydrate decomposition for hydrogen production and storage. Catalysis Today, 146 (1–2) (2009) 196–201.
[240] H. Kaneko, Y. Tamaura, Reactivity and xafs study on (1–x) ceo_2) &s066ndash;xnio (x=0.025–0.3) system in the two-step water-splitting reaction for solar h2 production. Journal of Physics and Chemistry of Solids, 70 (6) (2009) 1008–1014.
[241] Hiroya Miyauchi, Takashi Yamamoto, Ramesh Chitrakar, Yoji Makita, Zhengming Wang, Jun Kawai, Takahiro Hirotsu, Phosphate adsorption site on zirconium ion modified mgal-layered double hydroxides, Topics in Catalysis 52 (6–7) (2009) 714–723.
[242] Jung-Hyun Park, Bokie Kim, Chae-Ho Shin, Gon Seo, Seok Han Kim, Suk Bong Hong, Methane combustion over pd catalysts loaded on medium and large pore zeolites, Topics in Catalysis 52 (1–2) (2009) 27–34.
[243] Takehiko Sakamoto, Hiroyuki Morishima, Akihiro Yoshida, Shuichi Naito, Marked effect of mo and fe addition upon liquid phase methanol reforming

with water over al_2o_3 supported pt catalysts, Catalysis Letters 131 (3–4) (2009) 419–424.
[244] Mi-Young Kim, Young San You, Hyun-Sik Han, Gon Seo, Preparation of highly dispersive platinum catalysts impregnated on titania-incorporated silica support, Catalysis Letters 120 (1-2) (2008) 40–47.
[245] Sung June Cho, Jun Lee, Yun Sung Lee, Dong Pyo Kim, Characterization of iridium catalyst for decomposition of hydrazine hydrate for hydrogen generation, Catalysis Letters 109 (3-4) (2006) 181–186.
[246] Evan P. Jahrman, Lisa A. Pellerin, Alexander S. Ditter, Liam R. Bradshaw, Timothy T. Fister, Bryant J. Polzin, Steven E. Trask, Alison R. Dunlop, Gerald T. Seidler, Laboratory-based x-ray absorption spectroscopy on a working pouch cell battery at industrially-relevant charging rates, Journal of The Electrochemical Society 166 (12) (2019) A2549–A2555, https://doi.org/10.1149/2.0721912jes.
[247] Jennifer L. Stein, William M. Holden, Amrit Venkatesh, M. Elizabeth Mundy, Aaron J. Rossini, Gerald T. Seidler, Brandi M. Cossairt, Probing surface defects of inp quantum dots using phosphorus kαand kβx-ray emission spectroscopy, Chemistry of Materials 30 (18) (2018) 6377–6388, DOI: 10.1021/acs.chemmater.8b02590.
[248] Singfoong Cheah, Shealyn C. Malone, Calvin J. Feik, Speciation of sulfur in biochar produced from pyrolysis and gasification of oak and corn stover, Environmental Science & Technology 48 (15) (2014) 8474–8480, https://doi.org/10.1021/es500073r, PMID:25003702.
[249] G.T. Seidler, D.R. Mortensen, A.S. Ditter, N.A. Ball, A.J. Remesnik. A Modern Laboratory XAFS Cookbook. Journal of Physics: Conference Series, 712 (1) (2016). ISSN 17426596. DOI: 10.1088/1742-6596/712/1/012015.
[250] P. Bastia, TES detectors applications for scientific instruments in space and on the ground, Journal of Instrumentation 14 (10) (Oct 2019), https://doi.org/10.1088/1748-0221/14/10/c10009, C10009-C10009.
[251] K.D. Irwin, G.C. Hilton, Transition-Edge Sensors, pages 63–150. Springer, Berlin Heidelberg, Berlin, Heidelberg, 2005. ISBN 978-3-540-31478-3. DOI: 10.1007/10933596_3.